Final Design Report

Spoiler Alert!

Active Aero for Formula SAE

Senior Design Spring 2022

COLLEGE OF
ENGINEERING, ARCHITECTURE
AND TECHNOLOGY

Table of Contents

1 Introduction

1.1 Background

Formula SAE (FSAE) is a subset of the Society of Automotive Engineers, one of the largest automotive governing bodies in the world. Annual competitions are held across the globe, where over a hundred other colleges and universities compete in a combination of static and dynamic events. Examples of static events include a business report and technical inspection. Examples of dynamic events include acceleration, braking, skid pad (circle or figure-eight), autocross, and endurance. The vehicles are typically powered by ATV or motorcycle engines with a maximum displacement of 710 cubic centimeters and weigh between 400 and 600 lbs.

1.2 Problem Description

Before detailing the project design, the fundamentals of why an active aerodynamic package is of interest must be addressed. Why is an aerodynamic package on a racecar advantageous as compared to a racecar without one?

An aerodynamic package increases downforce, which increases normal force on the tires, increasing grip with the ground. The higher grip increases stability and maximum cornering speeds. Figure 1.2.1 is a bird's-eye view of a past FSAE competition endurance track. These tracks are short and tight, which means that cars typically do not go very fast, so maximizing cornering speed by increasing grip is of the upmost importance. Of interest in the figure are the slaloms and tight radius turns. In these corners, a vehicle's linear speed is not high, but it pulls substantial lateral g-forces which allows for higher cornering speeds, decreasing lap time.

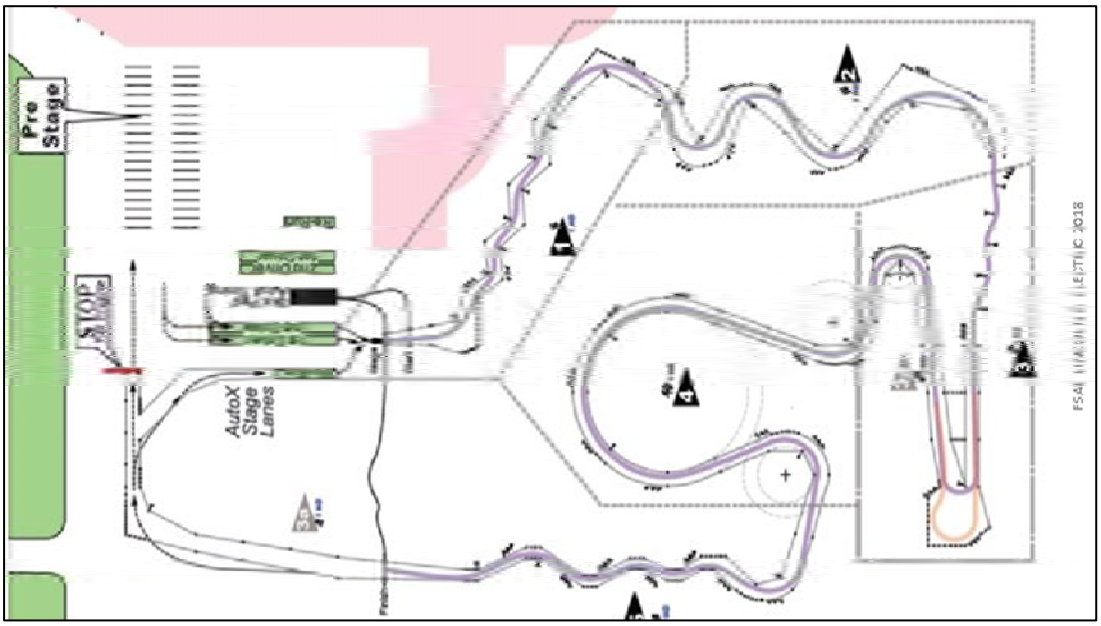

Figure 1.2.1 – Endurance Style FSAE Course

A natural progression from the above discussion is why it is advantageous to implement an active aerodynamic package as opposed to a static one. Simply put, FSAE cars compete against each other, and any small design advantages can have large impacts on performance. The largest disadvantage of a static aerodynamic package is that it increases drag, which reduces the vehicle's top speed. By utilizing an active aerodynamic package with adjustable-pitch flaps, downforce and drag can be actuated and modulated, optimizing the aerodynamics for any part of the track. High downforce is advantageous for cornering as discussed above, low drag is advantageous for straightaways where maximum grip is not important but linear speed is, and high drag is advantageous for late braking.

1.3 Project Objectives

The objective for this project is to develop a dynamic front wing for a Formula SAE car using independently actuated left- and right-wing elements. Making the project active will increase the handling of the car, however, it must be quantitatively proven through a decrease in lap time and/or qualitatively measure by an experienced driver's feedback. The front wing will have both static and dynamic control modes that will be able to be selected while the vehicle is stationary. The package also must be easily removable for testing purposes and for easy integration into future Bullet Racing, Oklahoma State Formula SAE cars.

Using data from Oklahoma State's FSAE team and comparing that to leaders of recent years FSAE competitions, the performance difference between the vehicles is close to 4.3 miles per hour in a constant 30 ft radius turn. The best FSAE cars have great suspension set-ups and well-developed aero packages. These aero packages include but are not limited to, front wings, rear wings, diffusers, etc. If we attribute 1/3rd of the performance difference between these two vehicles to be only due to the front wing package, the goal becomes 1.4 miles per hour. While the objective is not to compete and measure against other teams' suspension set-ups, an increase of about 1.4mph is the objective and expected performance gain.

More information regarding the testing of the vehicle and the measured performance gains of the vehicle occurs in Section 3.

1.4 Team Organization

The team is organized into four sub-teams focused on the different components of the project. Additional team management and support is provided by:

- C. Tanner Price, Team Lead
- Michael Schlotthauer, Team Planner
- Hunter Lovell, Team Purchaser

The Aerodynamics Team, focusing on the lift-generating control elements:

- Anthony Corpuz, Aero Lead
- Gwangmin Kim

- Levi Penwell
- C. Tanner Price
- Austin Wilkins
- Cameron Mendoza

The Electrical Team, focusing on system integration and control:

- Carson Elmore, Electrical Lead
- Jacob Robbins
- Michael Schlotthauer

The Mechanical Team, focusing on control surface actuation and structural implementation:

- Brian Guthery, Mechanical Lead
- Ian Babb
- Hunter Lovell
- Erin Matthews
- Luke Smith

The Testing Team, focusing on system validation and data collection:

- Weston Gorham, Testing Lead
- Kyler Martinez

1.5 Environmental, Health, and Safety Considerations

The project's impact on environmental health and safety were colored by the context of Formula SAE racing. Having less drag on a vehicle improves its efficiency which factors into the competition's static and dynamic events. The endurance event even measures the fuel used and gives a score based on how fuel efficient the vehicle is. However, while less drag improves the efficiency, automobile racing is a luxury from an environmental perspective.

Health and Safety considerations had a much higher impact on our design decisions, even going so far as to directly inform what products are specified for the project. The highest priority was compliance with the DML safety rules both in manufacturing and testing. This included a ban on urethane-based resins and epoxies, limiting material options for the aero and electrical teams. The electrical team communicated constantly with the Formula SAE drivers to ensure the project had a user interface and would take actions that wouldn't surprise the driver. In the worst case, if the driver didn't understand the implemented system, the conflicting control inputs could result in a crash. We consider this to be low risk given the size of the forces generated by the aero package, however, engineering leadership and ethics classes have influenced us to take proactive steps to prevent significant issues.

The social impact of our project does not spread outside the existing impact of FSAE. To the casual observer, there's no functional difference between a FSAE vehicle that has an aero package and

one without. Within the FSAE environment, our implementation could increase the standard and quality of high-performance engineering projects in teams at Oklahoma State and other universities. This will make the FSAE program more competitive and has the potential to increase the quality of engineers involved.

From an ethical perspective, both static and active aero packages are confirmed within the FSAE rules both as written and intended. The highest performing teams all use active aero packages, so we can be sure any competitive advantage gained by our system is fair.

2 Final Design

2.1 Active Wing Elements

2.1.1 Final Active Front Wing Element Configuration

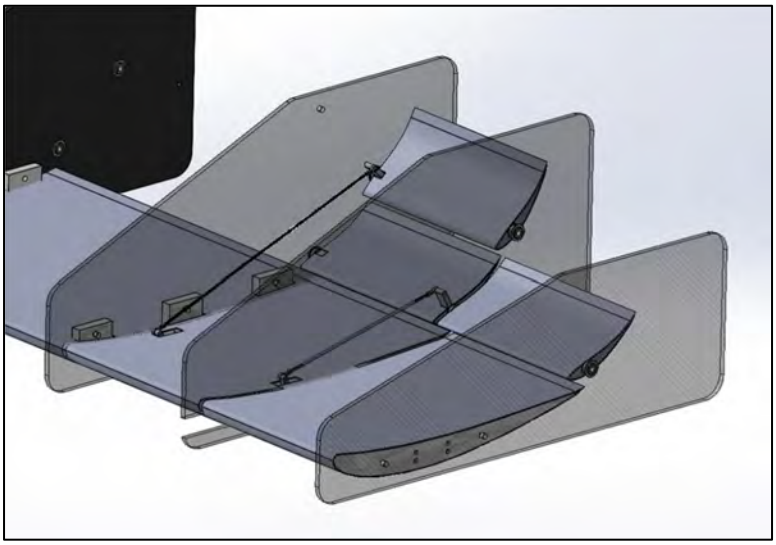

Figure 2.1.1 - Final Front Wing Configuration (One Side)

The final front wing design chosen consists of one static element in the center/chassis region and an active front wing split into two distinct sections on each side of the front wing assembly. The outboard, outermost, section of the wing consists of one static element and one active element. The next section inward, the inboard section, consists of one static wing element and two active elements.

The first active element for the inboard section and the one active element for the outboard section are coupled together for both to actuate in conjunction with each other in operation. The second active element in the inboard section actuates independently of the first tier, allowing for more freedom of movement for that element to maximize aerodynamics of the front wing package.

To stay in compliance with current year Formula SAE (FSAE) competition rules, the wing had to be split into an inboard and outboard section based on design space constraints. Based on Figure ,

it is seen that the section from the centerline of the car to the inside of the front wheel has a maximum build height of 500mm from the ground. Furthermore, the area in between the inside and outside of the front tire is constrained to a shorter maximum build height of 250mm from the ground. To maximize the aerodynamic potential of the front wing package, it was decided that the wing would be split based on the build height restrictions and that the inboard section would hold one more active element due to there being more available vertical build space. While a full two-active element wing would perform better aerodynamically across the entire span to the outer wheelbase, the outermost endplate, the wing needed to be split in order to satisfy the project criteria of designing the front wing package to be within compliance of FSAE competition rules.

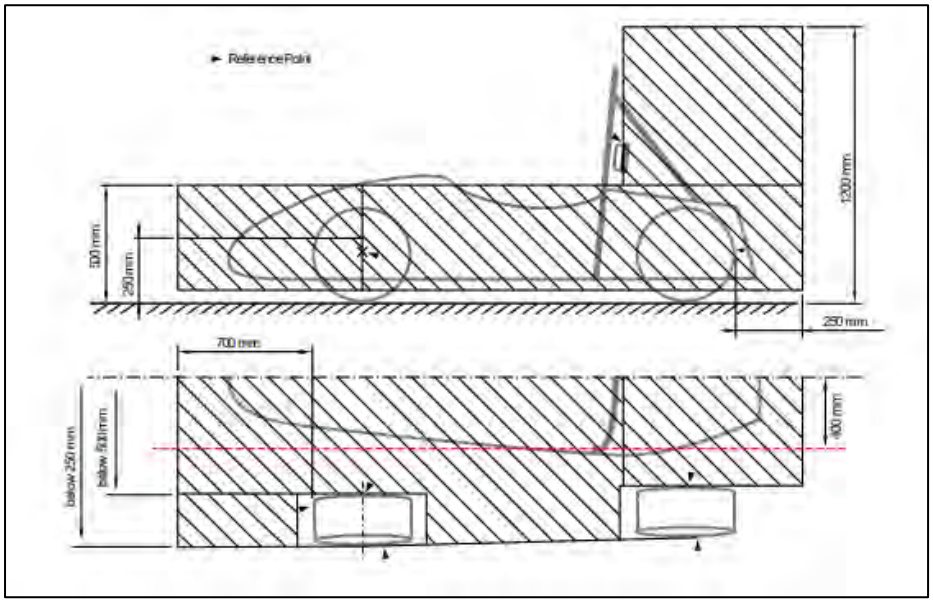

Figure 2.1.2– Aerodynamic Package Sizing Constraints (Formula SAE International)

2.1.2 Computational Fluid Dynamics Analysis

In order to best guide the design decision between one and two active elements on the front wing, 2-D computational fluid dynamics (CFD) simulations, using SolidWorks Flow Simulation was completed. The CFD was conducted in order to provide numerical data to support the final design choice. While 3-D CFD simulations offer more realistic analysis for the front wing package—modeling aerodynamic effects such as upwash, tire rotation, and 3-D flow—the simulations were found to be too time consuming, hardware intensive, and outside the scope of the project. 2-D simulations are idealized case-studies and recognized as such that the final application of the front wing will incur downforce losses and drag gain from the estimations calculated in this phase. Dr. Ryan Paul and Dr. Andy Arena of the Oklahoma State Mechanical and Aerospace Engineering Department were critical in the knowledge acquisition of CFD for the phase of this project.

Figure 2.1.3 – 2-D SolidWorks Travel-Refined Velocity Plot

A SolidWorks assembly consisting of wing elements, in their proper wing geometry, and a "floor" at a designed height above the ground was modeled to conduct the simulations. To test both one and two active elements, configurations were made with one static element and one active element and another with one static and two active elements. Depending on the study being analyzed, the corresponding configuration would be used. The end goal of the CFD studies ran were to analyze the drag, downforce, and torque of each element at various element deflection angles in a 2-dimensional area with a defined thickness ($1/100^{th}$ of an inch thick). These results would be used to estimate finite values for those parameters based on the length of each element to develop a basis to compare the configurations.

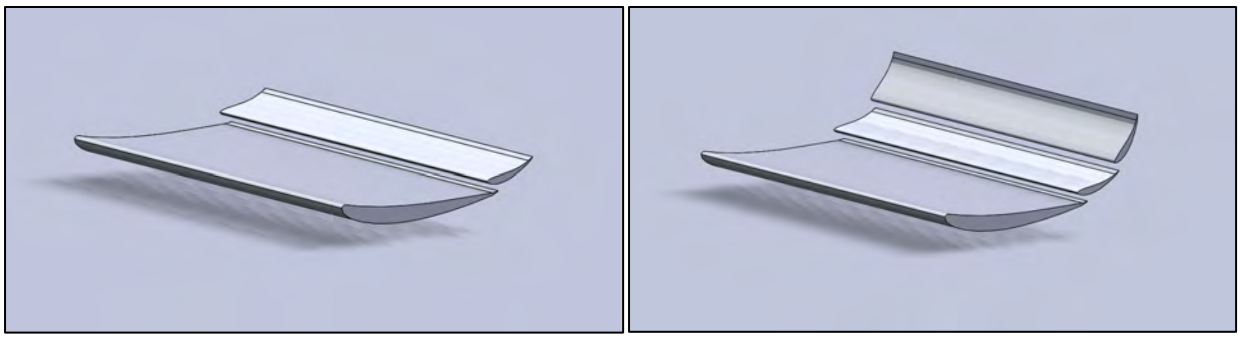

Figure 2.1.4 – SolidWorks CFD Assembly (One Active Element v. Two Active Elements)

A defined approach was taken in order to analyze the performance of each wing configuration at various deflection angles. For the one active element configuration, a separate study was ran deflecting the active element from 0-90 degrees, at intervals of 5 degrees per experiment. This resulted in fifteen studies for the one active element wing.

For the two-active element wing configuration, in order to calculate the drag, downforce and torque of each deflection angle configuration, studies were run that iterated through the second active element deflections from 0-90 degrees (at intervals of 5 degrees) at a set deflection angle for the 2nd element. From there, the second active element angle would be increased by an interval of 5 degrees and the process would be repeated.

To fully analyze the deflection values for the two active element system, almost four hundred separate CFD studies would have had to be set up. Due to the limited time constraint of the critical design phase and resources available to the team at the time of design, a little over a hundred CFD studies were ran. On average, each experiment took an estimated 8-10 hours per experiment to complete. With these points in mind, an engineering judgement decision was made to focus experiment efforts on the 0-20 first active element deflection range for the two-active element wing configuration to be able to find the optimal element deflections for the maximum and minimum downforce and drag. It was determined that reasonable data trends could be assumed for any first element deflection angles past 20 degrees and the necessary conclusions could be reached based on the data available.

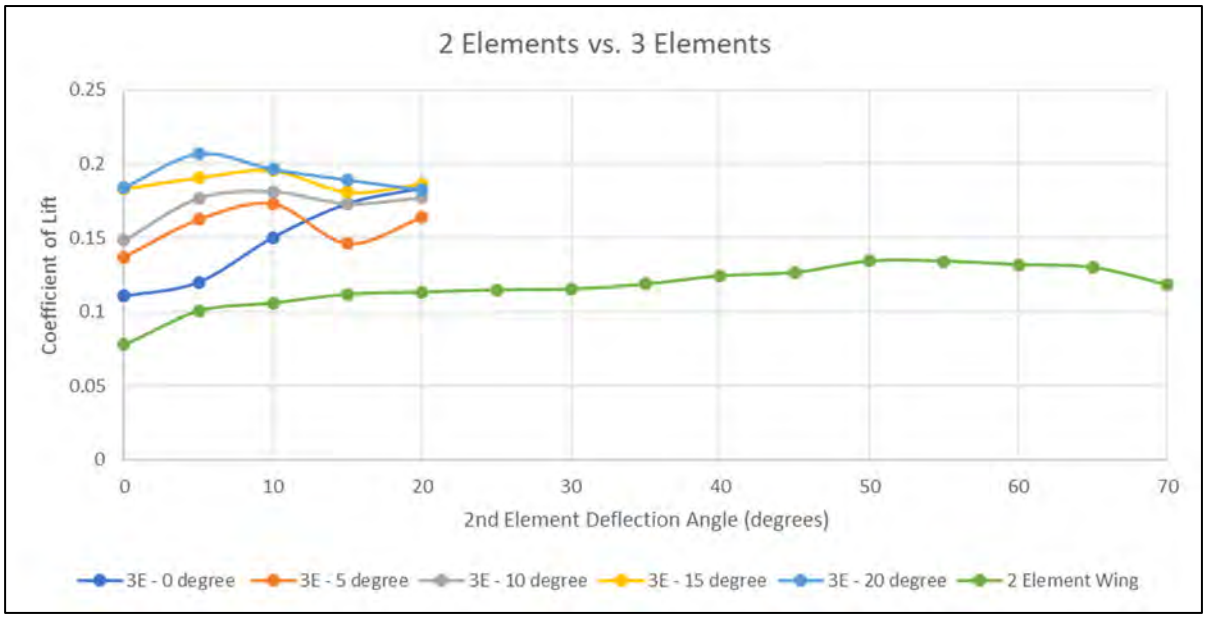

Figure 2.1.5– Coefficient of Lift v. First Active Element Deflection (Comparing One Active Element [2E] With Two Active Elements [3E])

From the data, coefficients of lifts were derived in order to serve as a metric to analyze the performance for both sets of wings and compare them directly to each other. A coefficient of lift is a dimensionless coefficient that relates lift from a lifting body to its surrounding fluid, which for all simulations was standard air at a freestream velocity of 66mph. As seen in the plot above, across a second (second wing referring to the first active element for both configurations) element deflection angle range of 0-20 degrees, there was over a 50% increase in coefficient of lift from two total elements to three elements, which justified the design decision of choosing two active wing elements over one active element. It should be noted that the two active element wing only displays data from a first active element deflection range of 0-20 degrees due to the computational reasons mentioned previously.

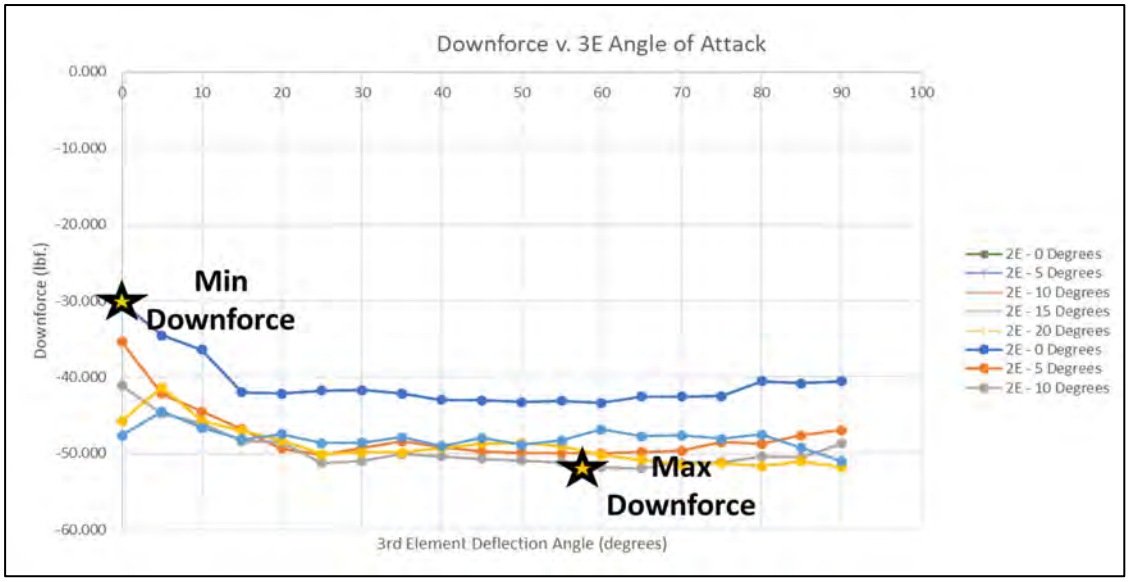

Figure 2.1.6– Downforce v. Second Active Element (3rd Element) Deflection Angle

The maximum downforce was found to be 51.6lbf. at a first active element deflection of 10 degrees and a second element deflection of 58 degrees. The configuration that produced the least down force was at 0-degree deflection for both the active flap elements and made only 30.2lbf of downforce.

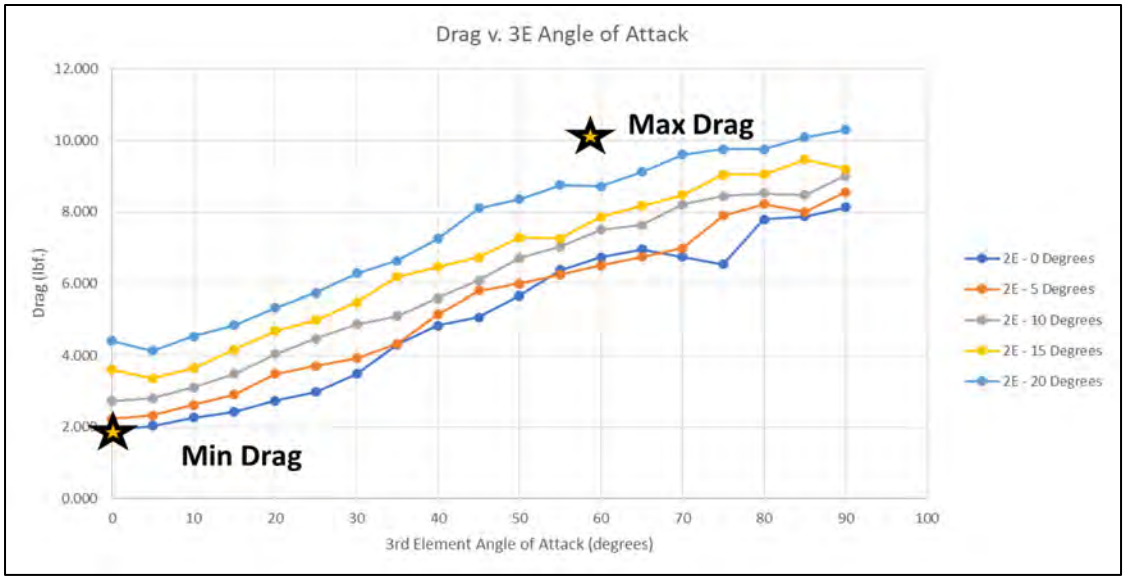

Figure 2.1.7– Drag v. Second Active Element (3rd Element) Deflection Angle

The total wing package produces a maximum drag of 10.7lbf. at a first active element deflection of 30 degrees, and a second element deflection of 58 degrees. For maximum drag, a single point study was conducted outside the range of the three-element total study to calculate the finite

amount of drag produced by the assumed maximum drag deflection configuration. This configuration was selected based on the farthest possible physical deflection angle constraints for both flap elements based on the maximum constraints set by the mechanical actuation system. The deflections that produced the least downforce, the front wing's minimum drag configuration, occurs at 0 degrees deflection for both flap elements producing only 1.9lbf of drag.

The minimum and maximum values for downforce and drag are marked as key points from the data collected because of the measured aerodynamic effects as a result of the active element deflection angles in question. A maximum drag deflection configuration was found for the purpose of "air-braking", allowing the front wing kit to use maximum available drag, and downforce, to assist the driver with the car's braking. The minimum and maximum downforce deflections are important to the front wing package for cornering; as maximum downforce is preferred on the inside wheel of the corner; minimum downforce is preferred on the outside wheel to provide additional tire grip and to mitigate the effects of body roll in the turn.

2.1.3 Wing Material Selection

The material selected for all 3 elements is 3k, 2x2 twill weave carbon fiber. Listed below are reasons carbon fiber is the proper material as opposed to fiberglass.

1. Double the strength to weight ratio
2. Tensile modulus is four times greater
3. Weighs 15% less than fiberglass composites

The carbon fiber that will be used has a tow rating of 3k. Tow rating of a specific carbon fiber defines the number of threads that will be used to weave the fabric. In this case, the chosen fabric has three thousand fibers in each thread. Each thread is contained within an eighth of an inch meaning there are three thousand carbon fibers used per every eighth inch. Other available tow ratings include 6k and 12k, however, with doubling the number of fibers, the weight is close to double as well. Collin Boettcher at the CEAT Design and Manufacturing Lab advised the team on this tow rating because it would provide sufficient strength for the loads that the front wing will be experiencing.

Figure 2.1.8 – 45 Degree Layer Offset Visualization

The threads will then weave in a 2 x 2 pattern, which means two threads going over two threads, and then under two threads to create the woven fabric. This 2 x 2 pattern allows for good formability and stability while laying up the part. Other available patterns include 1 x 1 or 4 x 4.

The carbon fiber fabric will be laid in such a way so that there will be a 45-degree offset between the stacked layers. For example, the fabric on the bottom would be oriented at 90 degrees and the

fabric laid on top would be oriented at 45 degrees. An example of this method of composite layup can be seen in Figure 2.1.8. The reason for the angle offset is to provide constant strength and stiffness of the material regardless of the direction in which it is loaded.

Finally, to reinforce the static main element and increase its rigidity, a Nomex honeycomb core will be embedded between two layers of carbon fiber.

2.1.4 Composites Layup Knowledge Acquisition

Knowledge acquisition for composites materials came from OSU Speedfest's Capstone composites layup training. Using the manufacturing processes learned, practice parts were made for testing purposes and hands-on learning experiences. The aerodynamics sub-team then manufactured sample wing elements utilizing pre-existing wing molds the Oklahoma State University Formula SAE team had already developed. The samples tested were 5in. by 5in. square pieces, also known as coupons, with varying thicknesses and cores materials. The samples to be tested are discussed further in more detail in Section 3.

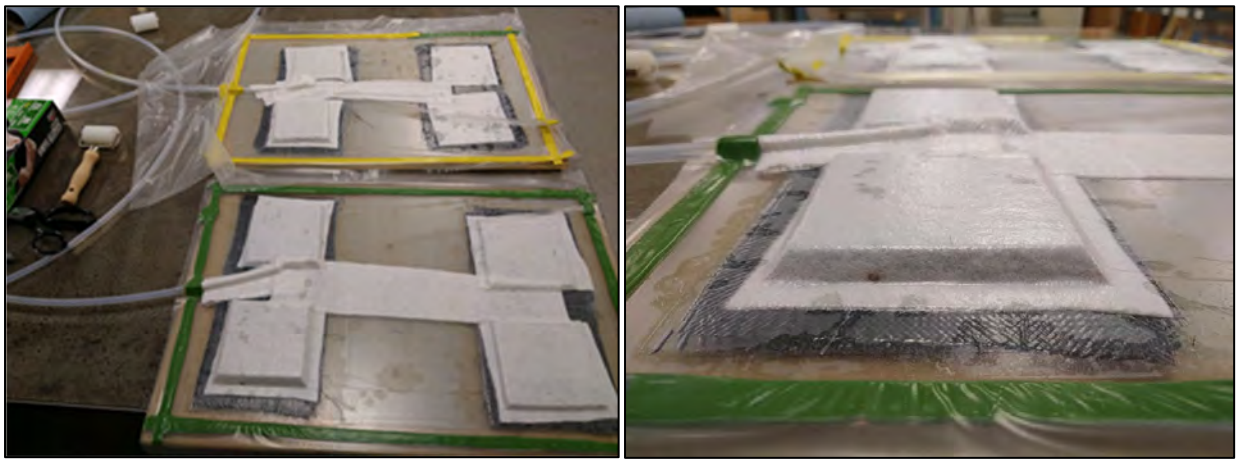

Figure 2.1.9 – Testing Samples (Left: Multiple Coupons Undergoing Vacuum, Right: Testing Coupon with Foam Core)

2.1.5 Manufacturing Plugs and Wing Element Molds

In order to manufacture wing elements correctly and efficiently, negative molds are required to lay the carbon fiber fabric down first on the "outside" face of the final part. To create a negative mold, a positive piece called a plug must be manufactured first. Before designing the plugs for the wing elements, time was spent practicing laying up carbon fiber on existing wing molds, and this revealed some changes that needed to be made in the new plugs and consequently, the molds. The new plugs were sized to be much longer than the actual wing elements with wider flanges on both the leading and trailing edges. This allows the team to create better quality parts using more efficient layup techniques.

Plug designs of the wing elements were created using SolidWorks where the airfoil shape was split in half using the element's trailing edge as the cutting line. This allows for a top half and bottom half positive plug to be made for the different airfoils used. After designing the wing plug, the aerodynamic team operated a Multicam 3000 CNC router at Oklahoma State's Design and Manufacturing Lab to machine high density, 20lb tooling foam board into the design of the plug. The bottom half positive plug is shown below in Figure 2.1.10. The foam board used is dense but still a manipulative material allowing for easy cutting and sanding into a part ready for fiberglass.

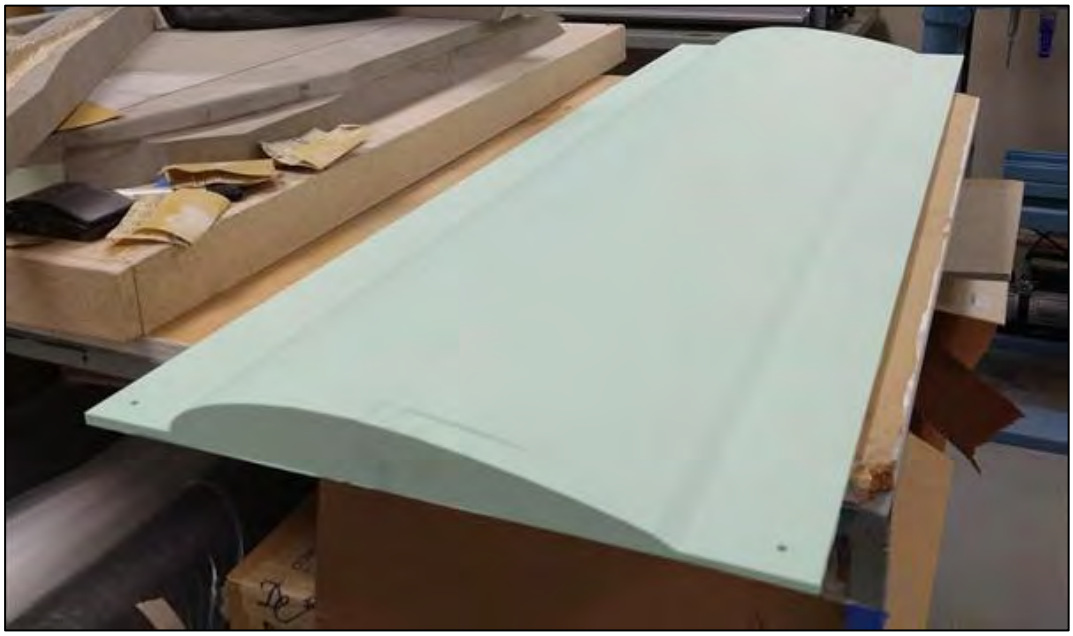

Figure 2.1.10 – Main Wing Bottom Half Plug

After the plug's surface is sanded smooth and all dust is removed, three coats of primer are put down, and the sanding process is repeated. Four wooden medium-density fiberboard (MDF) boards, also layered with three coats of primer and sanded, are screwed together and boarded to create walls surrounding the foam positive. After ensuring there are no cracks between the foam and the board, any of which are filled with filling plaster or clay, the end product is prepared with three preparation layers of wax and three layers of mold releasing agent for the layup.

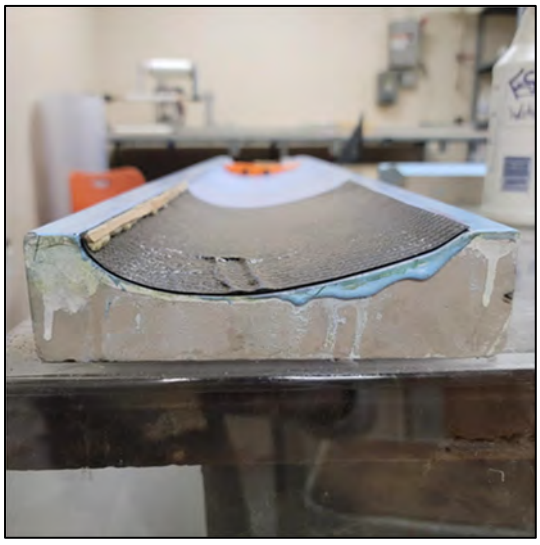

Figure 2.1.11 – Negative Mold Example with Carbon Fiber Wing Half

After the mold release has dried fully, two thick coats of tooling coat are applied to the inside walls and positive foam mold surface. Once the second coat is tacky, thirteen layers of fiberglass in addition to enough

epoxy to saturate it completely is laid up onto all of the inside surfaces in order to create the fiberglass negative mold. Once the process is complete and the mold has cured, the boards and positive foam piece are removed, and the negative mold is complete.

Figure 2.1.11 shows an existing negative mold used for layup practice. This figure also shows a trimmed and cured carbon fiber wing halve that depicts how the fabric sits in the mold. The outside face of a negative mold is sanded to a smooth, glass-like finish in order to have the outside face of the part be smooth with no physical disturbances on the surface that could negatively affect the airflow over and around the wing. The negative molds themselves were manufactured with fiberglass, which required them to be laid up in a similar process to that of a carbon fiber part.

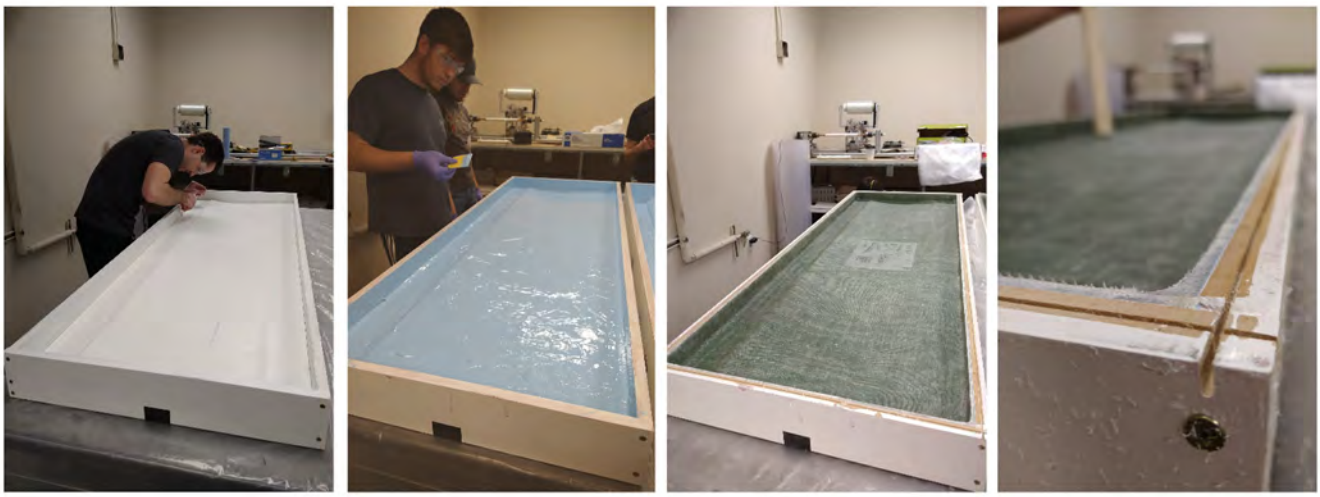

Figure 2.1.12 – Mold Making Process

The figure above is a visual overview of each major phase of the mold making process, involving the positive mold preparation, tooling coat application, fiberglass laying, and negative mold post-processing.

The steps for the positive mold preparation are as follows:

1. Sand tooling foam wing half plug up to 400 grit sandpaper (starting from 320)
2. Apply three layers of white paint primer
3. Sand the top layer of primer up to 1000 grit sandpaper (starting from 400)
4. Assemble the MDF board borders around the positive mold
5. Fill any cracks between the MDF board borders and the positive mold with modeling clay
6. Apply three layers of parting wax (removing the previous layer of wax before applying the next)
7. Apply three layers of PVA mold release spray, brushing enough PVA to cover all surfaces coming in contact with tooling coat in a thin layer (waiting roughly 20-30 minutes between each coat to allow the applied layer to dry)

The steps to apply tool coat are as follows:

1. Mix enough tooling coat to allow the MDF wall and positive plug surfaces to have a semi-thick layer of tooling coat
2. Mix thoroughly and pour newly mixed tooling coat into another mixing cup (WITHOUT scraping the sides of the cup)
3. Pour tooling coat onto the aforementioned surfaces, spreading using Bondo plastic putty knives until the poured coat is even across all surfaces (the working time with tooling coat is only ~15 minutes so this step will need to be done within that time period)
4. Pop any air bubbles that begin to develop across the coat for the next 15-20 minutes using a toothpick or sharp disposable tool\
5. Wait for the tooling coat layer to reach a "tacky" state (a member should be able to gently lay their finger on the coat, leave a print, and not pull up any tooling coat upon removal of the finger)
6. Repeat steps 1-5 to apply an additional coat, totaling two coats of tooling coat for each mold.

The steps for the fiberglass laying are as follows:

1. Pre-cut all layers of fiberglass needed for the part
2. Allow the fabric to overhang at least 1 inch over the sides
3. Prepare a properly-ratioed large batch of epoxy
4. Pre-saturate the first layer of fiberglass with epoxy on a large, covered surface
5. Lay the first layer of fiberglass onto the "tacky" toolcoat
6. Ensure that all critical areas of the mold, such as the corners and wing element surfaces are all properly covered with fiberglass with no trapped air pockets or delamination of the pre-saturated fiberglass layer
7. Lay twelve more layers of fiberglass over the first, adhering to step 6
8. Upon completion of the layup, allow the mold to cure for at least 24 hours from the laying of the last layer before moving on to the post processing stage.

The steps for post-processing the mold are as follows:

1. Use a hand-held circular saw to cut off the overhanging fiberglass (adjust the blade so that it cuts <0.25 inches into the MDF board), cutting down the middle of the MDF until the borders are removed
2. Use a hand-held router (rolling the guide bearing along the MDF exposed by cutting the overhanging fiberglass) to face off the remaining excess fiberglass so that the edge of the fiberglass mold is level with the rest of the MDF border wall
    a. NOTE: Steps 1 & 2 must be conducted with the proper PPE: Long-sleeved shirts, N95 masks, face shields
3. Remove the screws that hold the MDF border walls in place
4. Remove the MDF border walls
5. Wet sand the top flanges and wing element surfaces of the mold up to 1500 grit sandpaper (starting from 320)
6. Wipe off all residual debris
7. Mold is complete!

2.1.6 Manufacturing Carbon Fiber Parts

Once fiberglass molds have been correctly manufactured, the carbon-fiber layup process can begin. This process includes preparation of the mold, cutting carbon fiber, mixing epoxy, and laying all of the layers correctly. The preparation of the mold is the same process as is detailed in the previous section, with three layers of wax and three layers of release applied within the taped-off section of the mold. The carbon fiber should be sized larger than the necessary part, and the shape of the mold should be taken into account when measuring to make sure there is enough material to go around. After all the carbon fiber pieces necessary, those oriented at 90 degrees as well as those oriented at 45 degrees, have been cut using power trimmers, they should all be weighed on a scale. This total weight will be used to decide how much epoxy needs to be mixed for a given layup, using the chart seen in Figure 2.1.13. Once the mold is prepared, all carbon fiber layers are cut, and all epoxy is mixed, the laying up can begin. This process entails a beginning coat of epoxy directly on the mold, followed by laying each layer of carbon fiber and making sure that it is saturated with epoxy. This includes a layer of core material, if necessary, although it will not need to be saturated with epoxy. After all layers are placed and saturated, the tape must be replaced with chromate putty, and perforated plastic and breather fabric must be laid on top of the part. Lastly, the part must be put under a vacuum seal by laying a layer of plastic down onto the chromate putty, with a hose or medallion inside to connect to the vacuum hose. This vacuum hose must go undisturbed for 24 hours while the epoxy cures, then the part will be ready to take out of the mold and post-processed.

70 MIN EPOXY MIXING QUANTITIES

Weight after adding 400 resin 400 (Clear Resin)	Final weight in cup 215 (Yellow Hardener)
10	14
20	28
30	42
40	56
50	70
60	84
70	98
80	112
90	126
100	140
120	168
140	196
160	224
180	252
200	280
250	350
300	420
350	490
400	560
450	630
500	700
550	770
600	840
650	910

Figure 2.1.13: Epoxy Ratio Chart

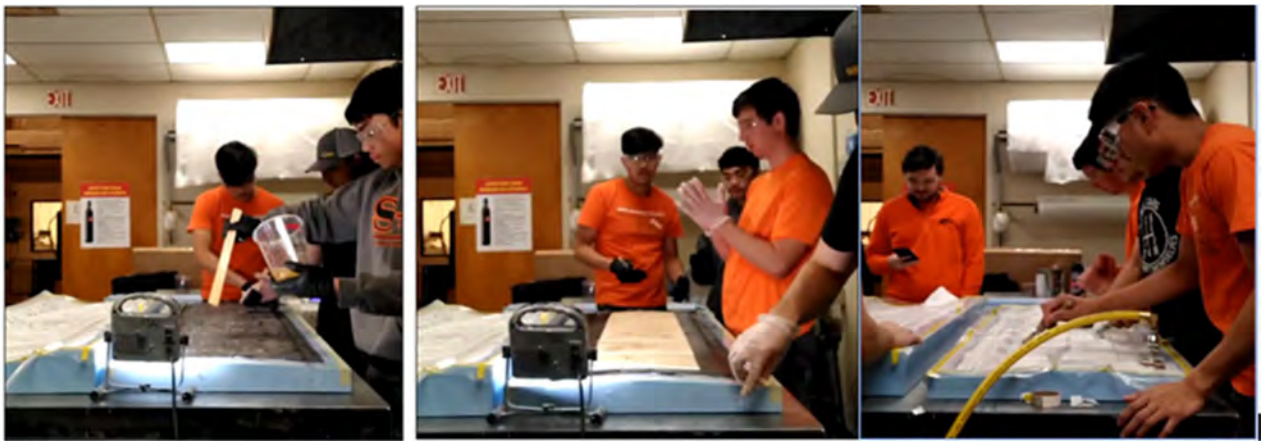

Figure 2.1.14: Carbon Fiber Layup Process

The steps for mold preparation are as follows:

1. Tape around the edges of the mold surface.
2. Apply three layers of wax to the mold surface, removing each layer with a clean towel in between.
3. Apply three layers of PVA release to the surface, allowing for each layer to fully dry in between. A layer should fully dry in approximately 20-30 minutes.

The steps for laying carbon fiber are as follows:

1. Cut as many layers of carbon fiber as needed, including both 90-degree and 45-degree orientations, and ensuring that there is at least an inch of extra material in every direction.
2. Weigh all carbon fiber layers on a scale to decide how much epoxy to mix.
3. Mix the correct ratio of epoxy elements and stir thoroughly.
4. Cover the mold surface with an initial layer of epoxy.
5. Lay down a layer of carbon fiber onto the mold, tapping lightly to ensure that the fabric becomes saturated with epoxy without disturbing the weave.
6. Add each subsequent layer of carbon fiber, adding epoxy onto each one and tapping to ensure saturation. If necessary, add a layer of core material when half of the layers are laid onto the mold.
7. After all layers are saturated, add a piece of perforated plastic that extends to the inside edges of the tape.
8. Add a layer of breather fabric that extends to the outside edges of the carbon fiber layers.
9. Add extra breather fabric around the hose or medallion end.
10. Pull up the tape and replace with chromate putty tape (if using a hose add a ring of chromate around it as well, at the spot where it will cross the border of chromate putty).
11. Add plastic bagging over the entire mold, using rollers to push it firmly onto the chromate border (and the chromate on the hose if necessary).
12. Plug in the vacuum and check to make sure there are no air leaks in the plastic bagging (roll more or add more chromate if necessary). Let cure for 24 hours.

The flaps for the wing are two layers thick with no core and only 3D printed ribs at the ends. The top and bottom halves are four layers thick with 5-pound core in the middle (layup order 90, 45, core, 45, 90) with sections of the layup without core for rib placement. A schematic of this is shown below.

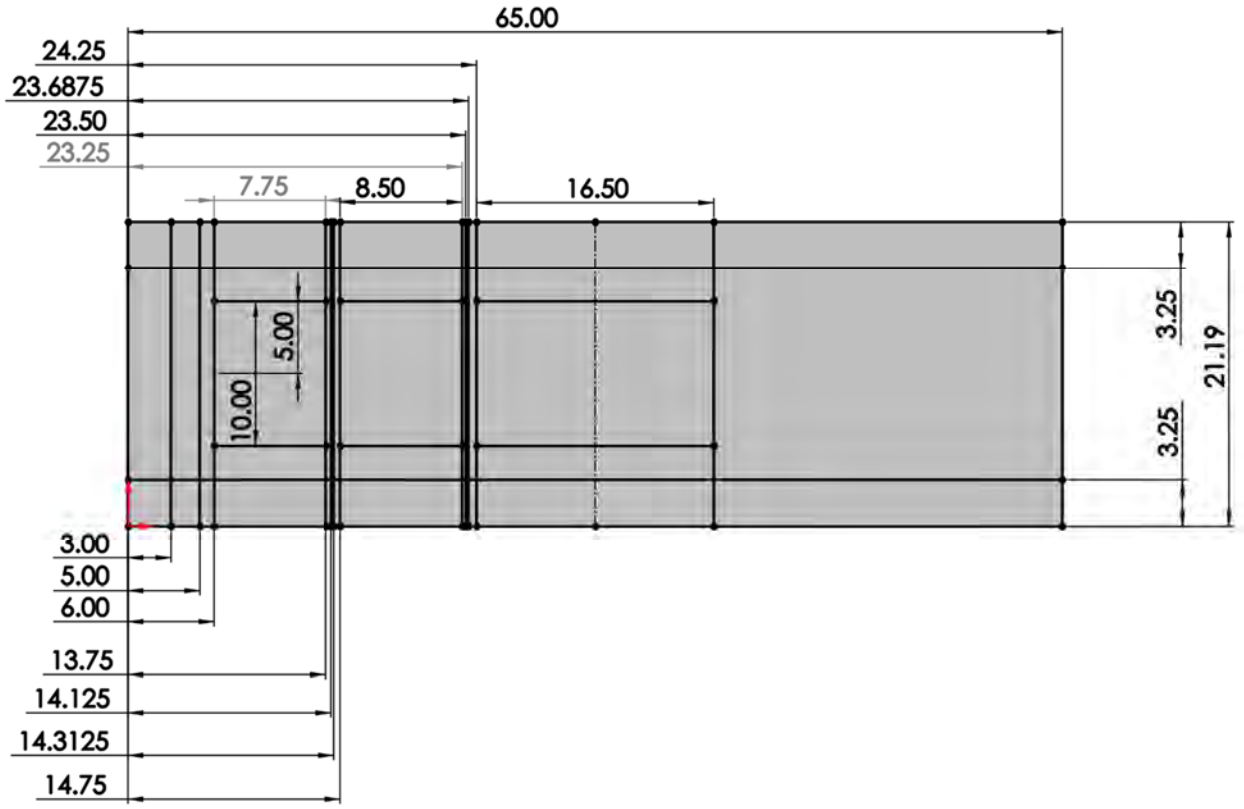

Figure 2.1.15: Main Element Schematic

The vertical lines from left to right, units in inches: beginning of mold, beginning of carbon fiber, beginning of part, beginning of outboard core, end of outboard core, beginning of first rib, end of first rib, beginning of inboard core, end of inboard core, beginning of second rib, end of second rib, beginning of middle core, mid-point of wing, end of middle core, end of mold. The left and right sides are mirrors of each other.

The horizontal lines from bottom to top, units in inches: beginning of mold, end of flange/beginning of part, beginning of core, end of core, end of part, end of mold. The core is centered in the layup between the leading and trailing edges. This schematic is also drawn out on the molds themselves.

The internal ribs are made of four-layer carbon fiber with 5-pound core in the middle CNC'd from a flat plate, like the endplates. The ribs which cap off the wing are 3D printed PLA+. The main structural design change suggested for the competition team would be to add a flat plate 4-layer with core spar in the main element to decrease twisting and bending. It is important for the spar to be one continuous piece the span of the wing, so a rectangular cutout on both the ribs and spar would be necessary for them to mate together in a puzzle piece-like fashion.

Post-processing steps are as follows:

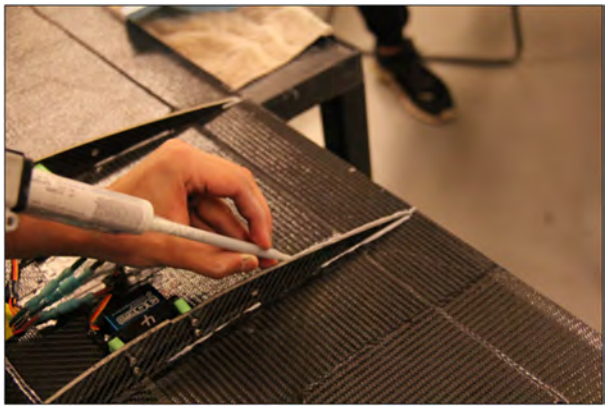

Figure 2.1.15: Adding Bonding Epoxy

1. Pull the carbon fiber part from the mold, applying water to the PVA release if necessary.
2. Use a Dremel to cut the part down to nearly the correct size, leaving about 1/8”-1/4” of margin in every direction.
3. Use sandpaper to make “fine-tuning” adjustments, making the part the exactly correct size.
4. If parts need to be bonded together, lightly scuff each surface of contact
5. Lay a bead of high strength epoxy on one part, in every area that will contact the other part. (If two knife edges must be bonded together, toothpicks or popsicle sticks can be glued to the inside of the part to allow for easier laying of epoxy beads).
6. Clamp the two parts together and turn them over, so that the part which has the bonding epoxy on it is on top. (This can sometimes be done by taping both parts into their mold with double-back tape, then clamping the molds together).
7. Let cure for 24 hours.

2.2 Wing Mount and Motion

2.2.1 Bolt Pattern Conversion Plates

To enable the current car, Bullet Racing’s 20.5 (BR20.5), for the implementation of a front wing, the vehicles ride height must be addressed as it is 1.25 in. This height is not enough for the current car with additional aerodynamic equipment attached to it. The quick and easy solution to this problem is to purchase larger wheels and tires. This results in 3.25 in. of safe and usable space to install the wing package. While this solves one problem, it introduces another. The wheel hubs on the BR20.5 car are designed for a smaller wheel using a smaller bolt pattern; to solve the bolt pattern misalignment a conversion plate has to be designed, manufactured, and installed on the hub and larger wheel simultaneously. When designing this part, finite element analysis (FEA) must be run to ensure proper tolerances and safety factors under the torques and loads the car experiences. Figure 2.2.1 shows the

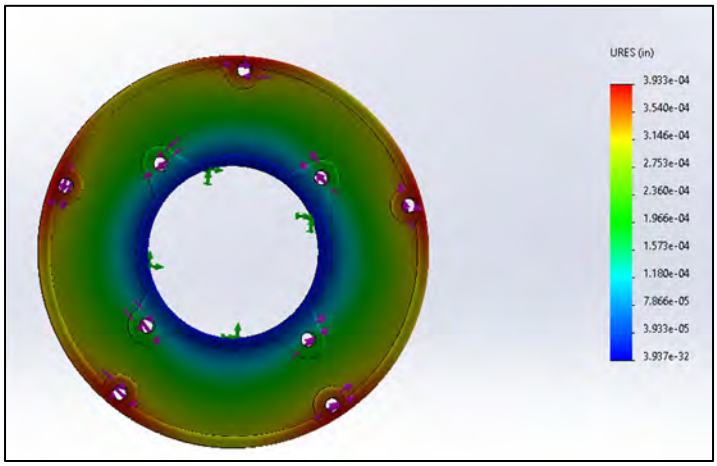

Figure 2.2.1 – FEA Analysis of version 1 Wheel Conversion Plate

displacement results of an FEA study ran on the first iteration. A three-dimensional part was printed using PLA to ensure fitment to the BR20.5's wheel hubs and larger 13 in, wheels. A second iteration was designed thereafter to remove more weight and reduce the estimated manufacturing time. To manufacture this part, first, the outside profile is water jetted out of a 0.5 in thick, 12 in x 44 in 6061 Aluminum plate at Oklahoma State's North Campus Laboratories. Material is removed from the interior circle to allow the plate to fit around the wheel hubs. Next, the plates are placed in a manual engine lathe and turned in 0.005 in. increments until the plates are trued: ensuring there is minimal to no wobbling and the plates are flat. This is needed because the aluminum plate initially used is not normally flat. Figure 2.2.2 shows final assembly installed on car. To be sure that there was no vibration developed by the wheel assembly, it was taken to Pioneer Wheel & Tire, and balanced. To safely attach each wheel, the wheel studs in the hubs had to be removed and replaced with longer wheel studs. This allowed safe attachment for each wheel.

Figure 2.2.2 – Bolt Pattern Conversion Plate

2.2.2 Endplate Design

To attach the wing kit to the chassis of the car, the team will be using specifically designed endplates. Figure 2.2.3 to the right shows the endplate naming convention. Endplates one and two are responsible for mounting and supporting the wing kit to the vehicle. On the car side, six steel tabs will be welded onto the frame rails providing strong, fixed mounting points. Due to the design of the chassis, the width of the frame where the main weight-bearing endplates will be mounted is not constant. To solve this problem, spacers were designed to fill the gap between the tabs and the carbon fiber end plates; these spacers will also double as a bushing press-fit into endplates to ensure strength. More information about the bushing-spacer configurations used are discussed in Section 3.1.1. Figure below showcases the wing kit attached to the front of the car using the welded-on tabs and spacers.

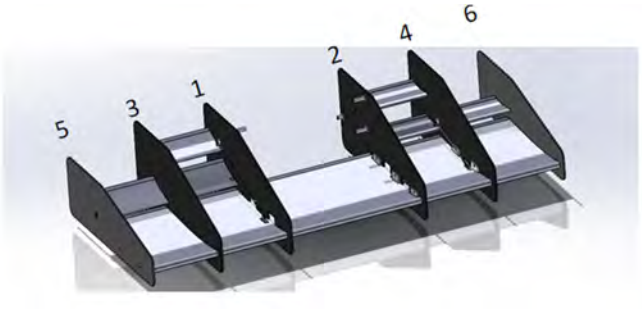

Figure 2.2.3 - Endplate Naming Convention

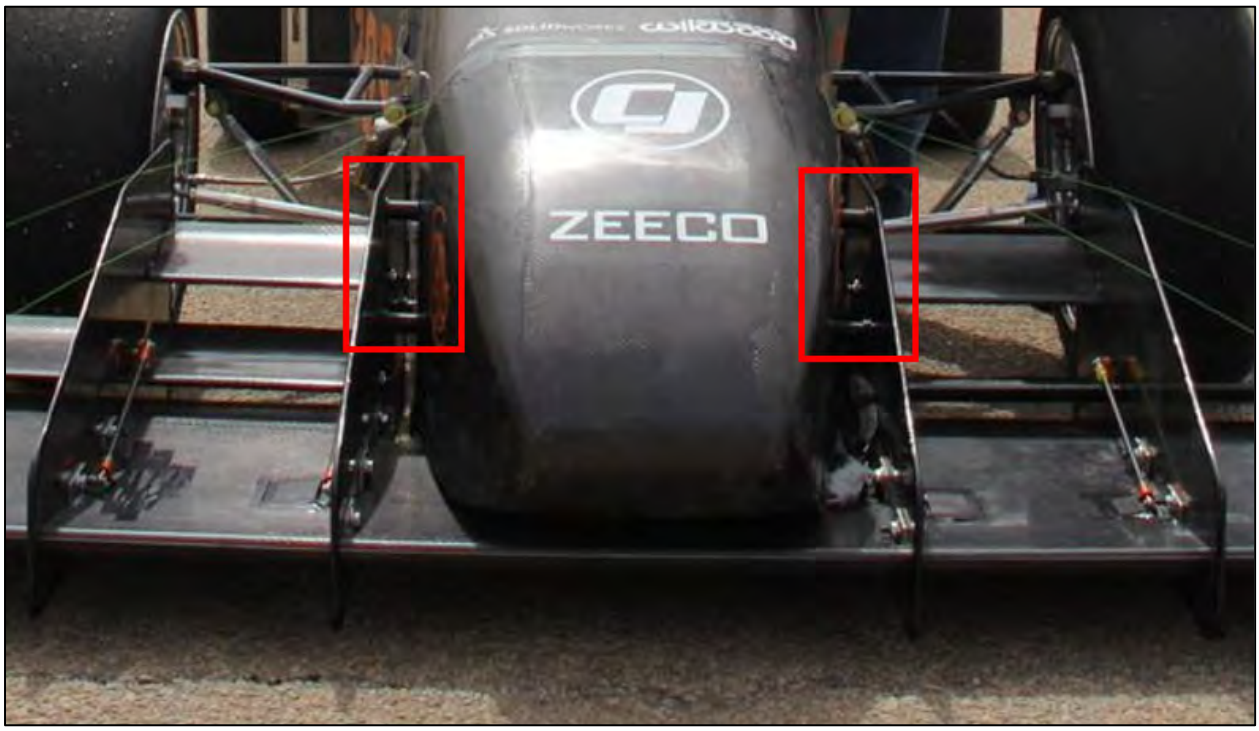

Figure 2.2.4 – Endplate to Frame Connection

Along with our main inside endplates (1,2), two more individual end plates were designed to be used at different positions throughout the wing. At location 3,4, the endplate acts as a marker between the larger (inside) and small (outside) build boxes. It has the same form and application method as end plate 1,2, however it will not be experiencing the loading that endplates 1,2 will be.

The final end plates 5,6, are the caps of the main element wing. They are shorter in height and only have to support one active element. It will mount directly to the side of the main element, bolting to its outer most rib.

The endplate construction will be a carbon fiber sandwich. Each end plate will be made with a total of 4 layers of carbon fiber and an 1/8 in thick, 5 lbs. density foam core. Section 3.1 discusses the advantages and disadvantages of the different layers and core materials in further detail. All three variations of the endplate will be constructed in the same fashion with the same material. Large, square carbon fiber layups will be placed in the CNC Router and cut to the specific design for the endplate made. This allows accurate placement and precise results for the overall design and bolt locations. Endplates cut imprecisely will introduce error through misaligned pivot points and poorly assembled products. Figure 2.2.5, Figure 2.2.6, and Figure 2.2.7 show the different and unique design differences between the different endplates.

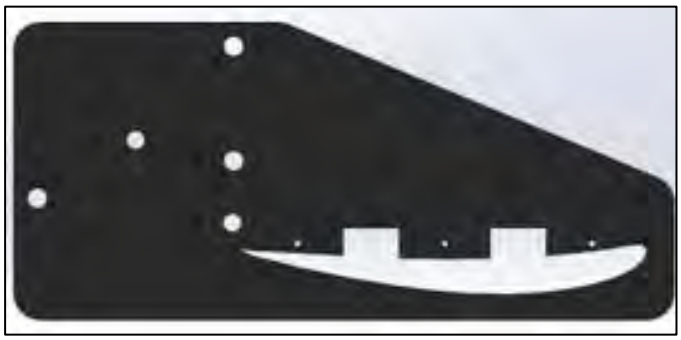

Figure 2.2.5 – Endplate Design 1,2

Figure 2.2.6 – Endplate Design 3,4

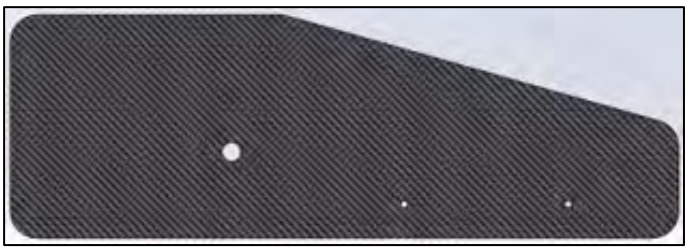

Figure 2.2.7 – Endplate Design 5,6

2.2.3 Rib Design

To secure the static main element to the endplates, 6 different ribs with 3 different designs will be used. Following the naming convention of the endplates, ribs 1,2 will have 3 attachments to the endplates along with holes allowing a servo to be mounted in the main element that will allow the active elements to be actuated. The next set of ribs, 3 and 4, will have 2 mounting points that will attach to the endplates, this rib will also have holes allowing a servo to be mounted. The outermost ribs, 5 and 6, will have 2 holes allowing the outermost endplate to be bolted on to the rib. Ribs 1,2,3 and 4 will all be made of 4 layers of carbon fiber with a 5-pound density core. This design will offer enough strength to support the main element based on material testing covered in Section 3.1 later. The outermost ribs, 5 and 6, will be 3-D printed to allow for more surface area while being bonded with the carbon fiber. Figure 2.2.8, Figure 2.2.9, and Figure 2.2.10 below shows the different designs for the ribs used in the main static element.

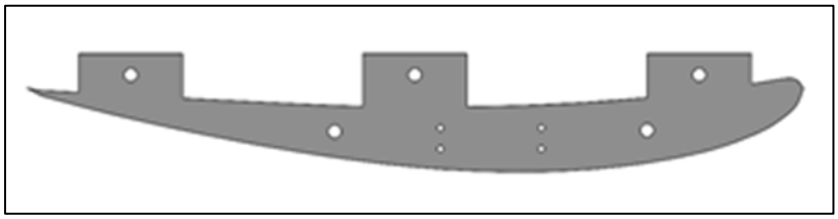

Figure 2.2.8 – Rib Design 1,2

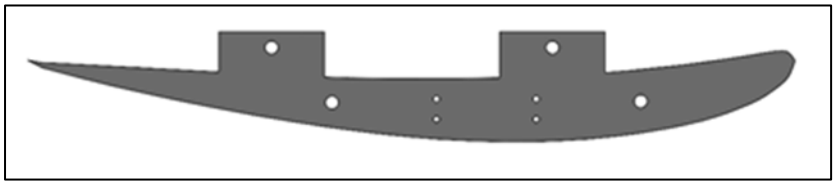

Figure 2.2.9 – Rib Design 3,4

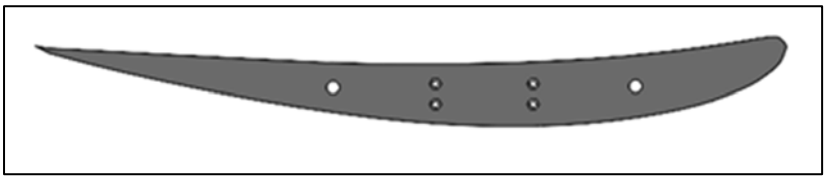

Figure 2.2.10 – Rib Design 5,6

The active ribs designs can be seen in Figure 2.2.11, Figure 2.2.12, Figure 2.2.13, and Figure 2.2.14 below. To allow for actuation, a tower lever arm in line with the pivot point is inserted onto the ribs. The towers are place on the inside of endplates 3 and 4 for element 2 and on endplates 1 and 2 for element 3. The rib design for the active element with the tower has one hole in the middle of the airfoil that will be used to connect the active elements to the bearings in the endplates. To couple the 2 elements together at endplates 3 and 4, the ribs shown in Figure 2.2.15 and Figure 2.2.14 will be used. These ribs are designed to hold a D-pin that will force element 2 to have the

same angle on both sides of endplates 3 and 4. All the active ribs will be 3-D printed to allow for maximum surface area while bonding with the carbon fiber.

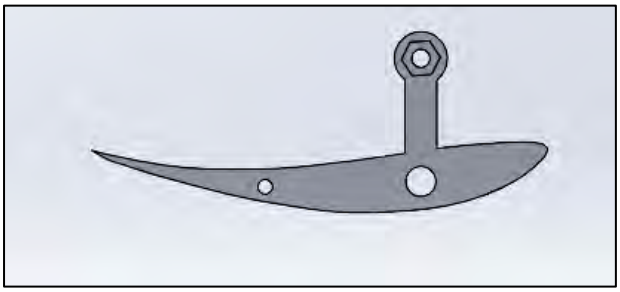

Figure 2.2.16 - Rib Design Active Element with Tower

Figure 2.2.17 – Rib Design Active Element

Figure 2.2.18 – Rib Design Active Element with D-Pin

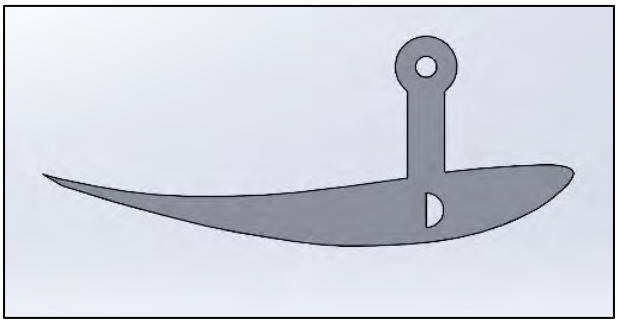

Figure 2.2.19 – Rib Design Active Element with D-Pin and Tower

2.2.4 Linkage Design

The first linkage design concept in Figure 2.2.20 contains M4 ball joints connected with servo arms by threaded rods. A double servo arm creates a push-pull effect between the 35kg servo and the active elements. Threaded rods provide some adjustability in fine-tuning the exact lengths and

tension along the setup. Servo arms with multiple ball joint mounting locations could give the design some added flexibility during the assembly and testing process.

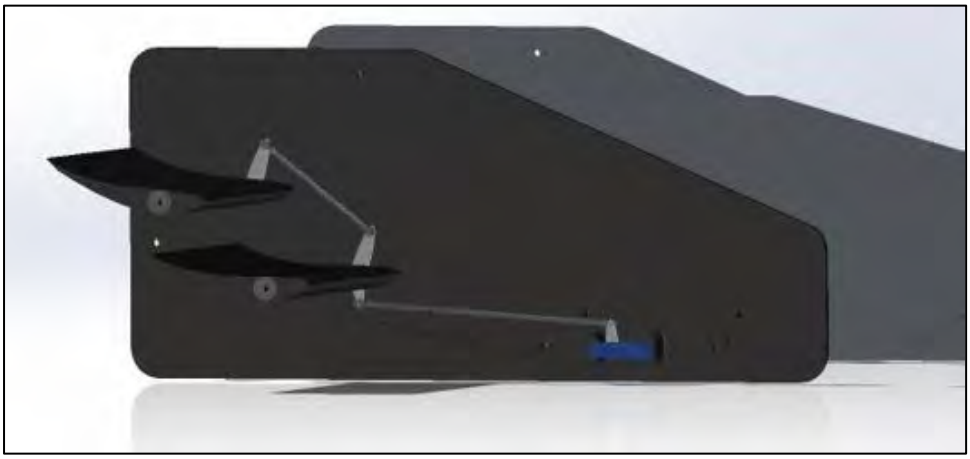

Figure 2.2.21 – Linkage Design Concept 1

The second linkage design concept in Figure 2.2.22 contains M4 ball joints connected with carbon fiber rods glued into place to actuate the wing elements. Individual servo motors, the same used in the first linkage design, actuate the different elements that allow for more precise control and prevent any chance of servo motor burnout. These 35kg motors will be placed on mounts built into the ribs 1, 2, 5 and 6 and holes will be cut to allow proper actuation.

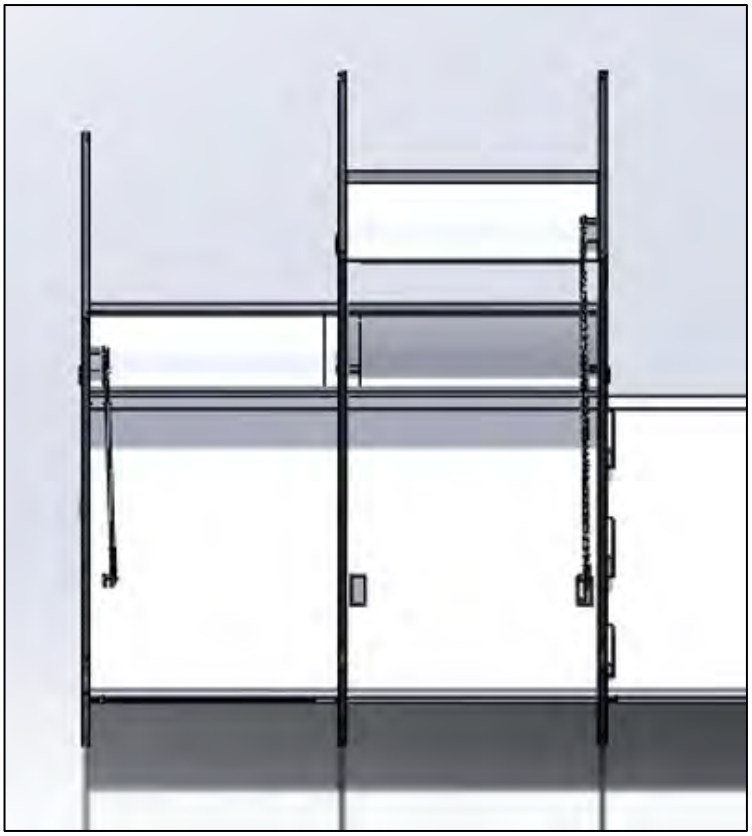

Figure 2.2.23 – Linkage Design Concept 2

The third linkage design concept in Figure 2.2.24 has a similar design as concept 2 containing M4 ball joints, a 35kg servo motors, and carbon fiber rods to actuate the wing elements. However, the key difference between concepts two and three is the placement of the 35kg servo motors. The outermost servo motors have been relocated to ribs 3 and 4, to prevent any unusual twisting in active elements 2 during usage while the innermost motors stay in the same position.

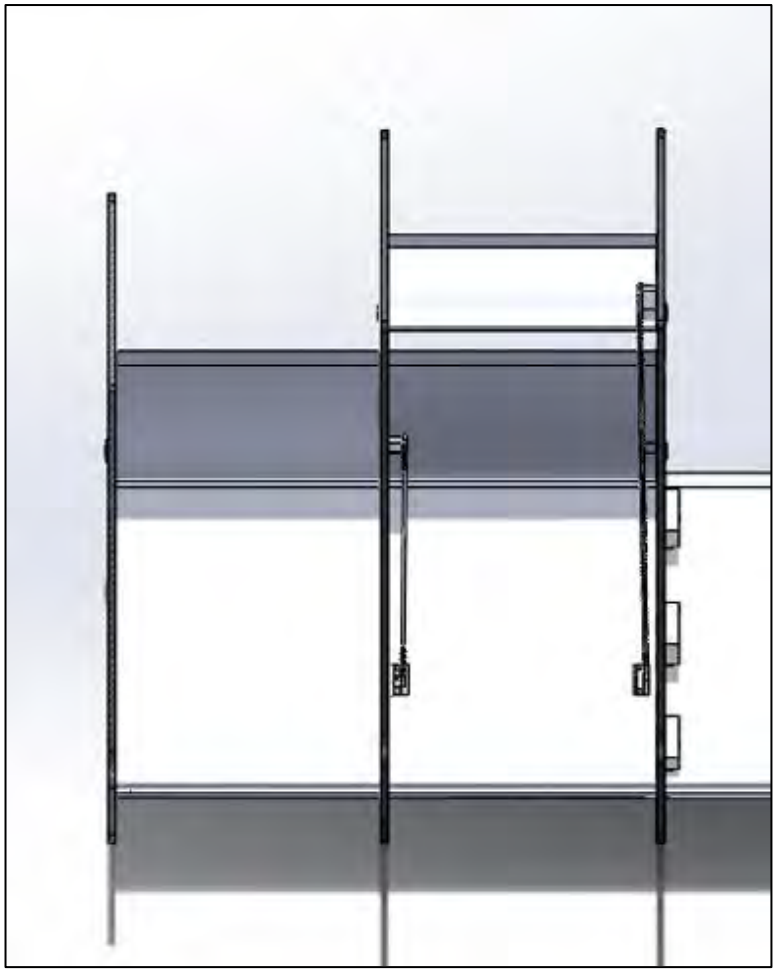

Figure 2.2.25 – Linkage Design Concept 3

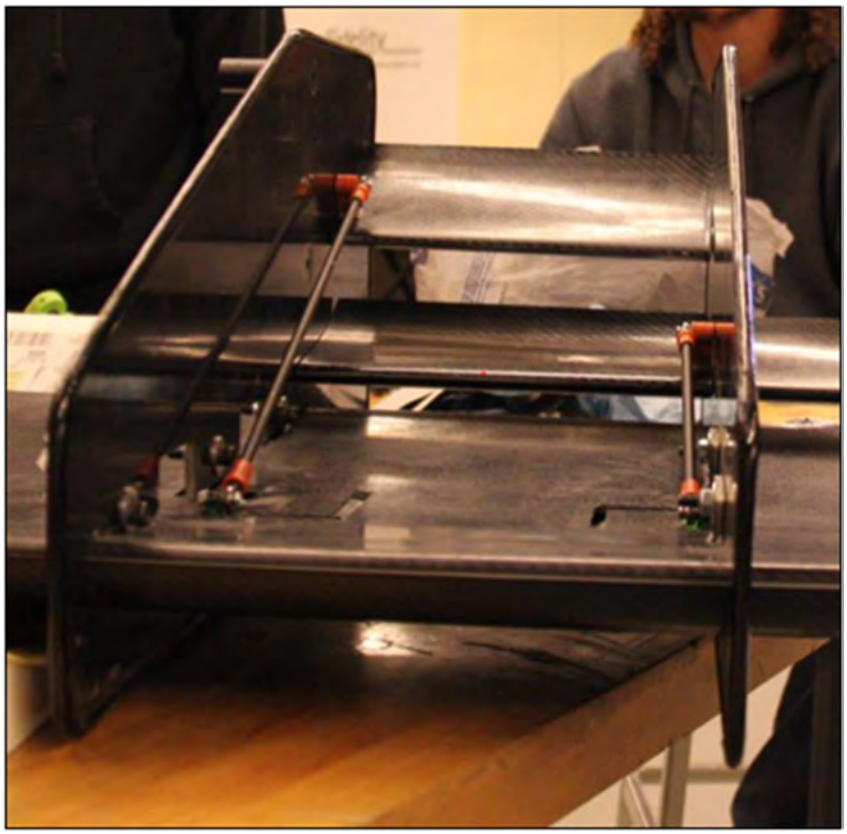

Figure 2.2.26– Linkage Design Final

2.2.5 Tab Nuts and Carbon Couplers

To securely attach the wing to the car at the 6 mounting points on Endplates 1 and 2, six individual tabs had to be welded onto the frame. When the wing was initially attached to the vehicle, it was held on by standard nuts on the backside of the tabs, but this became a problem as soon as the nose had to be put on. To put the current nose on the car, it had to go on before the wing since the bushings would block it from sliding into place. This meant that there had to be a permanent fastener attached to the backside of the tabs. The first iteration of permanent fastener was with a rivet nut, commonly known as a rivnut. This seemed like an easy fix but because the tabs are very thin and the angle required to use the rivnut gun has to be exact, none of them came out the same. Upon first installation of the wing kit with the rivnuts on the tabs, the bolts began to get stuck in the rivnuts and spin in the holes. This prevented removal of the wing from the car, and thus a new solution had to be developed. The mech team's second attempt at permanent fastening was to design a nut that could be welded to the backside of the tab and have precise threads. To manufacture, a 5/8" diameter mild steel bar was CNC turned down and drilled out. After the drilling operation, it was hand threaded with ¼", 20 thread pitch, and welded to the back of the tabs. This solution solved the installation problems with the wing kit.

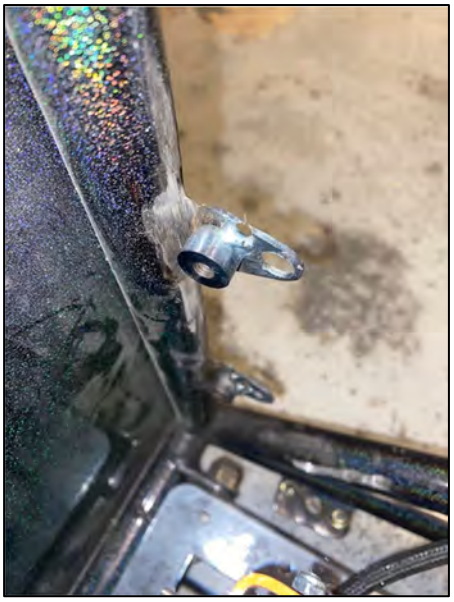

Figure 2.2.27 – Tab Nut

The most difficult part in actuation of the active element wings is to ensure that the angles determined from CFD were achieved. Since the carbon fiber rods were hollow, threadless, and too long when they were purchased, they had to be cut to the appropriate length. This was accomplished by sanding the carbon rod to a length shorter than shown in the CAD model and designing a rod coupler. The coupler ensured that the nut on the end of the carbon fiber rod was directly in the center of the rod. To manufacture the coupler, it was 3D printed out of PLA+, then painted orange. Once dry, the coupler was epoxied to the carbon rod, the surfaces of the nut that would be in contact with the coupler were sanded, and then the nut was epoxied inside the coupler. If the sanding step is skipped, the epoxy will not bond the nut to the coupler, and it will come out. After 24 hours, the rods were cured and could then have the M4 rod ends threaded into the top and bottoms. Then the total assembly was attached to the wing, and working with an angle finder, adjusted to the correct lengths for the required angles to be achieved.

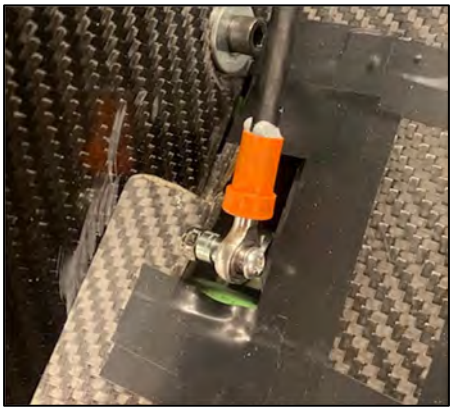

Figure 2.2.28 – 3D Printed Rod Coupler

2.3 System Control

To put the “active” in active aero, an electronic control system was developed in conjunction with the aerodynamic and mechanical subsystems. Utilizing a microcontroller, 6-axis inertial motion unit, and four servo motors, the system actively adjusts the wing element angles to provide the optimal amount of downforce throughout a turn according to two active control modes.

2.3.1 Electronic Components

The electronic system runs on 5V while the car’s battery outputs 13V, so a voltage converter located in the rear of the vehicle steps down the battery’s voltage to a useable level.

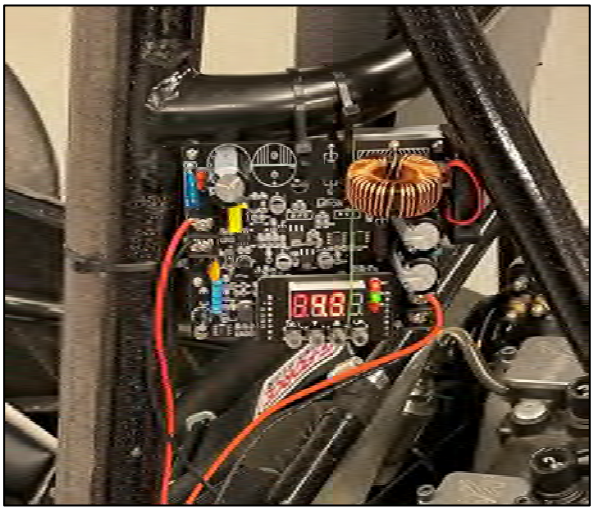

Figure 2.3.1 – DROK DC Buck Converter

For central processing, Adafruit’s ItsyBitsy M0 Express was chosen for its high performance and smaller, more vibration-resistant form factor compared to a larger Arduino or Raspberry Pi.

Figure 2.3.2 - Adafruit ItsyBitsy M0 Express development board for the Cortex M0

The ItsyBitsy M0 collects sensor data from a standard binary brake sensor as well as a GY-521 IMU with a standard MPU-6050 chip. This is perhaps the most common IMU on the market and there is an abundance of supporting documentation for it.

Figure 2.3.3 GY-521 IMU board for the MPU6050 accelerometer/gyroscope chip

The central controller uses the data from these sensors to actuate five 35kg servos, shown below in Figure 2.3.4.

Figure 2.3.4 The servo, a generic 35kg model with two torque settings.

For the system wiring, standard automotive wiring with ring connectors connecting to the PCB is used. A segment of this was tested with a simulated control signal and confirmed to reliably transmit it without significant attenuation. The control signal was simulated at 3.3V using an average PWM specifications of 1.5ms pulse width and a 20ms period. The voltage measured 2.65V, which is above the (5V) TTL $V_{Hi,In}$ level read by the servo. Heat shrink automotive quick disconnects with full insulation are used at junctions to prevent shorting to the vehicle frame.

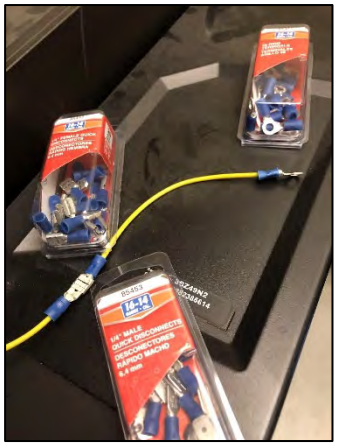

Figure 2.3.5 The sample wire along with basic versions of the automotive quick connectors.

Configuration and mode selection is accomplished using three locking toggle switches on the dash of the vehicle.

Figure 2.3.6 A locking toggle switch. The handle must be pulled to change positions.

An additional momentary switch on the steering wheel allows the driver to activate the Drag Reduction System (DRS) for the rear wing, which minimizes drag for as long as the switch is depressed. The switches on the car's dashboard along with the momentary DRS button are shown below in Figure 2.3.7.

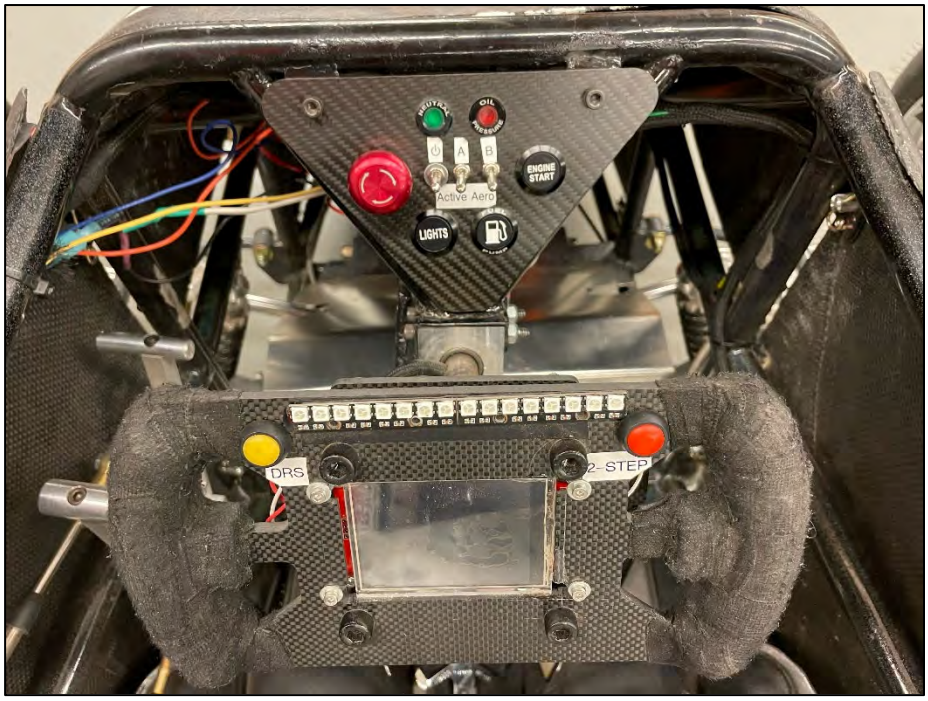

Figure 2.3.7 - Driver Control Interface

2.3.2 Custom Printed Circuit Board

A custom 4-layer printed circuit board (PCB) was designed to connect these components more efficiently and effectively than using individual wires, and the PCB also provides a platform to easily align the IMU to the primary axes of the car. All exterior connections are on ring terminals for maximum reliability in a high vibration environment.

2.3.2.1 Physical Design

Anecdotally, electrical connectors and connections coming apart is attributed as the primary driver of failure in consumer electronics. More rigorous estimates from the US Air Force find “vibration and shock cause 20 percent of the mechanical failures in airborne electronics” (Steinberg, 2000). Since our stated deliverable was intended to last beyond a senior design expo to be used by the OSU Formula SAE competition team, the design trends recommended by Steinberg were applied to the physical layout of the PCB from the earliest design phase. Without the resources to conduct a full vibration analysis of the completed vehicle, the team targeted a physically small and dense design with oversized traces. External connections were made around the perimeter using ring terminal connectors, which were soldered to the board for maximum electrical reliability and then bolted in place.

To maintain a small PCB board required using small components. The team selected an ATSAMD Cortex M0 processor mounted in an Adafruit ItsyBitsy Cortex M0 over the more typical Arduino type prototyping boards. The Cortex M0 is a 32bit processor running at 48MHz, 6 times the clock frequency of the 8 bit Arduino Uno considered as a baseline. This freed the team to use more

complex algorithms when processing the data and allowed the testing / fine tuning stages of the project to continue without allocating finite development resources to low power embedded device techniques. The ItsyBitsy also occupied a footprint around a quarter the size of a standard Arduino. Onboard voltage conversion from the nominal 12V to 5V was planned with four LM7805 linear voltage regulators. These failed during testing and a separate buck converter was utilized in the final version. The MPU-6050 IMU was mounted on header pins over the ring terminal connectors. This was a space saving measure that complicated manufacture and remanufacture during testing.

The board was intended to be potted with a silicone epoxy compound after completion. Due to the need to reconfigure the electrical layout of the board this was not accomplished before the testing and fine-tuning phases of the project.

The measures taken to protect against vibration were validated by the reliability of the arrangement during testing. The measures might well be more intense than necessary, presenting an opportunity for future research into vibration mitigation and physical fatigue in automotive racing electronics. The scope of the project required us to err on the side of reliability and the monetary costs associated with these decisions largely did not warrant a higher level of scrutiny. The chief exception was the ring terminals, which if replaced with traditional through-hole soldered connections would have saved not only the terminals but around 3 minutes of billable effort every time each connection was soldered or desoldered.

2.3.2.2 Electrical Layout

Using the online documentation (lady ada, 2018) for the ItsyBitsy M0, a pin arrangement was developed and implemented to guide a PCB layout. Terminals were manually placed in KiCad 5.1.10's Legacy Toolset. Automatic netlist layout was rejected due to the need to create library parts with nominal internal connections for almost every single part, deemed outside the scope of the project. To maximize extensibility, an additional connection was provided for a servo to control a future rear wing and the mode select switches were originally connected to analog inputs to support more complex input systems in future vehicles.

We selected professional manufacture for the boards from JLC PCB to enable us to use a four-layer routing. The PCB physical layout was optimized to organize the connections that would be later used by the competition team, necessitating a four-layer design. The top layer contained the 5V power routing for ease of reverse engineering in the event the documentation was ever lost. The first internal layer contained the 12V power, for extra protection against accidentally connecting future modifications to the high (by CMOS standards) voltage line. The bottom layer contained the servo connections, leaving ground to the second internal layer. JLC PCB would also assemble certain parts for us, allowing the team to specify surface-mounted pull-up and voltage dividing resistors. The LM7805 voltage regulators were also ordered through JLC PCB, with the resulting order looking like the 3D visualization in Figure 2.3.8.

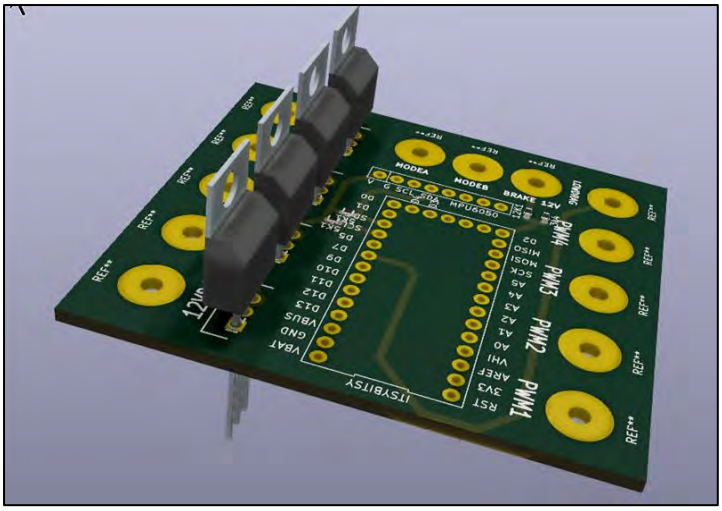

Figure 2.3.8 - A 3D rendering of the circuit board as ordered.

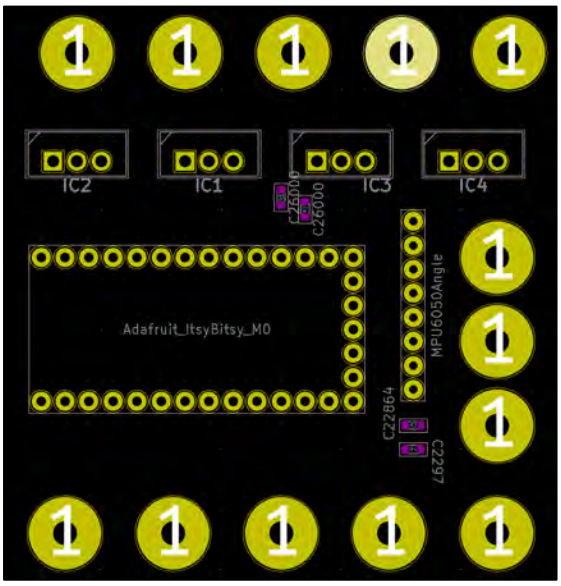

Figure 2.3.9 PCB Connections, from the top

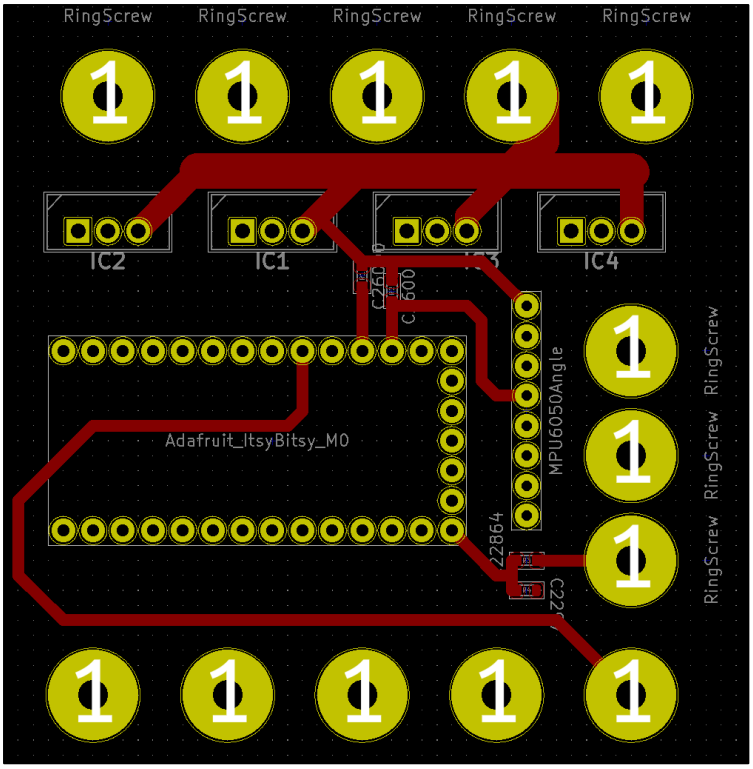

Figure 2.3.10 PCB front copper layer, used for 5V, I2C, and the DRS connections

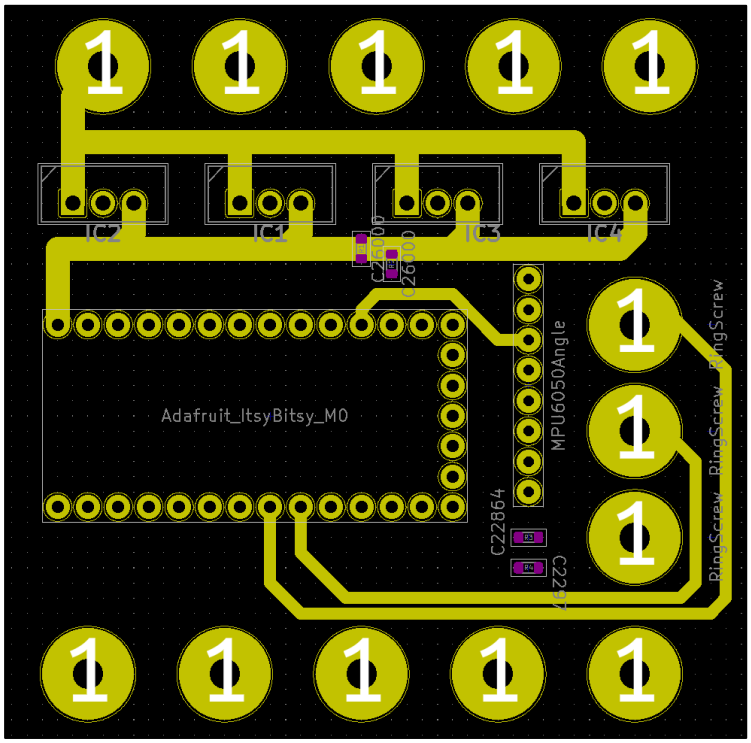

Figure 2.3.11 Internal layer 1, used for 12V, I2C, and mode sensor connections

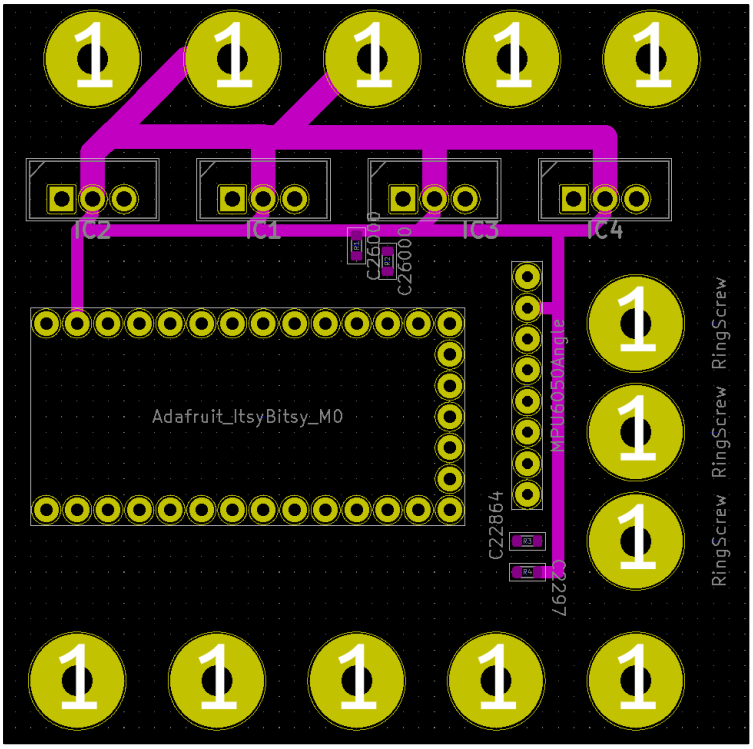

Figure 2.3.12 Internal layer 2, used for ground connections

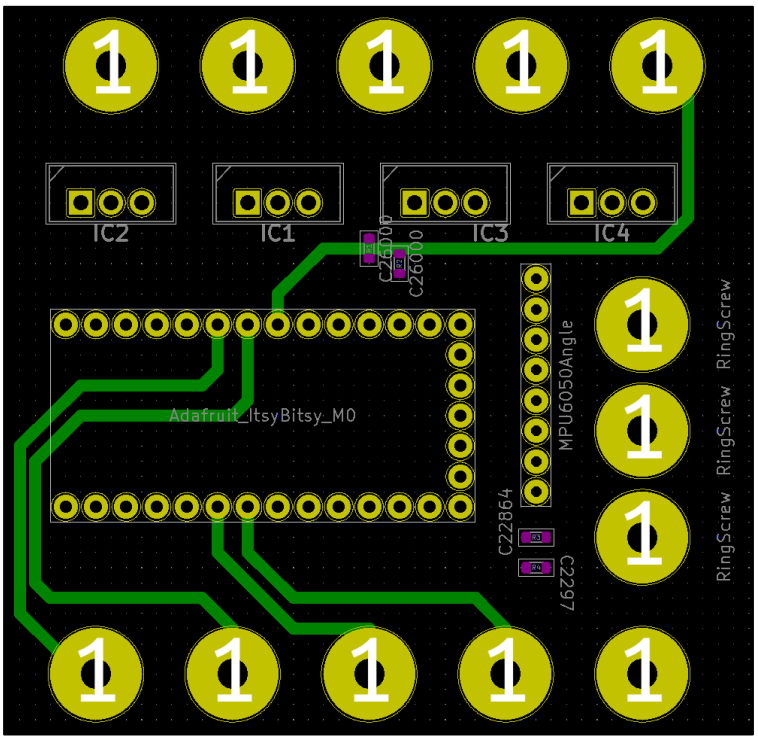

Figure 2.3.13 Back layer, used for servo connections

In addition to the core requirements of this project, the PCB is extended to support the rear wing servo output and four control inputs. This includes a brake sensor at the 12V level used by the team to activate the brake lights, passed through a voltage divider to the control board. Two mode switch inputs allow up to four preloaded modes to be selected at runtime using the toggle switches on the dash without connecting the board to an external system.

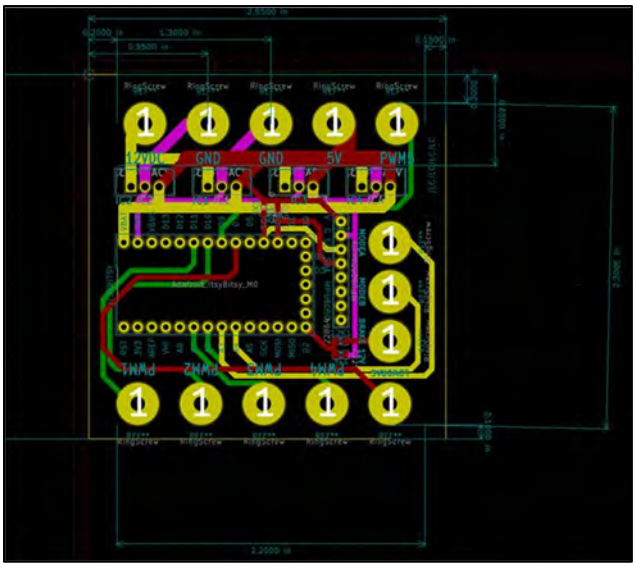

Figure 2.3.14 - The overall design of the PCB.

2.3.2.3 Discrepancy Correction

Five copies of the board were ordered from JLCPCB with the power conversion components, I2C pullup resistors, and brake sensor voltage divider to be soldered on by the original manufacturer. The microcontroller and IMU sensor were ordered and attached separately. The extra boards were ordered for backups, and three were damaged in testing due to faulty voltage regulators. Therefore, the FSAE team will have the working PCB installed on the car and one extra copy to experiment with.

Testing quickly revealed an omission in the Adafruit claim of 13 PWM out pins: not all of them could be set to drive servos at once, being connected to the same timers. The electrical team solved this issue by writing a program to test every combination of pins connected to the breakout slots on the PCB and devising a pin remapping that allowed us to continue to use the PCBs originally ordered. This pin remapping is documented in Table 2.3.1.

WARNING TO THE COMPETITION TEAM:
THE PCBS USED BY THE SPRING 2022 TEAM DO NOT HAVE UPDATED LABELS.
FOLLOW ALL PROVIDED DOCUMENTATION.
DO NOT RELY ON THE SCREEN PRINTING.
FAILURE TO FOLLOW THESE INSTRUCTIONS MAY RESULT IN EQUIPMENT FAILURE.

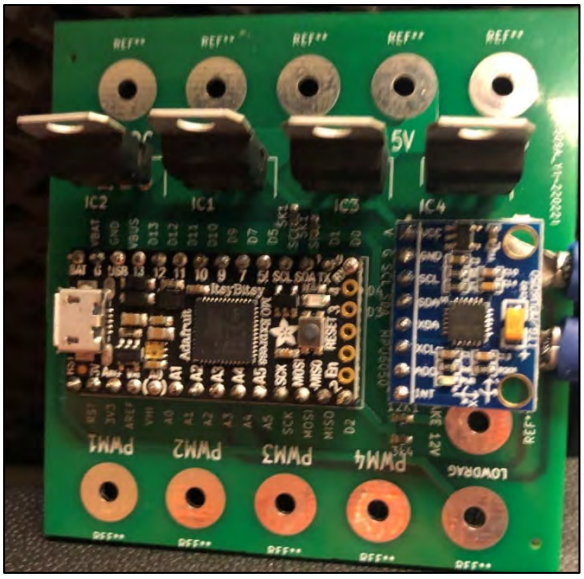

Figure 2.3.15 Completed PCB with Itsybitsy, MPU-6050, and two ring terminals

Original Function	ItsyBitsy Pin Name	Arduino Pin Number	PCB Label	Final Function
5V power out	BAT		5V	5V power in
Ground	GND		GND, GND	Ground
Servo 3	A1	15	PWM3	Mode A
Servo 4	A2	16	PWM4	Servo 4
MODEA	A3	17	MODEA	Servo 2
MODEB	A4	18	MODEB	Servo 3
12V (divided) Brake	D2	2	BRAKE	Brake
I2C – SDA	SDA	26		
I2C – SCL	SCL	27		

Original Function	ItsyBitsy Pin Name	Arduino Pin Number	PCB Label	Final Function
DRS button	D7	7	LOWDRAG	DRS button
Servo 5	D9	9	PWM5	Servo 5
Servo 2	D10	10	PWM2	Mode B
Servo 1	D11	11	PWM1	Servo 1

Table 2.3.1 - ItsyBitsy Pin Assignments, PCB Labels, and their Functions

2.3.3 PCB Enclosure and System Integration

A specialized enclosure was designed to protect the PCB from the harsh environment and secure it to the car, shown below in Figure 2.3.16.

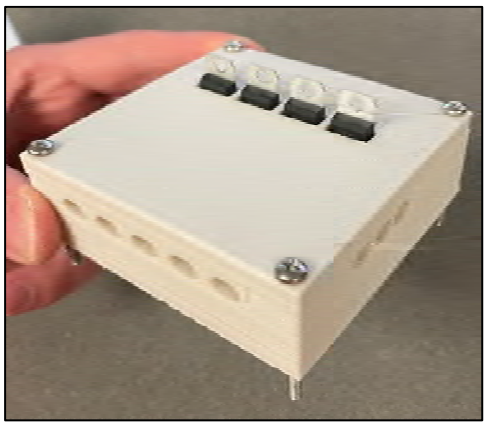

Figure 2.3.16 – PCB Enclosure

The enclosure is 3D printed in PLA, and this method of manufacturing was chosen for its simplicity and speed. For assembly, the enclosure is split into two halves. The bottom has cutouts for hex bolts to pass through which secure the PCB mount to the car, and these cutouts allow nuts to be tightened onto the hex bolts without having access to the head of the bolt after the PCB is installed in the enclosure bottom. The bottom half of the mount without the PCB installed is shown on the left side of Figure 2.3.17 below. Only two of the four 1/4” hex bolts are shown for simplicity, and the PCB before installation is shown in the middle of Figure 2.3.18 with rubber washers on the 2-56 mounting screws to dampen vibration. Three screws are used because there is not adequate space in the bottom left of the PCB for a mounting screw’s head to not contact the ring terminal. After the rubber washers are placed on the mounting screws, the PCB is placed into the bottom half of the enclosure and bolted into place.

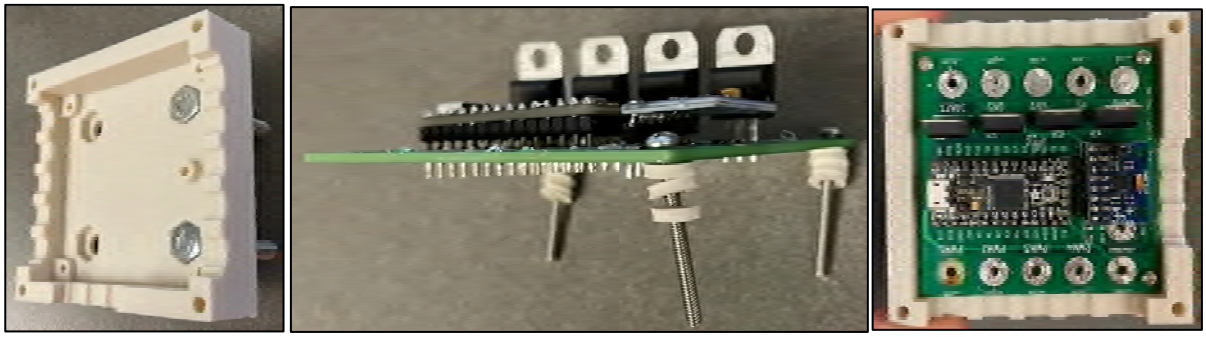

Figure 2.3.17 – PCB Enclosure Assembly

On the underside of the enclosure's bottom shown below in Figure 2.3.18, cutouts allow nuts to be placed on the PCB mounting screws and tightened without the use of a socket wrench. These cutouts also allow the PCB mounting screws to be shortened so that they do not collide with the mounting brackets when the PCB enclosure is placed on the car. In addition, the cutout in the middle of the two mounting bolts allows a bolt to directly connect the PCB's ground to the frame of the car, safely grounding the active aero system with the rest of the car's electronics.

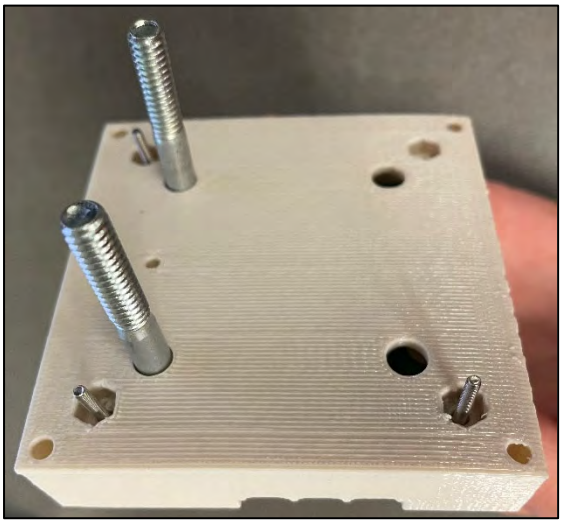

Figure 2.3.18 – PCB Enclosure Bottom

Once the PCB is secure in the mount bottom, the mount top is bolted into the mount bottom using 1/8" machine screws, and the entire assembly is bolted onto two brackets at the front of the car beneath the front cross bars, shown below in Figure 2.3.19. This location was chosen for ease of accessibility and proximity to the wing kit. Vibration damping bushings and washers are used between the mount and the brackets to lessen the impact of the car's vibration on sensor readings.

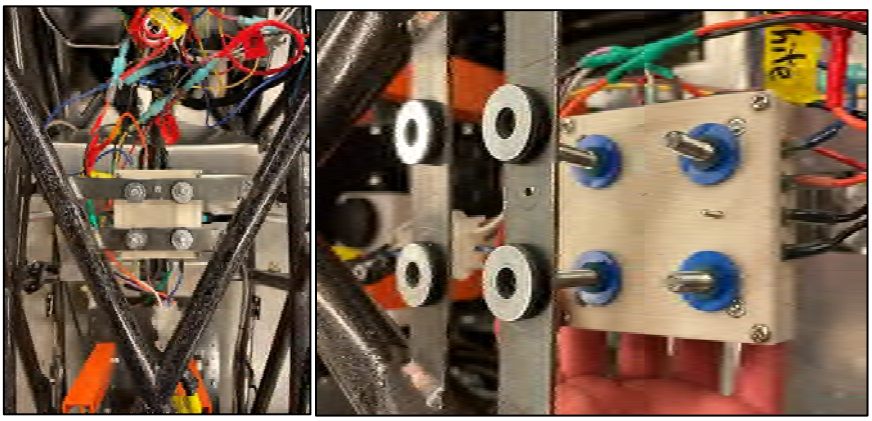

Figure 2.3.19 – PCB Enclosure mounted on car

2.3.4 Wiring Diagram and Harness

A simplified wiring diagram is shown below in Figure 2.3.20 and a detailed wiring diagram of the entire system can be found in Appendix C. The voltages associated with this project are all 12V DC nominal or less. The highest current possible would be with 5V power supply line to the servos, which can supply up to 6 amps, or stall current for three servos. The project connects to the vehicle's existing electrical distribution through the voltage converter and draws up to 5 amps based on the fuse.

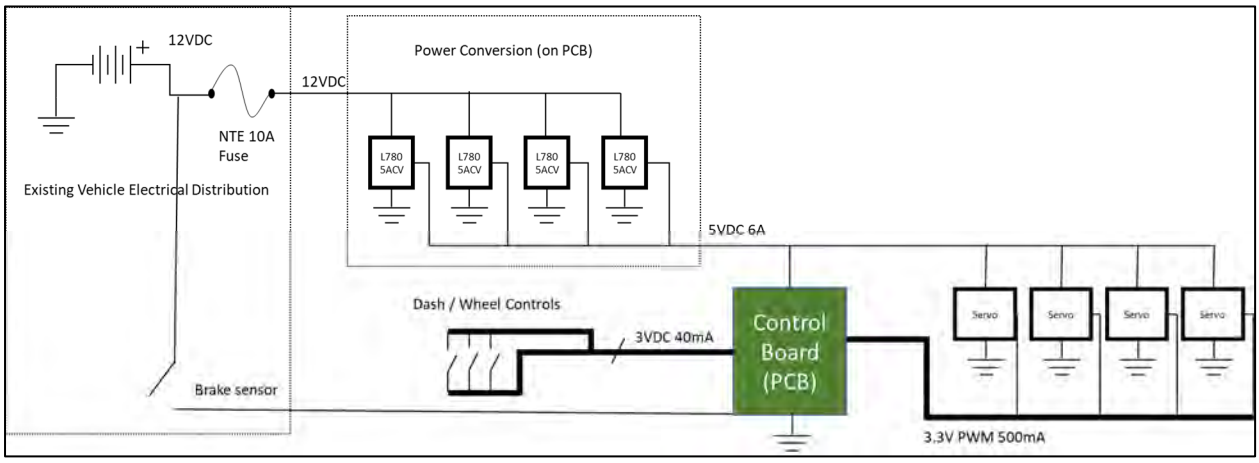

Figure 2.3.20 – Simplified Wiring Diagram

2.3.5 Control Logic

Switch A and B on the dashboard allow the driver to switch between four modes for the wing kit: low drag, discrete, continuous, and high downforce. Low drag and high downforce are static wing modes, which means the wing kit will stay fixed at one position. For low drag, the wings are fixed at a flat, neutral position producing the lowest drag possible; for high downforce, the wings are fixed at angles producing the highest downforce possible as determined by Aero team's CFD in

Section 2.1.2. The active modes are discussed in the following sections, and the switch positions corresponding to each system mode are shown below in Table 2.3.2.

A Switch	B Switch	Mode
0	0	Low Drag (Neutral)
1	0	Discrete
0	1	Continuous
1	1	High Downforce

Table 2.3.2 - Mode Switches Configuration

2.3.5.1 Data Collection

Although the PCB enclosure was mounted to the car with rubber washers, the accelerometer data from the IMU was very noisy. The slightest vibration would cause massive spikes up to 1/8 of a g in the x and y direction, and in addition the x-direction acceleration would not settle to zero even when the car was sitting still. To fix these issues, we first coded in a calibration at start-up to counter the offset from zero and then took a rolling average of the acceleration. For calibration, the car's engine has to be turned off and the car should not be jostled or moved when the active aero power switch is turned on. This ensures a reliable offset is calculated. Once the wings begin their startup sequence, the engine can be started and normal operation resumed. The calibration routine calculates the average of the first 200 data points from the accelerometer, and then this average is subtracted from the raw acceleration data every time a data pointed is retrieved from the IMU for both the x-acceleration and y-acceleration. For the rolling average function, a matrix stores the last 18 points of raw acceleration data from the IMU, and these 18 points are averaged every time the function is called to update the average acceleration value. The IMU data is sampled at a frequency of 100 Hz, which means 100 data points are taken every second. Taking the size of the rolling average matrix and dividing by the sampling frequency, the time length of the rolling average is approximately 0.2 seconds, so the system would need about .05 seconds to notice a change in the average acceleration trend and react. The length of the rolling average and sampling frequency were chosen to optimize the reaction time of the wings on the track.

2.3.5.2 Discrete Mode

The first active control mode is based on an if-elseif logic shown below in Figure 2.3.21. The microcontroller takes the average acceleration value, a_c, from the rolling average function and compares this value to the initial and final acceleration thresholds, shown as a_{low} and a_{high}. The optimal values for a_{low} and a_{high} were determined through testing and are shown below in Table 2.3.3.

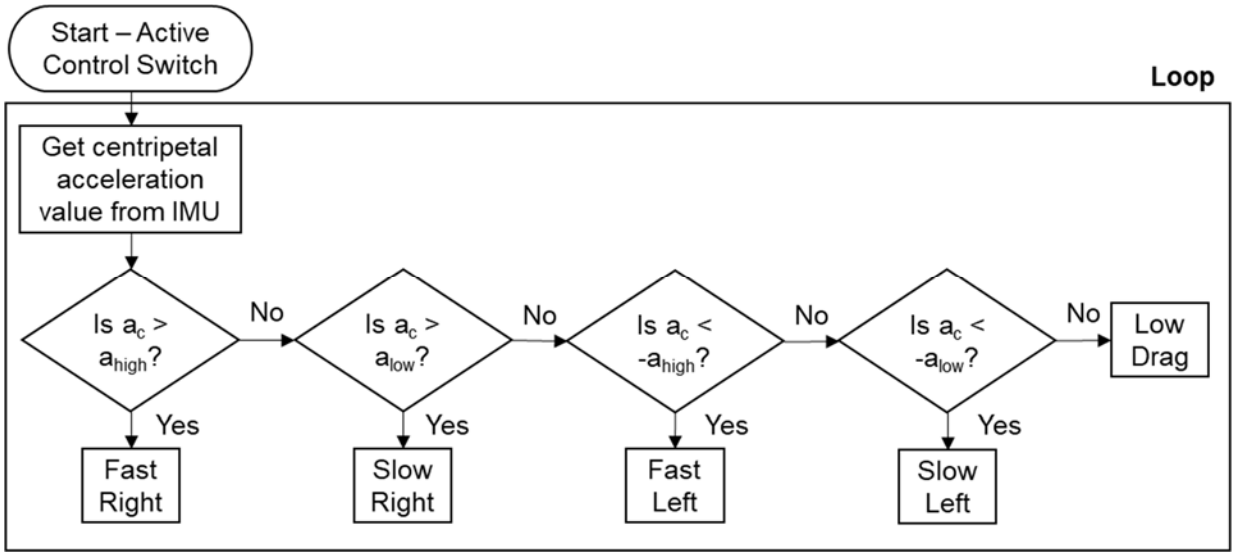

Figure 2.3.21 - Discrete Mode Control Logic Flow Diagram

	Lateral Acceleration (g)
a_low	0.5
a_high	0.8

Table 2.3.3 – Discrete Mode Acceleration Thresholds

Based on where the average centripetal acceleration falls within the thresholds, the state of the car is determined as fast right, slow right, fast left, slow left, or low drag. These are the only five possible wing configurations for discrete mode, and the servo positioning key shown below in Table 2.3.4 shows the servo positions for each state while the actual servo angles at these positions can be found in Table 2.3.5 and Table 2.3.6 below. This organization allowed a else-if type structure to be used in the code that prevented a servo from being written the incorrect angle and burning out. Due to the different orientation of the servos in the main wing element, the control arms of servo one and three face the left of the car while the control arms of servo two and four face the right of the car, which means writing an angle of 180 degrees to all four servos would not result in all the servo arms being at the same position. The switch-case structure allowed angles for each servo's position to be pre-programmed as variables so that the servo.write() function always used a variable indicating a value from the lookup table instead of a calculated number, thus preventing any errors or confusion in the servo orientation.

		Servo Position			
		Servo 1	Servo 2	Servo 3	Servo 4
State of Car	Low Drag	0	0	0	0
	High Drag	3	3	3	3
	Low Downforce	1	1	1	1
	High Downforce	2	2	2	2
	Slow Left	1	1	0	0
	Fast Left	2	2	0	0
	Slow Right	0	0	1	1
	Fast Right	0	0	2	2

Table 2.3.4 – Servo Positioning Key

Servo 1		
Position	Servo Angle (deg)	1st Element Angle (deg)
0	60	0
1	70	5
2	85	10
3	112	30

Servo 2		
Position	Servo Angle (deg)	2nd Element Angle (deg)
0	130	0
1	107	20
2	68	40
3	68	40

Table 2.3.5 – Servo 1 and 2 Angles

Servo 3		
Position	Servo Angle (deg)	2nd Element Angle (deg)
0	46	0
1	89	20
2	106	40
3	106	40

Servo 4		
Position	Servo Angle (deg)	1st Element Angle (deg)
0	124	0
1	114	5
2	99	10
3	64	30

Table 2.3.6 – Servo 3 and 4 Angles

2.3.5.3 Minimize Roll Logic

The second active control mode is based on a closed loop PID controller minimizing body roll of the vehicle, as shown below in Figure 2.3.22. The PID controller was implemented using the Arduino `PID_v1` library (maintained by Brett Beauregard). A continuous Proportional on Measurement PID controller was implemented with an input from a truncated X acceleration value

where any value greater than 1G was capped. The PID output was then fed into a map function that calculated wing angles between the ±1G limits.

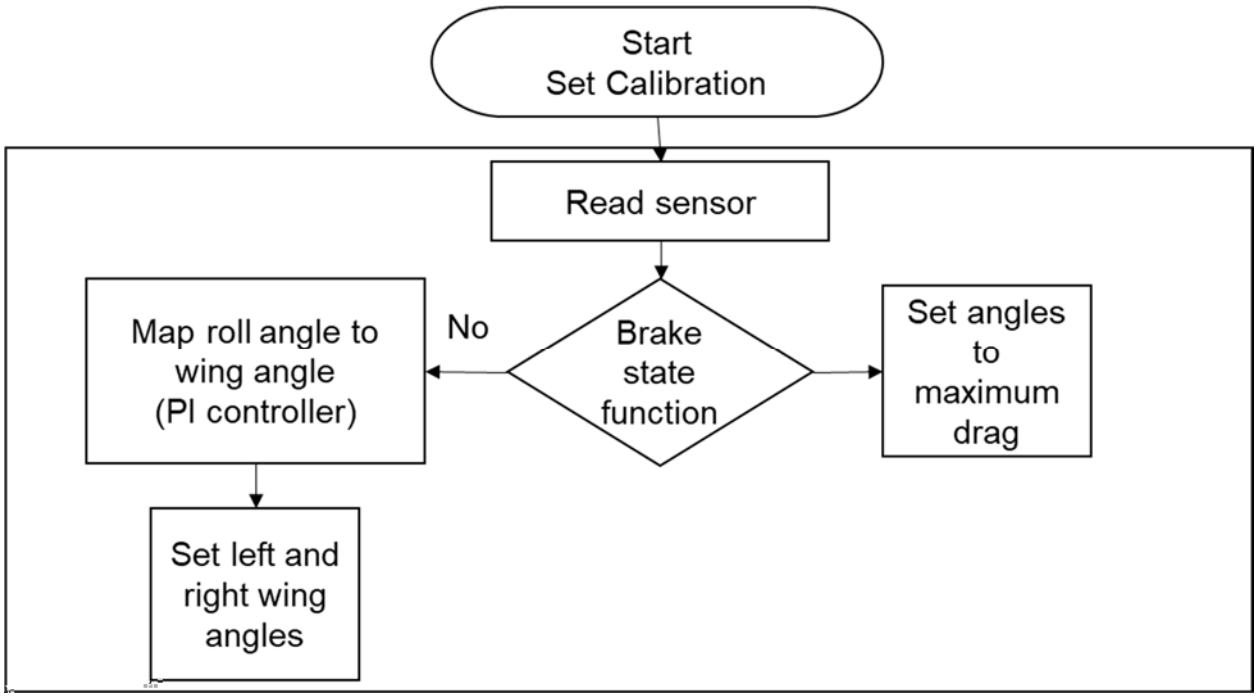

Figure 2.3.22 - Minimal Body Roll and Air Brake Logic

2.3.5.4 Air Brake Logic

In Figure 2.3.22, the air brake logic is also demonstrated. This logic is relatively simple and focuses on accurate implementation. The air brake should come on when the system detects a threshold of either time or deceleration in conjunction with a binary sensor input taken from the brake light indicator. Testing was cut short due to weather and the deceleration air brake not implemented to a finished state.

3 Testing and Quality Plan

3.1 Material Testing

Material testing is required to determine the type of layup, core material, and layer count for a specific part. Parts that need this type of testing include the endplates (inboard and outboard sections), the main element, and the second and third elements. Endplate testing is priority number one as it ensures the wing package will not “fall off the car” and minimizes the overall deflection measured at the wing tip. If the plate is not resistant to bending by a big enough margin, the outside endplates will have more deflection and result in being out of rules tolerance of the maximum allowed 5mm (about 0.2in).

3.1.1 Independent Variables

The variables to be changed and observed include the layer count, core material, and hole diameter. Layer count refers to the total number of layers of carbon fiber used in the part; a four-layer part means four layers of carbon fiber are stacked on top of one another. The core material refers to the type of material that is being sandwiched between the carbon fiber layers. Utilizing a core material will require a minimum of two layers of carbon fiber but can have any other number of layers. Usually, however, the layer count will be an even number when using a core material as this means the same number of layers will be used on both sides of the core material. Lastly, the hole diameter refers to the size of the hole that the load is being applied through. This was not considered to be an independent variable at first but after the first round of testing it was evident a bushing of some material would need to be analyzed to try and increase the area the load is applied through. Below is an example of a 4-layer part with a Nomex core material.

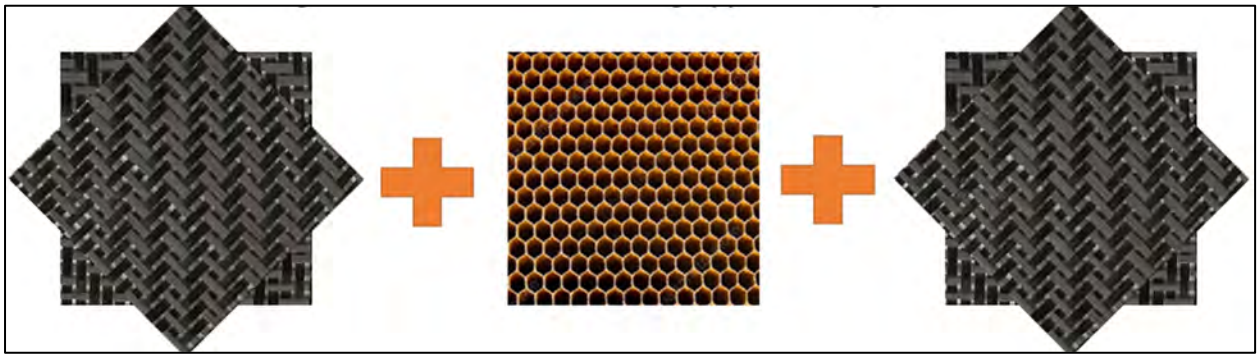

Figure 3.1.1 - 4-layer Nomex Core example

3.1.2 Shear Testing

Shear testing was the first set of tests to be conducted on the carbon fiber samples. The first round of testing included a total of 8 samples, all two layers, using four different core materials. Core materials include a 7lb, ¼ in. foam core, 1/8 in. Nomex Honeycomb, ¼ in. Nomex Rectangular block, and no core. Figure 3.1.1 displays the results of half the samples from the first round of testing.

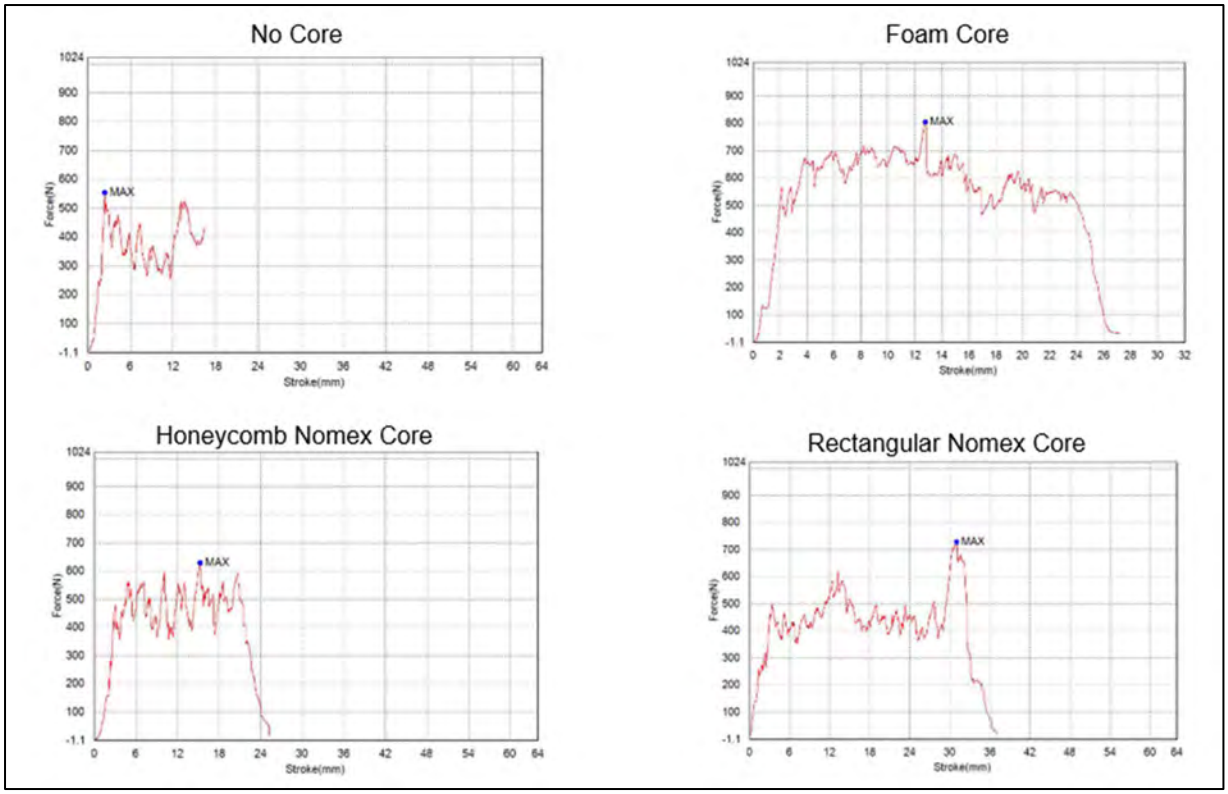

Figure 3.1.2 – Primary Testing Results with different Core Materials

As can be seen, the graphs do not have very much load and a zigzag pattern can be observed. The zigzag pattern relates to the sample cracking and breaking as the load is being applied; in the case of the no core sample, this is the carbon fibers themselves. The Nomex cores are drastically less consistent than the foam core. This is a result of the bolt shearing through each "wall" of the core material as load is applied. The load builds up to the point the Nomex wall breaks and a drop in load is observed.

The results of the tests proved a need for stronger samples. The first way is to increase the layer count; however, an increase in layers is an increase in weight limiting the number of layers to be increased. This led to the second idea of increasing the hole diameter – creating a bushing using the same ¼ in bolt as before while increasing the outer diameter would increase the load applied as it would require more force to shear the increased area through the material. Lastly, the rectangular core did not perform as well as the other cores and, as it is a harder material to handle, was eliminated from being used in further testing. With these independent variables defined and selected, a new set of tests would be conducted.

The Second round of testing included 13 new samples, 6 of 4-layer ¼ in. foam core, 6 of 4-layer 1/8 in. Nomex Honeycomb, and a single 4-layer no core sample. A comparison of the no core samples with 2-layers to 4-layers can be seen below in Figure 3.1.3 and Figure 3.1.4.

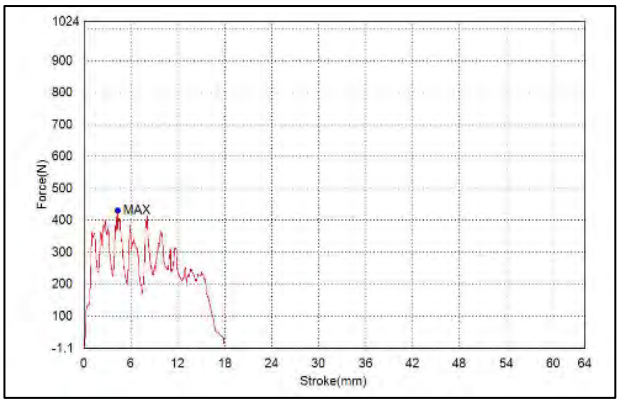

Figure 3.1.3 - 2-Layer No Core

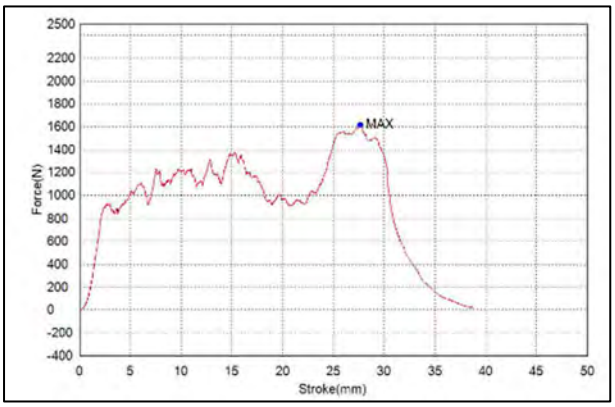

Figure 3.1.4 - 4-Layer No Core

With the scales in consideration, the overall maximum of the 4-layer sample can be seen to be four times as high as the 2-layer. Comparing the "safe loads" of the samples—loads where the material is not cracking or yielding—the 4-layer is also four times as high as its counterpart. This means, doubling the layers and, effectively, doubling the weight of the sample increases the strength by four times as much and doubles the strength to weight ratio.

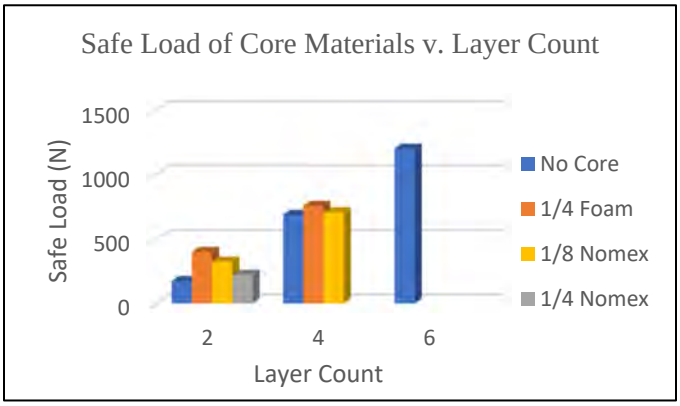

Figure 3.1.5 - Safe Load of Core Materials v. Layer Count

Comparing the first round, two-layer, test samples with core materials to the four-layer tests an increased strength of about 2:1 is observed. Figure 3.1.5 above displays the effect of increased layer count. Figure 3.1.5 also shows the result of a single 6-layer no core test; this occurred in the third round of testing and will be addressed later.

The second round of testing also includes tests for different bushing sizes. These tests include no bushing, using the standard ¼ in. hole, a 3/8 in. bushing with a ¼ in. hole for the same bolt used, and a ½ in. bushing with the same ¼ in. I.D.—interior diameter. Figure 3.1.6 shows the effect of bushing size observed in these tests. The 1/8 in. Nomex core performs better as the bushing size increases, however, the foam does not. The ¼ in. foam increases its safe load substantially using the smaller bushing size, 0.375in., but does not continue to increase in the 0.5in. samples. Originally, the bushing width was made to be the same width as the sample. During testing, it was

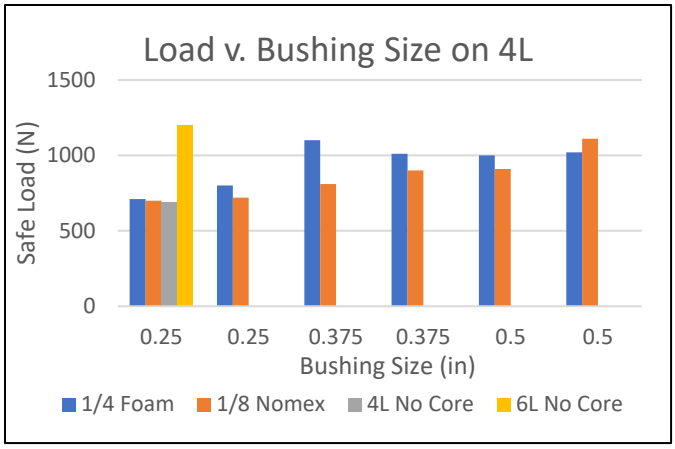

Figure 3.1.6 - Safe Load v. Bushing Size

observed that the bushing would shift in the foam samples and would not perform as consistently as seen in the first round of testing where no bushing was used. The bushings intention was to increase the area the load would be applied through in every layer and the core material. When the bushing would shift, the bushing would only be active through one side of the sample, only half the layers carbon fiber layers, and semi-active in the core material. The Nomex core samples did not have this problem as these samples are thinner overall and do not allow the bushing to shift. This led to the proposition that if the bushings were wider for the foam core tests conducted, shifting would be less likely to occur allowing for more consistent results and, hopefully, and increased load being applied.

The second round of testing with increased layer count and the inclusion of bushing size was successful. The safe loads applied were much higher by simply increasing the layer count. The bushings allowed more load as well with some less consistent results in the foam core samples. The maximum experienced safe load was a 4-layer sample utilizing the ¼ in. foam core at a load of 1100N (about 247lbf). This is better than the first round of testing, however, as the need to be slightly stronger arose, a third round of testing would be conducted. Table 3.1.1 below shows the results for the samples tested in round two.

Sample	Layers	Core	Hole Size (in)	Weight (g)	Thickness (in)	Safe Load (N)	Ultimate Load (N)
1	4	1/4 Foam	0.25	48	0.425	710	1616
2	4	1/4 Foam	0.25	50	0.427	800	1476
3	4	1/4 Foam	0.375	46	0.424	1100	1810
4	4	1/4 Foam	0.375	49	0.424	1010	2020
5	4	1/4 Foam	0.5	47	0.425	1000	2252
6	4	1/4 Foam	0.5	44	0.423	1020	1844
7	4	1/8 Nomex	0.25	41	0.236	700	1348
8	4	1/8 Nomex	0.25	38	0.237	720	1035
9	4	1/8 Nomex	0.375	40	0.236	810	1872
10	4	1/8 Nomex	0.375	39	0.237	900	1819
11	4	1/8 Nomex	0.5	39	0.237	910	1580
12	4	1/8 Nomex	0.5	39	0.235	1110	1624
13	4	None	0.25	29	0.042	690	1624

Table 3.1.1 – Second Round Testing Data

As seen above in Table 3.1.1, some observations include the foam core samples being much thicker than the Nomex core. A foam core sample of 4-layers is rougly 18 grams heavier than a no core 4-layer sample while a Nomex sample is roughly 10 grams heavier. With the observed weight of sample 13 being 7.25 grams/layer, it becomes clear almost 3 additional layers of carbon fiber will equal the weight of a single layer of the ¼ in. foam core. The question now was if a 6-layer no core part would perform better than the 4-layer foam core sample.

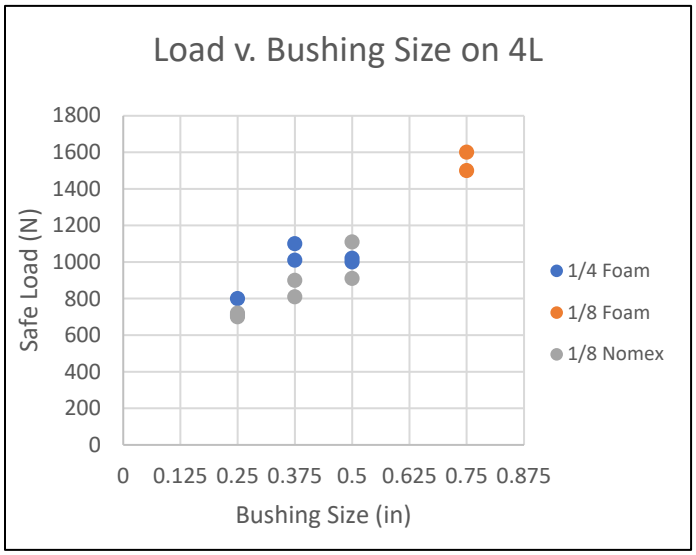

Figure 3.1.7 - Safe Load v. Bushing Size during Round 3

Round three of shear testing was fueled by the data collected in the second round and the data tabulated in Table 3.1.1 above. First, a new material was introduced in the form of a 5lb, 1/8 in. thick foam core. As foam core samples seemed to perform better, this material was introduced in an effort to make parts thinner and lighter while still increasing the applied safe shear load. Second, a bigger bushing size with an outside diameter of 0.75in. would be tested. Lastly, a single 6-layer no core test would be conducted to analyze further if no core and more carbon fiber layers would perform better.

Figure 3.1.7 to the left shows the effect of the increased bushing size with the new 1/8in. foam core material. As can be seen, the two samples testing are much higher reaching an average safe load of 1550N (337lbf). Multiplied by the 6 attachment points to the vehicle results in a safe load of over 2,000lbf. The 6-layer no core test also performed better than any of the 4 layer samples in Round 2, however, did not perform as well as the 1/8 in. foam samples. The weight of the 6-layer sample was also 19% heavier than the 1/8 in. foam.

Testing Round	Sample	Layers	Core	Weight (g)	Thickness (in)	Core Material Weight	Weight/Layer CF
2	1	4	1/4 Foam	47	0.425	20.50	6.71
2	7	4	1/8 Nomex	39	0.236	12.50	6.71
2	13	4	None	29	0.042	N/A	7.25
3	14	4	1/8 Foam	32	0.177	5.17	6.71
3	16	6	None	37	0.059	N/A	6.17

Table 3.1.2 - Tabulated Values and Materials of Testing Rounds 2 and 3

Table 3.1.2**Error! Reference source not found.** above displays the overall values for the materials tested in rounds two and three. As can be seen, the materials of sample 13, 1/8 in. foam, are exceptionally light compared to samples one and seven. Sample 13 is also 25% thinner than the Nomex core and 58% thinner than the ¼ in. foam.

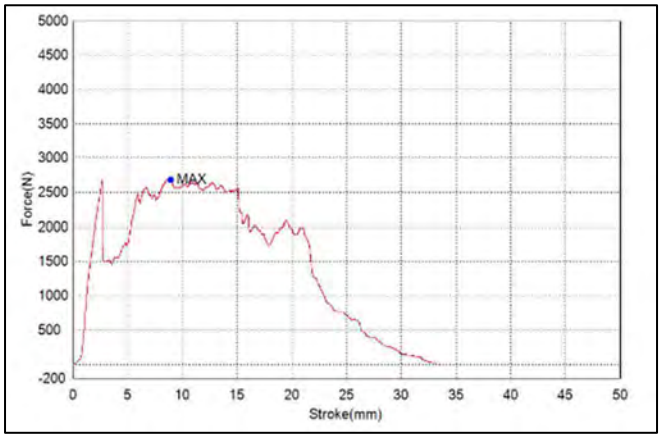

Figure 3.1.8 - Chosen Material Shear Testing Performance

From the results in round three of shear testing, the optimal endplate material is a 4-layer, 1/8 in. thick, 5lb density foam core material. This material is being chosen as it had the highest loads witnessed of all tests conducted and is thin, light, and durable. Figure 3.1.8 to the left shows the performance of this material. A sharp drop in load is seen at the 3mm mark; this is where the sample first yielded. Up to this point there had been no cracking or shifting of the bearing. The gap from range 5mm to 15mm also has very minimal "zigzag" pattern as observed in round one of testing. The overall ultimate load was also the highest observed of all tests reaching a maximum load of 2685N (603lbf). Multipling this by the six attachment points to the chassis results in 3618lbf of consistent shear load to break the wing off the vehicle at the endplates. The next section covers the performance of these samples under bending loads.

3.1.3 Deflection Testing

Deflection testing was conducted on the samples after shear testing was complete to determine the maximum bending/compression load that could be applied to the different core materials. The goal is to estimate the total displacement at certain loads to ensure rules compliance is met of 5mm total deflection allowed at the wing tips.

As seen in Figure 3.1.9 below, all materials performed close to the same. All samples increased load in a linear line until the sample yielded and the test was stopped. Analysis of the tests are done with two variables in mind, the load withstood by the material, and the displacement witnessed at the maximum points. As can be seen, the no core sample performed the worst in both conditions reaching less than 200lbf of bending at the most deflection observed of 0.5in, out of

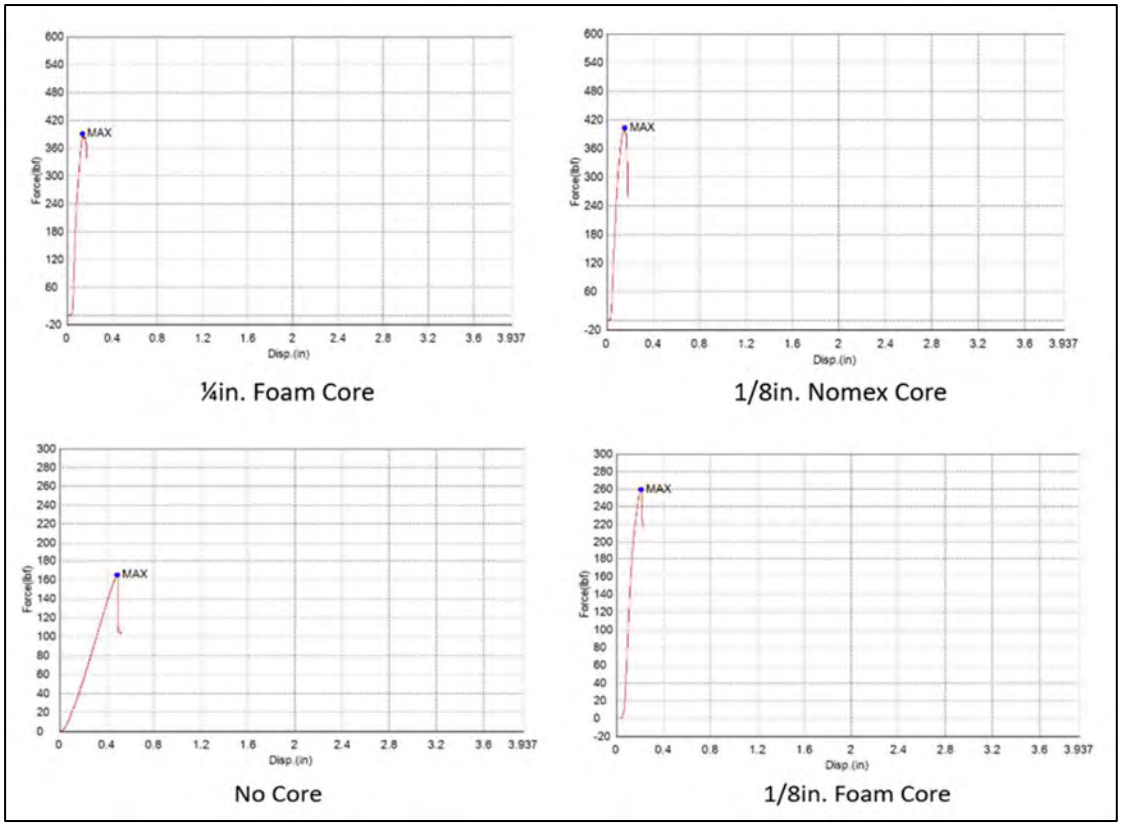

Figure 3.1.9 - Results of Bending Loads applied on Core Materials

rules tolerance. The ¼ in. foam and 1/8 in. Nomex performed almost the same reaching right at 400lbf at 0.2 in. of displacement. Lastly, the 1/8 in. foam performed right in the middle with 280lbf of load applied yielding at the same 0.2 in. of displacement. As mentioned in Section 3.1.2, the material chosen for the endplates is the 1/8 in. foam core with 4-layers. While this does not perform as well in bending as the others, the material is not expected to deflect much and is still within rules tolerance as opposed to the no core sample. Lastly, the results of the deflection testing also aids the material selection for the main element and active elements of the wing. The Nomex core is flexible enough to work with easily and has sufficient loads at the measured displacements making it the ideal material for these components.

3.2 Performance Testing of Front Wing

The performance testing of the vehicle will take place using different FSAE style tracks at numerous locations. FSAE style tracks include a straight line, for acceleration and braking, skid pad, for cornering speed, and autocross style for the combination of acceleration, braking, and cornering.

3.2.1 Straight Line Testing

3.2.1.1 Straight Line Testing Plan

Straight-line vehicle testing was initially planned to take place to determine the braking performance and stopping distance, and the downforce generated on the vehicle. Brake testing would be conducted by entering the testing path at a constant speed and applying as much brake pressure to stop the car without locking up the front wheels. Conducting this test without any aero, with aero in the drag reduction mode, and at maximum air braking mode will determine if the vehicle stops in a quicker distance with the front wing package. With active air braking the vehicle should be able to stop quicker for two reasons: first, more downforce is being applied to the front tires allowing for more brake pressure to be applied without locking up the front tires. Locking up the front tires reduces the friction factor applied and will not slow the car down quickly. Secondly, in the air brake mode, while more downforce is being applied, so is more drag; drag will help slow down the vehicle, however, this should be minimal compared to the overall drag of the vehicle and exposed surfaces where drag cannot be measured.

Straight-line vehicle tests would also be conducted with linear potentiometers placed on the front springs. Figure 3.2.1 shows an example of a linear potentiometer to be used. This would allow an active and real measurement of the displacement of the front springs without aero, with air in the drag reduction mode, and at maximum air braking. Conducting this test at a constant speed is crucial but will allow for the true calculation of the downforce generated at the different aero deployment levels.

Figure 3.2.1 - Linear Potentiometer

3.2.1.2 Straight Line Testing Results

On April 19, 2022, testing was scheduled to occur at the Life Church parking lot in Stillwater, Oklahoma. This parking lot has a long straight where straight line vehicle testing could easily take place. As will be seen in Section 3.2.2.2, skid pad testing also took place at this location and time. As skid pad testing finished, problems arose with the testing vehicle. The engine had leaked oil all over the parking lot, ruining the testing surface and preventing the opportunity to record reliable straight line testing data since the car's tires could no longer predictably grip the surface. Along with this issue, the car could not be safely operated with low levels of oil, so testing had to end before straight line data could be recorded. Although the team was not able to perform straight line testing, important test parameters such as downforce generation was able to be approximated during skid pad testing.

3.2.2 Skid Pad Testing

3.2.2.1 Skid Pad Testing Plan

Skid pad testing would take place to determine the cornering speed of the vehicle and the lateral acceleration the vehicle achieves. The skid pad used, seen in Figure 3.2.2, is set up like a figure eight but can be set up as a single circle. The inside diameter of each circle is 15.25m while the outside diameter is 21.25m. This means the average radius of the track is 9.125m or 30ft. The test is conducted by the vehicle entering the course at the bottom, completing two full circles in the right-hand direction, transitioning to the left-hand direction between laps two and three, completing laps three and four before exiting through the top of the course.

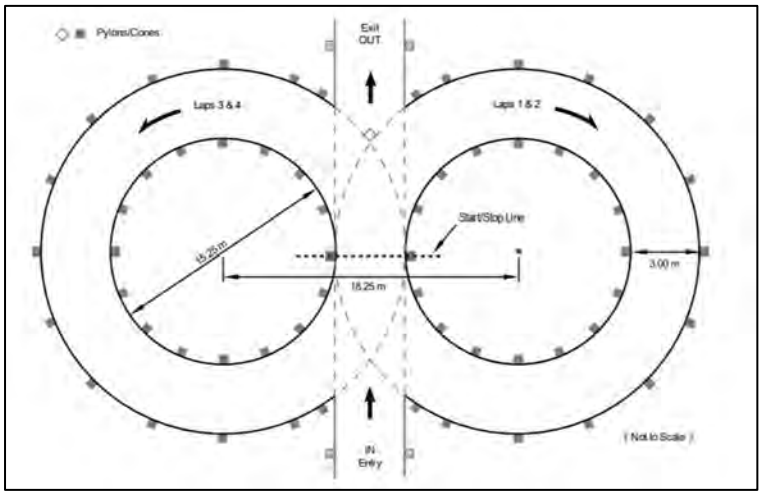

Figure 3.2.2 - FSAE Skid Pad Layout

As mentioned in Section 1.3, the expected performance gain is estimated to be 3.5 miles per hour in a constant 30ft radius corner. Using data from the current Oklahoma State FSAE car, 0.975 lateral g-force is the maximum recorded lateral acceleration. Using equation 3-1, this is 20.918 miles per hour. The top ten vehicles in FSAE competition reach a maximum of 1.414 laterals g's. This is 25.194 miles per hour, or 4.276 miles per hour quicker. Obviously, in autocross and endurance style tracks with different corners and radii, the speed measured can be greater or smaller than the constant 30ft radius skid pad, it just depends on the corner radius. An increase of 4.276 mph translates to a 20% cornering speed increase on the vehicle.

$$\text{G-Force} = \frac{\frac{v^2}{r}}{32.2 ft/s^2} \qquad \textit{Equation 3.2.1}$$

3.2.2.2 Skid Pad Testing Results

Initial skid pad testing took place on April 16th, 2022, at the O'Brate stadium parking lot where the current FSAE team—Bullet Racing—does their testing. Cones were arranged in the configuration as seen in Figure 3.2.2. After collecting data for one driver through the different static and active modes (neutral, high downforce, discrete, and continuous), the data was collected and analyzed. Additional testing was conducted on April 19th, 2022, at the Life.Church parking lot located in Stillwater, Ok. Below is the average course completion time for each of the different control modes for the front wing package.

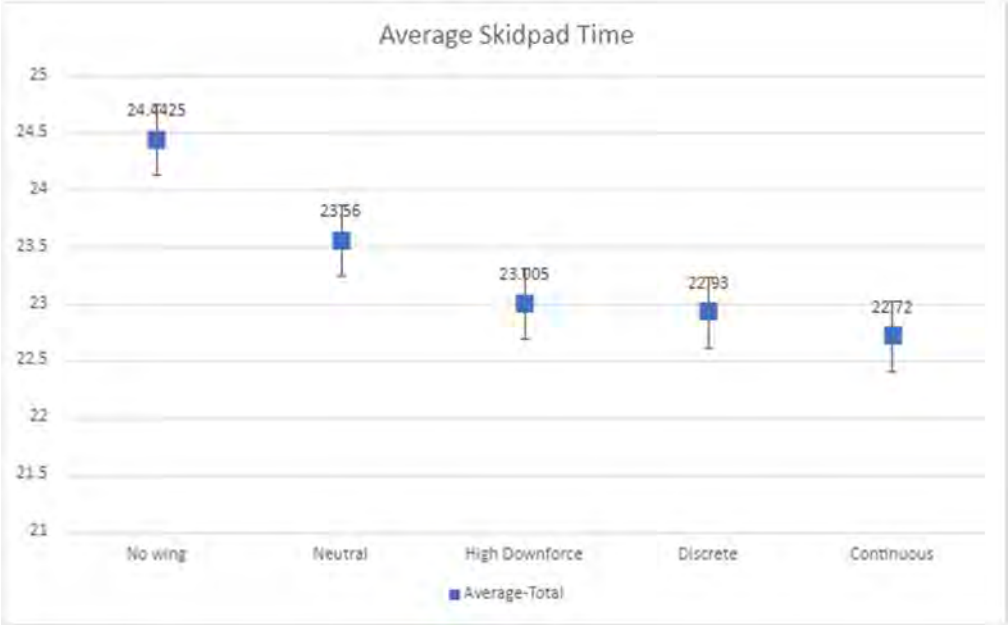

Figure 3.2.3 - Average Skidpad Time for Different Wing Deployments

As can be seen in Figure 3.2.3, the average time between drivers one and two was 24.4 seconds without the front wing. Putting on the front wing immediately decreased the lap time to 23.6 seconds, a 0.8 second increase. This was with the wing in the "neutral" configuration when the flap elements were in the lowest drag mode. The average times for the higher tier deflection modes, high downforce, discrete, and continuous mode, yielded even quicker lap times by over 0.5 seconds.

What stands out in the higher deployment modes is the standard deviations. The lows and highs of each mode all roughly correlate with one another. The skid pad times can be seen for each individual driver in Figure 3.2.4. Driver one is seen to have a quicker lap time in the high downforce configuration while driver two is quicker using continuous mode. Neither driver was faster in the discrete mode. What makes the data more interesting is the inclusion of driver comments. Driver one preferred using the continuous mode but was quicker in high downforce. Driver two preferred the high downforce mode but was quickest in continuous mode.

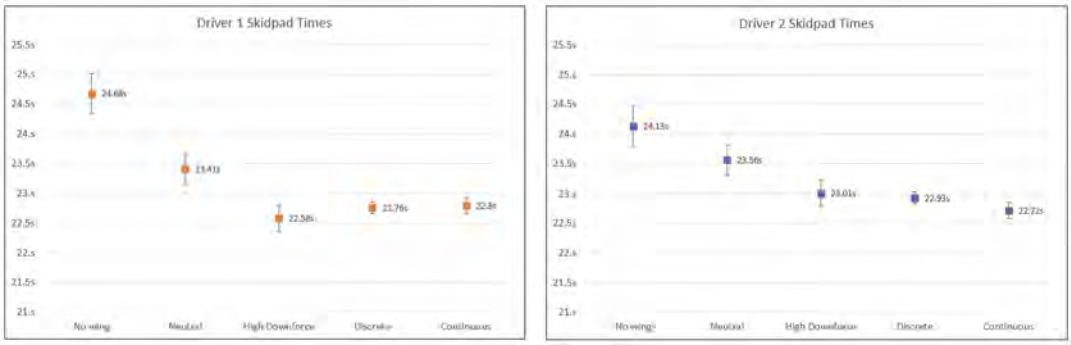

Figure 3.2.4 - Individual Driver Lap Times

Comparing the data collected to the initial project goal and vehicle baseline comparison, a clear increase in performance can be seen. Table 3.2.1 shows the cornering speed increase and lateral acceleration improvements while using the wing. As can be seen, an increase in G-force of 0.179 was achieved. This translates to a 1.8 mph increase, 0.4 mph over the initial estimate, but still 2.4 mph under the achieved cornering speed of a full aero car. Applying this data to the 2021 FSAE Michigan competition, the vehicle would experience an eight-position increase in the skid pad competition, and this would place the vehicle in 23rd place overall.

		Goal (full aero car)	No Wing Baseline	Highest Achieved
time	sec	5.1	6.143	5.645
distance	ft	188.496	188.496	188.496
velocity	ft/sec	36.96	30.687	33.39167
velocity	mph	25.194	20.918	22.762
radius	ft	30.000	30.000	30.000
Lateral Acceleration	ft/sec^2	45.535	31.390	37.167
G-Force	-	1.414	0.975	1.154

Table 3.2.1 - Skid Pad Comparison

While downforce estimation was not able to be calculated with the lack of straight-line testing, an approximation for the downforce generated by the front wing was able to be made with the data collected from the skid pad tests. With the skid pad tests being conducted in left and right-hand circles, a lateral acceleration is induced on the vehicle. The other force in the horizontal direction opposing the lateral acceleration is the friction force of the tire. This can be seen in Figure 3.2.5.

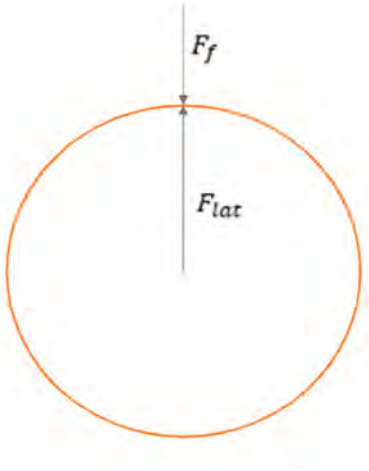

Figure 3.2.5 – Skid Pad Circle with Horizontal Forces

$$F_f = F_{lat}$$ *Equation 3.2.2*

Equation 3.2.2 is derived from Figure 3.2.5 above. Figure 3.2.6 below shows the free body diagram of the vehicle. Assuming the tire is the limiting factor, there is no change in the friction coefficient with the increased downforce, and the turn is constant radius at constant speed, the following equations can be derived below.

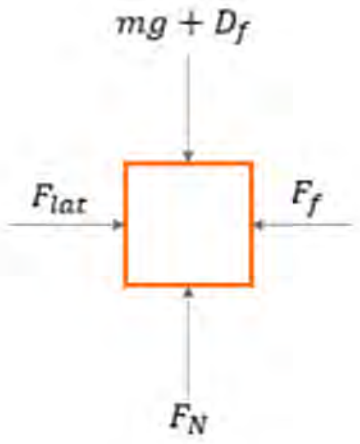

Figure 3.2.6 - Free Body Diagram of Vehicle

$$\mu F_N = \frac{v^2 m}{r}$$ *Equation 3.2.3*

$$F_N = mg + D_f$$ *Equation 3.2.4*

$$D_f = \frac{v^2 m}{r\mu} - mg$$ *Equation 3.2.5*

Equation 3.2.5 is the derived equation for downforce. Using test data without the wing, D_f is set to zero and friction factor, μ can be solved. It is estimated that friction factor falls between 0.975 and 1.05. Figure 3.2.7 below shows the relationship between the estimated downforce as a function of friction factor. The red lines represent the bounds of the friction coefficient. As can be seen, the downforce is very dependent on the friction coefficient; a small change in μ has a large impact on the downforce.

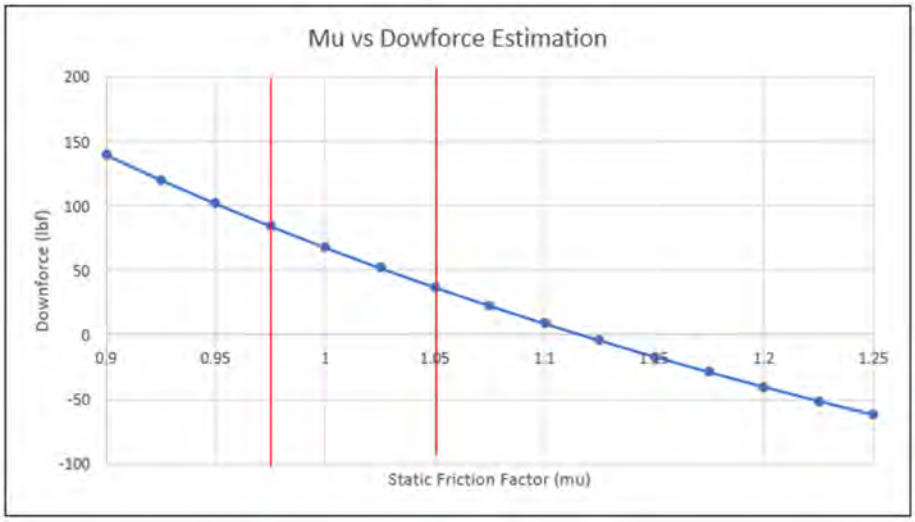

Figure 3.2.7 - Downforce Estimation

Implementing the data of the highest achieved lateral acceleration in the car with aero results in 38 lbf of downforce. While the two-dimensional CFD calculation estimated 26 lbf, it's important to note that Equation 3.2.5 does not consider the added static weight of the wing. When accounting for the 10 to 12 lb the wing weighs, the projected downforce at the speed tested becomes much closer to the CFD projection. Figure 3.2.8 below points out where this real-world downforce calculation lies on the above figure.

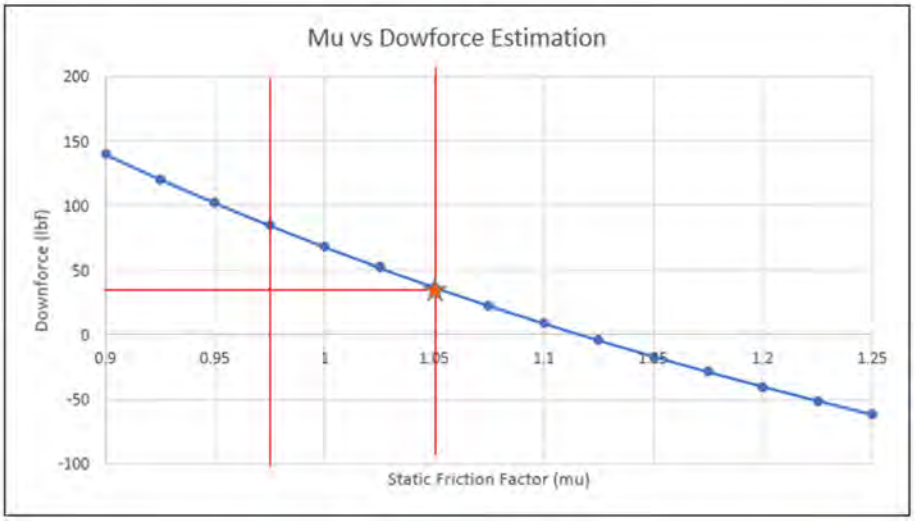

Figure 3.2.8 - Downforce Estimation with Data Highlighted

3.2.3 Autocross Testing

3.2.3.1 Autocross Testing Plan

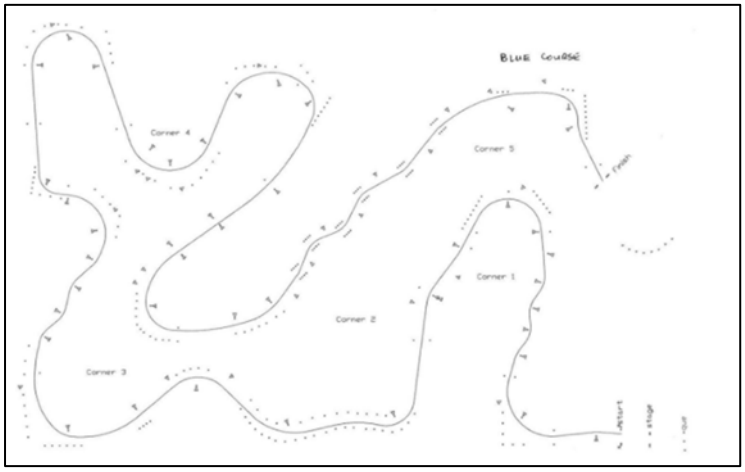

Figure 3.2.9 - FSAE 2012 Lincoln Autocross Track Layout

The final form of testing took place using and autocross style track set up in traditional FSAE style. The autocross track serves as a combination of both the straight-line testing and cornering testing. Track configuration will use cones to set up different radii turns, different length straightaways with slaloms set up in some locations. The goal is to have a quicker lap time using the active front wing than without. Based on the testing in the previous sections, this goal will be met by cornering faster around turns with a higher lateral acceleration, braking later into turns with a decreased stopping distance by using the maximum air braking control mode, and by minimizing the drag in the straights by going into drag reduction mode on long straights of acceleration. Figure 3.2.9 above shows an example of an autocross track that was planned be modified and made to fit in the Wes Watkins parking lot or O'Brate stadium parking lot. Figure 3.2.10 below shows the Wes Watkins parking lot where the testing planned take place.

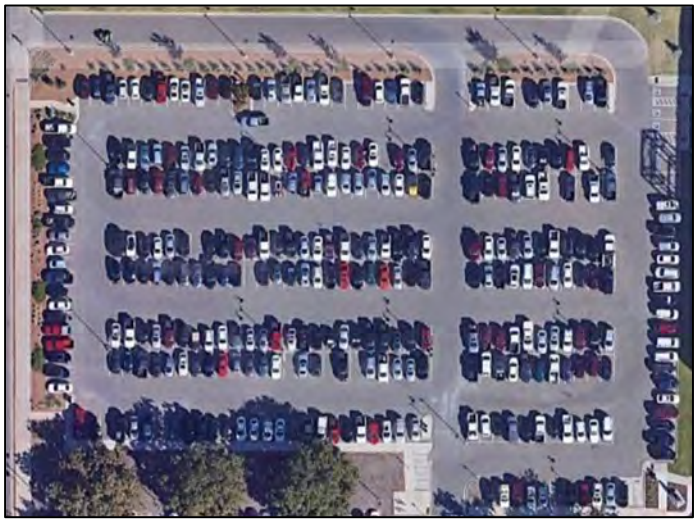

Figure 3.2.10 - Wes Watkins Parking Lot (testing location)

3.2.3.2 Autocross Testing Results

While attempting to schedule testing times at the locations mentioned in Section 3.2.3.1, the senior design and competition teams both struggled to secure either location. This led to two new track configurations at two different locations.

First, initial testing of the wing package on an autocross style track took place at the Design and Manufacturing Lab parking lot on April 10th, 2022. A makeshift track was made using the limited space; however, speeds were slow and lap times were not being paid attention to. This day mainly served to ensure the wing was functioning and allowed for any immediate tuning to be made to the wing and vehicle. As a result of this day's testing, the wing was realized to be too low to the ground and, with the excessive body roll of the vehicle, would contact the ground during cornering regardless of speed. To fix this issue, the endplates were taken off the wing assembly and cut by 3/8 inches for additional ground clearance.

Figure 3.2.11 - JRP Speedway Track Configuration

The second round of autocross testing took place on April 13th, 2022, at JRP Speedway located in Tulsa, Oklahoma. JRP Speedway is a known go-kart track in the area but allows testing of Formula SAE and other similar vehicles on their track. The track configuration, as seen in Figure 3.2.11, has tight, slow turns in some areas, wider, fast paced turns in others, and two distinct straightaways. On the front straight away, cones were spaced out 35ft apart in the center of the track to simulate a slalom and keep the speeds down. The track configuration as shown is 0.41 miles long and takes just over 40 seconds to complete. The average speed for the vehicle at this track is 30 to 35 mph while the top speed reaches 57 mph on the back straightaway.

First, two drivers got in the vehicle and spent 7 minutes driving the track and getting familiar with the car. This was done without the wing package on the car. Driver one then got back in the vehicle and was timed for four hard, fast laps, pushing the car to its limit, ensuring they got all the performance able out of the vehicle. Driver two then repeated this process. This marked the benchmark for the vehicle without aero, any testing done with the wing on would be compared to these laps. The wing package was then put on the vehicle. The following process then repeated itself for the different driving modes. Table 3.2.2 shows the average results of the two drivers with the varying levels of deployments.

	No Wing	Neutral (static)	High Downforce	Discrete
Average lap time	43.00 seconds	42.20 seconds	40.81 seconds	40.86 seconds

Table 3.2.2 - Autocross Lap Time Results

As seen in Table 3.2.2, the addition of the wing in the reduced drag mode yields a 1.87% quicker lap time. Once again, the higher deflection angles were much better an improved the performance by over 5%. Taking this unique set of results from JRP and applying it to a more traditional environment allows for a calculation of how much better this vehicle would have placed at competition.

The Bullet Racing 20.5 was only used in competition at the UTA Autocross weekend in November of 2021. The course from this event is shown in Figure 3.2.12 below, and the best finish for the car was in 26th place. Applying a correction factor of 1.67 to account for the size differences between JRP Speedway and this track, the car's lap time would decrease by approximately 3.66 seconds, which means the car would now finish in 12th place overall, a substantial increase.

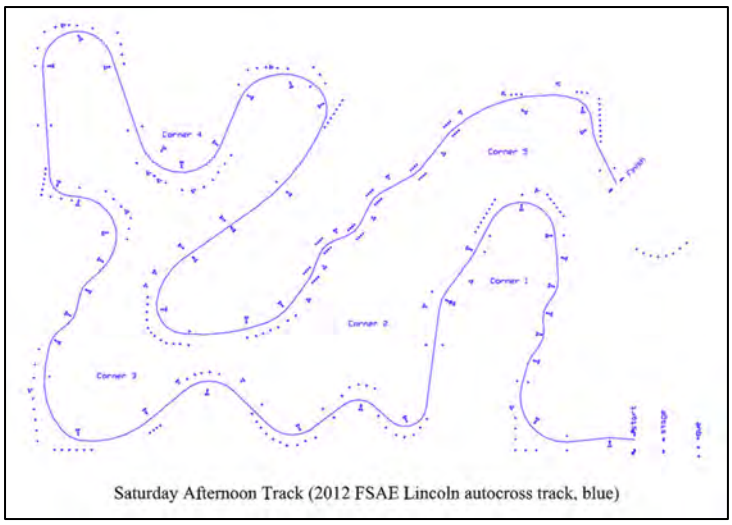

Figure 3.2.12 - 2021 UTA Autocross Track

3.2.4 Vehicle Handling Characteristics

To understand how the addition of the front wing impacts the vehicle handling from a qualitative standpoint, a foundational knowledge on vehicle handling must be set. To achieve the best speed, a driver must be comfortable and confident. A driver will only gain confidence after getting lots of seat time, but more importantly, seat time in a car that they can push and believe in. There are three versions of handling: understeer, oversteer, and balanced.

3.2.4.1 Understeer

On one end of the handling spectrum is Understeer (tight). Understeer occurs as the front wheels are turned to corner, but the vehicle continues in a straight direction. There are many causes for understeer. In a good handling car, understeer usually happens when the driver misses the corner and doesn't enter correctly. In a car in which understeer is inherent, it occurs because there is a significant lack of front-end grip and an overwhelming amount of rear traction. This combination is detrimental to corner speed, vehicular momentum, front tire wear, and most critically, driver confidence. There is nothing more demoralizing that an understeering car. The reason it is so hard

on driver confidence is that it limits the amount the driver can push into the corner. After the driver has made the corner, the car will still want to push out, away from the apex of the corner, further hurting corner speed. The two ways to stop a car from being tight, or experiencing understeer, is to use lots of brake in the corner to keep it settled in the racing line, or to change suspension setups. If one was to imagine how the car would rotate around the corner, imagine it is pivoting around a point behind the driver, in a rear engine vehicle, it would pivot more around the engine.

3.2.4.2 Oversteer

The opposite handling extreme is oversteer (loose). When a car is loose, it is wanting to turn very easily, so easily in fact that the rear end of the car begins to slide and if not corrected will induce a spin. A loose car will not develop the same lack of driver confidence that a tight car will, but it will develop as poor, if not worse lap times. The reason that lap times suffer so greatly, is that instead of driving around a corner, the car instead wants to spin the rear tires and almost float around the corner. This handling characteristic is caused by the front of the car having too much traction, while the rear of the car has none. A loose car can make driving a lot of fun, but in a competitive situation, it is ineffective and expensive. The reason it is expensive is that while in a slide, or drift, the driver is more likely to lose control of the car, thereby causing and accident, which then could hurt the car, or cause injury. The other reason is that the rear tires will be spinning and gaining lots of heat. Both will cause a significant decrease in tire life. As a run caries on, the more the rear tires will be worn, and the more loose the car will get. To correct this handling problem, simply using less throttle on corner entry/exit, and, if the problem is severe enough, a suspension adjustment/overhaul may be required. If one was to imagine how the car might pivot, a loose car will pivot about a point by the drivers' feet, or close to the front axle.

3.2.4.3 Balanced Steering

A balanced handling vehicle will display and feature the perks of both a tight and a loose car. The car will feel easy to rotate around the tightest of hairpins, slaloms, or high-speed corners, but will still be stuck in a straight line and powering through the corner at speed. The ability to keep momentum high in the corners is critical to lap time, and any extra steering, brake, or throttle input needed to force the car to turn will take away from the momentum. Carrying more momentum into and through a corner will also maximize the g-loading that the tires can take, thus optimizing the grip in total. A well-balanced car will be able to push every corner to the maximum g-load available and make the corner repeatedly. It will also be able to drive off the corner and enter the corner with control and drive, meaning one can stay in the gas more and feel secured that the car will do what you tell it to.

3.2.4.4 Bullet Racing 20.5 Handling

The test vehicle, Bullet Racing's "20.5" FSAE car, in standard form without the wing is, quite simply, a poor handling racecar. The reason it is not a good handling vehicle is to do with its inability to transfer weight in corners, poor suspension geometry, and the wheels and tires being used having more sidewall flex than designed. As a result of bigger wheels and tires being required for the increased ride height, more sidewall flex occurred, inducing body roll. The car had two similar, but different handling characteristics in right and left corners, but one major overarching

theme, understeer. The car was extremely tight and felt like it was pivoting around the rear differential. Along with being extremely tight, the car would pick up the left front tire in hard left corners and lock up the left front in almost every corner. This made the car extremely tricky to drive and very difficult to gain confidence and comfortability. In the skid pad testing, it was most obvious the difference between how the car reacted to right- and left-handed corners. In the right section, the car would stay as stable as a heavy understeering car could be expected to. In the left-handed section, the vehicle would aggressively and suddenly become bound up, and drive in a straight line until the throttle was relaxed and heavy braking introduced. These handling characteristics also manifested in different ways, while doing auto-cross testing at JRP. In the slow, hairpin styled corners, the front end wanted to chatter the tires and take significant encouragement to go around.

As soon as the drivers pulled the car onto the testing track, either auto-cross, or skid pad, they knew instantly that the car's handling ability and personality had changed. To start every winged test, the wing was set in static, neutral mode. This means that the wing is always producing the least amount of drag, but at the same token, the least amount of downforce. The results shown 3.2.5, show the decrease of lap time, but in a driver's point of view, the car had finally become tamed. The most notable of the changes is the swing in balance of the car, particularly on corner entry to mid-corner. With the wing in the neutral position, the front end had tremendous amounts of grip and would go where the drivers pointed the steering wheel.

When the drivers finished their stint in neutral, they would then be sent back out in high downforce mode, the second tested static mode. While having more drag than neutral mode, much more downforce was made as well. This made the car feel even better. The front of the car felt planted, and it made the car's handling and spirit come to life. The only negative effect felt was a balance shift so far forward that the car would start to get loose on corner entry if the driver did not use enough throttle. The shift of the pivot points now felt like it was in the center of the car, under the driver's seat, exactly where it's supposed to be. Because the drivers were able to feel such a remarkable change in the car, the confidence behind the wheel also grew. Because the drives felt more confident, they drove faster and driving faster increases downforce resulting in even more confidence.

The next two stints, each driver ran the active modes, discrete and continuous modes. Starting with discrete mode, the car behaved almost exactly like the car had with high downforce. It felt good and planted to the track, the rear of the car could get loose if the driver wasn't aggressive enough on corner entry. Although lap times may have been slightly lower, the couple tenth's difference could be assigned to driver confidence as much as actual improvement of handling. Once continuous mode was selected, the change in the car was almost as drastic as when the wing was first put on the car. The continuous mode was only used in skid pad testing, but the difference was notable. Because of the logic behind the continuous mode constantly reading the change in lateral acceleration, any change in steering, brake, throttle position, or any bumps on the track would cause a change in the deflection angle of the active elements of the wings. Because the wings would go from max deflection to a lower mid deflection almost randomly, the front of the car begin to feel unstable. Instead of feeling planted and stuck in the track, the front end began to feel like it was on a very slippery surface and the driver would chase the nose around. The obvious

solution meant gentle driving was needed to get the most out of it, with no alterations in the turning radius or throttle position. While this was liked by some drivers, others preferred the static high downforce mode for its predictability and constant nature. Ironically, the driver who preferred the high downforce mode, was faster in continuous mode, while the driver who liked continuous mode the best, was fastest in high downforce.

3.2.5 Overall Testing Results

Overall, the front wing package produced positively affects the balance of the BR20.5 FSAE car by making it easier to drive with the increased downforce allowing for a significant decrease in lap time. Both active aero modes—discrete mode and continuous mode—showed similar performance to the static, high downforce mode. The current problems with the active aero modes are downforce predictability and consistency. Based on the current state of this front wing package, the drivers recommend the high downforce mode. While the BR20.5 showed a significant increase in performance, future Bullet Racing cars will be able to utilize the full advantages of this front wing package as the suspension geometry is corrected and the car's designed tire is used. Solving these issues will allow the vehicle to have proper tire contact with the racing surface and greatly reduce the body roll of the vehicle—keeping the front wing level to the ground and improving downforce consistency.

Given the limited number of laps at JRP Speedway, potential for a drag reduction mode showed promise. This would be a semi-active, driver-controlled mode. The front wing would be in a high downforce configuration unless the driver activates a button, moving the active elements into a low drag mode for long straightaways. This would increase the top speed of the vehicle on the straights while providing all the downforce needed on the front wheels at every other time. Spoiler Alert's advice to the competition team—Bullet Racing—is to explore the idea of this more as it is outside the scope of this initial project. Spoiler Alert also recommends conducting more tests with the continuous mode as there is room for improvement and can potentially achieve greater performance than the static, high downforce mode.

4 Project Management

4.1 Risk Management

A risk matrix was used to establish the risks of the project and evaluate their impact. The matrix used can be seen in Figure 4.1.1. For each risk, a likelihood and impact are assigned. The risk level for each event is then established and mitigation strategies are arranged. Using this risk matrix, a negligible impact has a low risk level regardless of impact, but a severe impact can have medium to high-risk while being unlikely to happen.

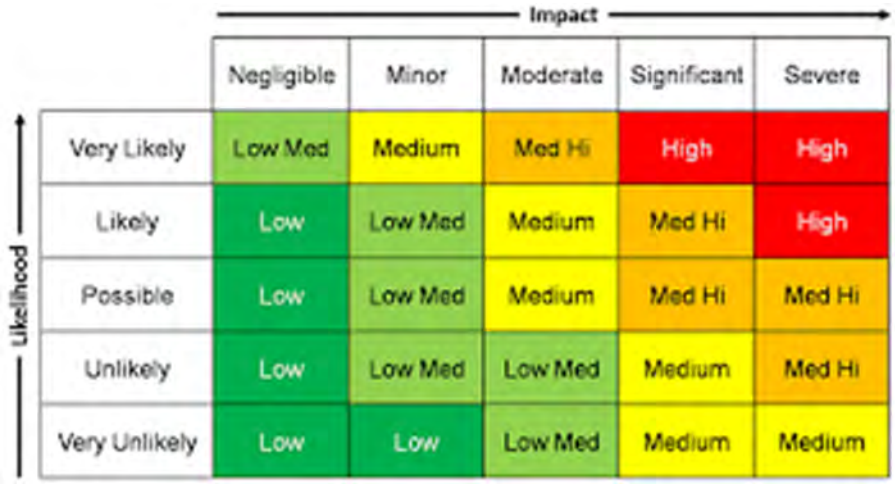

Figure 4.1.1 - Risk Matrix

Some safety risks for this project are tabulated in Figure 4.1.2 below and show the risk level and mitigation strategies instituted. An example from the list below includes the risk of a flat tire. A flat tire during testing could have hindered the project delivery and have a severe impact to the car, people surrounding it, and the driver. While the risk was possible, a mitigation strategy used to reduce the likelihood was to walk the track before the car was tested. Walking the track will ensure no objects or foreign debris are in the racing path and can puncture a tire. Another strategy is to sweep the track surface before driving a vehicle on it. At an official FSAE event, before an event starts people will walk the track with brooms and sweep all gravel and loose material out of the set path. This helps minimize the opportunity for punctures and reduces the overall risk level.

Risk	Type	Likelihood	Impact	Risk Level	Mitigation
Flat tire	Project delivery	Possible	Severe	Medium High	Walk the track and Pre-check tires to ensure nothing out the ordinary
Wing not being able to shear off properly	Safety/ Project delivery	Unlikely	Moderate	Low Medium	Checking bolt and build design to make sure it can shear off properly.
Tire Locking Up	Project delivery	Unlikely	Moderate	Low Medium	Hit the break, keep things under control, and hold the tires at the point of them locking up.

Figure 4.1.2 – Safety Risks and Mitigation Strategies

The risks listed below in Figure 4.1.3 are electrical risks that may hinder the project delivery, such as power deficiency problems and servo failures. While no risks listed were above medium risks, mitigation strategies were still documented to reduce the risk level.

Risk	Type	Likelihood	Impact	Risk Level	Mitigation
PCB Error (design or fabrication)	Project delivery	Low	Severe	Medium	Concurrent development of a protoboard alternative
Power Deficiency	Project delivery	Low	Moderate	Medium	Prepare an alternative tunable voltage regulator
PCB Power Supply Lines Inverted	Project delivery	Medium	Low	Low	Resolder power connectors in the correct orientation
Servo Fails to Resist Air Pressure	Project delivery	Low	Moderate	Low	Reconfigure internal servo gearing to increase torque

Figure 4.1.3 – Project Delivery Risks

Lastly, scheduling and time management issues are tabulated in Figure 4.1.4. Some of these risks played major parts during the course of this project such as having team members unavailable for health reasons or severe weather shutdowns. While the risk levels are medium or medium high, mitigation strategies were developed and deployed by having team meetings on Microsoft Teams and working from home during university weather shutdowns. During the critical design phase, the team had to present the CDR presentation on teams due to inclement weather. Work hours were also shifted to make up for lost time from multiple snow days. Some other issues listed are the risks we faced, such as car issues. During testing at Life church in Stillwater, a problem developed with the car and began leaking oil onto the skidpad. The car had to be retired for the day and testing was halted for the time being until the issue was resolved. The biggest risk encountered involved university parking services. After reserving certain parking lots on campus to conduct testing, and receiving confirmation of the reservation, parking services would annonce the day of they would not be able to reserve the lot. The team then searched for different locations until solutions were found. While testing locations had a medium to high risk level, ultimately, the problemwas non-impactful to the testing and conclusions of this project.

Risk	Type	Likelihood	Impact	Risk Level	Mitigation
Having a Team Member out for health	Project Delivery/ Schedule	Very Likely	Moderate	Medium High	Having Microsoft teams available so the work can continue
Severe weather shutdown	Project Delivery/ Schedule	Possible	Moderate	Medium	Have makeup days scheduled/ using teams
Engine oil leak	Project Delivery	Possible	Severe	High	Had to shut the car down, until we could repair the leak.
Not being able to test with parking services	Schedule	Very Likely	Moderate	Medium/ High	Used Life Stillwater, and JRP to test.

Figure 4.1.4 – Time Management Risks

4.2 Cost Report

The overall budget for this project is $10,000 with several major costs from the start such as new wheels, tires, battery, and fabrication materials. These items account for $4,595 of the budget but were necessary for the implementation and fabrication of the project. Many items can take weeks or months to arrive, therefore, waiting to purchase them is not an option.

For future production, costs would be significantly less than for the first version. In this table shown below, this shows a cost breakdown between the three main stages of this project. This does not account for labor cost or tool maintenance. This is strictly the cost of raw materials needed throughout the project.

Layup Process:			
Material (Unit)	Qty	Cost/Unit	Total
Carbon Fiber (roll)	31.25	49.95	1560.94
RS-WB-400 (gal)	0.46	55.15	25.37
RS-CS-215 (gal)	0.21	59.63	12.52
BF-D316 60" (lbs)	63	8.25	519.75
Divinycell 5lb Foam Core	2	40	80
Lord 310 A/B Epoxy	2	21	42
Trim Edge	1	10	10
SEAL-D313Y 1/2 CS (CS)	0.25	165	41.25
Breather Bleeder (roll)	0.25	135	33.75
RF-D5300 P3 48" (roll)	0.25	910	227.5
	Total Layup Cost:		2553.08
Mechanical Process Cost:			
Nuts	48	0.25	12
Bolts	48	0.25	12
Washers	65	0.15	9.75
Carbon Rods	4	4.49	17.96
Ball Joints	8	12.95	103.6
Bearings	10	12.99	129.9
Bushings	6	27.07	162.42
Wheel Weights	10	0.5	5
	Total Mechanical Cost:		452.63

Electrical Cost:			
Servo Motors (35kn)	4	34.99	139.96
Vibration Bushings	4	1.26	5.04
Vibration Washers	4	0.34	1.36
Machine Screms 1/8'	4	0.17	0.68
Nylock Nuts	4	0.042	0.168
1/8" Washers	9	0.2	1.8
Insulated Terminals (Male)	2	10.06	20.12
Insulated Terminals (Female)	2	8.36	16.72
Ring Terminal	13	0.77	10.01
Wire	8	14.82	118.56
IMU	1	6.99	6.99
ItsyBitsy M0 Express	1	11.95	11.95
2-56 Bolts/Nuts	16	0.26	4.16
Flame Retardant Sleeving	1	36	36
	Total Electrical Cost:		373.52
	Total Unit Cost:		3379.23

In summary of total cost, we had ~$140 left from the given $10,000 budget. After completion of the assembly, we had ~$1,500 left which we then used to replenish materials and worn tools that were borrowed from the DML or competition team.

4.3 Project Plan

The project plan was a fluid document as the team learned path dependencies and true task durations throughout the detailed design phase; this trend continued moving into the fabrication and testing and validation phases. In this overview of the project plan, the timeline and completion of each project phase is reviewed to summarize the lessons learned in project management by the team. The following Gantt chart images show the planned timeline as gray while the actual timeline as completed is shown in light blue and teal.

For the aerodynamics sub-team, 3D CFD analysis proved to be more computationally intense than time allowed and overall, outside the scope of the project. After spending multiple weeks attempting 3D studies, a move back to 2D CFD analysis was made and thus, a loss of time. This loss of time pushed back most Aero team tasks in the detailed design phase. Regardless, the CFD analysis provided valuable results and allowed the aero team to finalize the active wing element placement and incidence angles in time for fabrication to begin on schedule. Aero team's detailed design phase project plan is shown below.

	Task Name	Duration	Start	Finish
1	**Conceptual Design**	**13 days**	**Wed 1/12/22**	**Fri 1/28/22**
24	**Detailed Design**	**25 days**	**Mon 1/31/22**	**Fri 3/4/22**
25	**Aero**	**25 days**	**Mon 1/31/22**	**Fri 3/4/22**
26	Conduct 3D CFD integrating front wing designs with the full car assembly	11 days	Mon 1/31/22	Mon 2/14/22
27	Optimize active wing element incidence angles for each configuration	8 days	Mon 2/7/22	Wed 2/16/22
28	Finalize wing element placement and location	3 days	Fri 2/11/22	Tue 2/15/22
29	Manufacture carbon fiber coupons for material strength testing	5 days	Fri 2/11/22	Thu 2/17/22
30	Coordinate with mech team for system mounting and integration	25 days	Mon 1/31/22	Fri 3/4/22
31	Establish manufacturing method and protocol for wings	4 days	Tue 2/15/22	Fri 2/18/22
32	Establish manufacturing workplan	2 days	Mon 2/21/22	Tue 2/22/22
33	Use CNC router for main wing plug	1 day	Wed 2/23/22	Wed 2/23/22
34	Make fiberglass mold for main wing	3 days	Thu 2/24/22	Mon 2/28/22
35	Use CNC router for minor wing plugs	3 days	Mon 2/28/22	Wed 3/2/22
36	Make fiberglass molds for minor wings	2 days	Thu 3/3/22	Fri 3/4/22
37	Layup carbon fiber for main wing	3 days	Tue 3/1/22	Thu 3/3/22

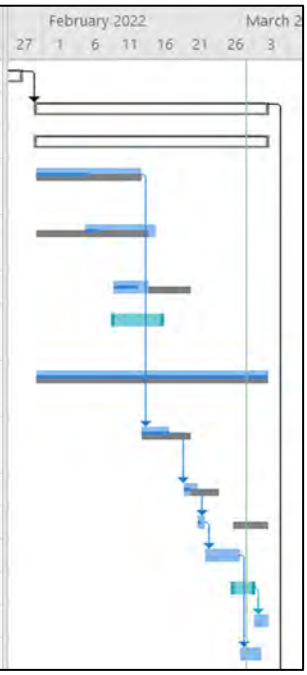

Figure 4.3.1 – Aero Detailed Design Review

For the mechanical sub-team, the wheel hub conversion plate and battery mount were designed and manufactured on schedule while the detailed CAD model of the entire mounting system took almost twice as long as expected to develop. This was mainly due to the difficulty of determining

the linkage arm lengths; the mech team tried to use Freudenstein's four bar linkage equation, but it proved to be too complex and unnecessary. A simpler calculation method was used instead. Many tasks had to be added for the mechanical sub-team because the initial plan was not detailed enough; this was a common theme for each sub-team. Mechanical team's detailed design phase project plan is shown below.

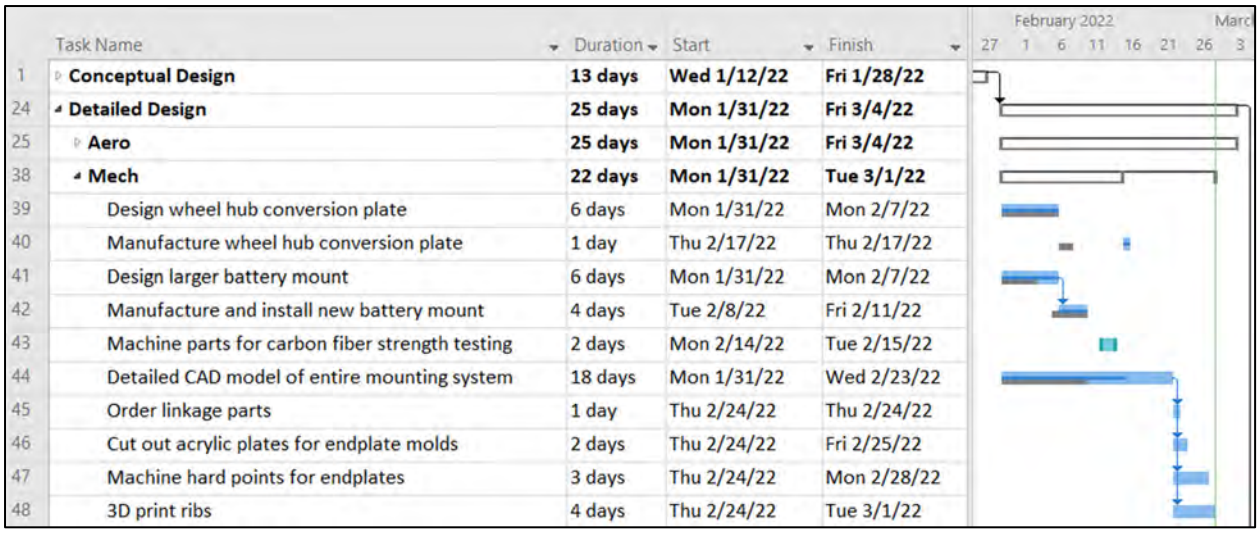

	Task Name	Duration	Start	Finish
1	**Conceptual Design**	**13 days**	**Wed 1/12/22**	**Fri 1/28/22**
24	**Detailed Design**	**25 days**	**Mon 1/31/22**	**Fri 3/4/22**
25	**Aero**	**25 days**	**Mon 1/31/22**	**Fri 3/4/22**
38	**Mech**	**22 days**	**Mon 1/31/22**	**Tue 3/1/22**
39	Design wheel hub conversion plate	6 days	Mon 1/31/22	Mon 2/7/22
40	Manufacture wheel hub conversion plate	1 day	Thu 2/17/22	Thu 2/17/22
41	Design larger battery mount	6 days	Mon 1/31/22	Mon 2/7/22
42	Manufacture and install new battery mount	4 days	Tue 2/8/22	Fri 2/11/22
43	Machine parts for carbon fiber strength testing	2 days	Mon 2/14/22	Tue 2/15/22
44	Detailed CAD model of entire mounting system	18 days	Mon 1/31/22	Wed 2/23/22
45	Order linkage parts	1 day	Thu 2/24/22	Thu 2/24/22
46	Cut out acrylic plates for endplate molds	2 days	Thu 2/24/22	Fri 2/25/22
47	Machine hard points for endplates	3 days	Thu 2/24/22	Mon 2/28/22
48	3D print ribs	4 days	Thu 2/24/22	Tue 3/1/22

Figure 4.3.2 – Mechanical Detailed Design Review

For the electrical sub-team, selecting specific sensors and actuators for purchasing took slightly longer than expected. The decision was made to design a custom PCB which required additional tasks to be added such as designing the PCB mount. These tasks pushed back writing the initial code for the control system and prevented testing of a preliminary electronic system in the detailed design timeframe. The electrical team also considered adding a GPS to the PCB to record the car's location on the track as the wing elements are actuated. This led to the possible purchase of an expensive datalogger for the testing phase; however, after discussion, the datalogger was deemed unnecessary and outside the scope of the project. The electrical team's detailed design phase project plan is shown below.

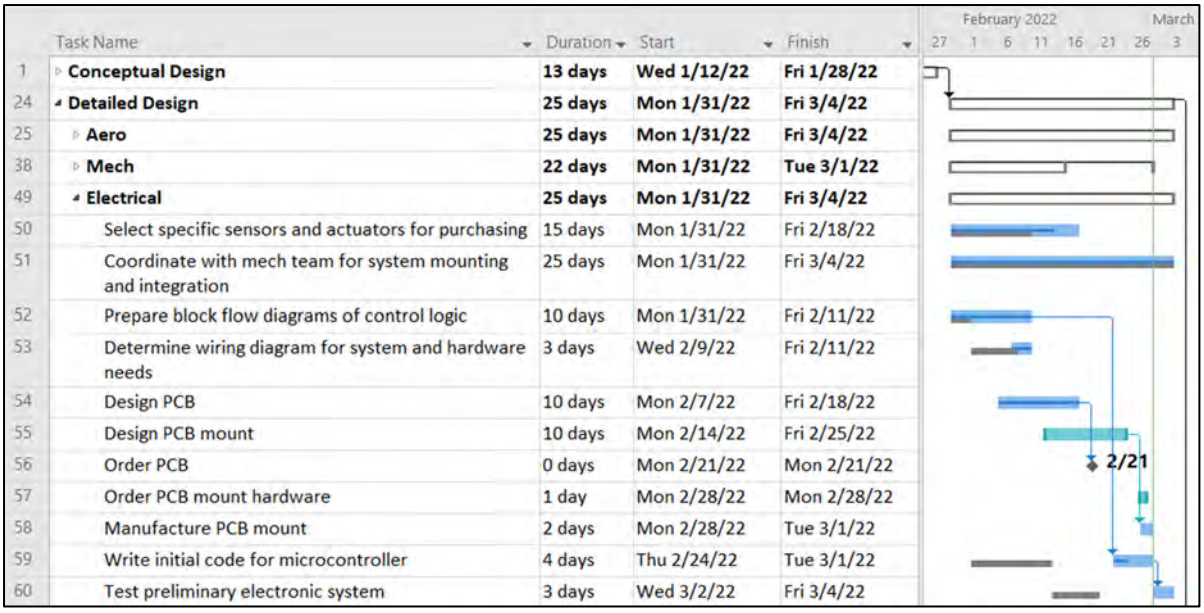

	Task Name	Duration	Start	Finish
1	**Conceptual Design**	**13 days**	**Wed 1/12/22**	**Fri 1/28/22**
24	**Detailed Design**	**25 days**	**Mon 1/31/22**	**Fri 3/4/22**
25	**Aero**	**25 days**	**Mon 1/31/22**	**Fri 3/4/22**
38	**Mech**	**22 days**	**Mon 1/31/22**	**Tue 3/1/22**
49	**Electrical**	**25 days**	**Mon 1/31/22**	**Fri 3/4/22**
50	Select specific sensors and actuators for purchasing	15 days	Mon 1/31/22	Fri 2/18/22
51	Coordinate with mech team for system mounting and integration	25 days	Mon 1/31/22	Fri 3/4/22
52	Prepare block flow diagrams of control logic	10 days	Mon 1/31/22	Fri 2/11/22
53	Determine wiring diagram for system and hardware needs	3 days	Wed 2/9/22	Fri 2/11/22
54	Design PCB	10 days	Mon 2/7/22	Fri 2/18/22
55	Design PCB mount	10 days	Mon 2/14/22	Fri 2/25/22
56	Order PCB	0 days	Mon 2/21/22	Mon 2/21/22
57	Order PCB mount hardware	1 day	Mon 2/28/22	Mon 2/28/22
58	Manufacture PCB mount	2 days	Mon 2/28/22	Tue 3/1/22
59	Write initial code for microcontroller	4 days	Thu 2/24/22	Tue 3/1/22
60	Test preliminary electronic system	3 days	Wed 3/2/22	Fri 3/4/22

Figure 4.3.3 – Electrical Detailed Design Review

For the testing sub-team, the Standard Operating Procedure, SOP, was the main focus of the detailed design phase. The document was actually completed ahead of schedule and submitted to the College of Engineering, Architecture, and Technology's Safety Review Board, CEAT SRB. This allowed for material testing to be added to the testing schedule in preparation for the Critical Design Reports. One dependency the Gantt chart did not illustrate was the need for the Aero team to manufacture the carbon fiber coupons in testing. This error did not prevent the completion of any project deliverables for the Aero team as 2D CFD studies were in the process of running and occupying the team's computers. This was, however, an important lesson and introduced the idea of thinking critically about dependencies of one team to another moving into future project phases. The testing team's detailed design phase project plan is shown below.

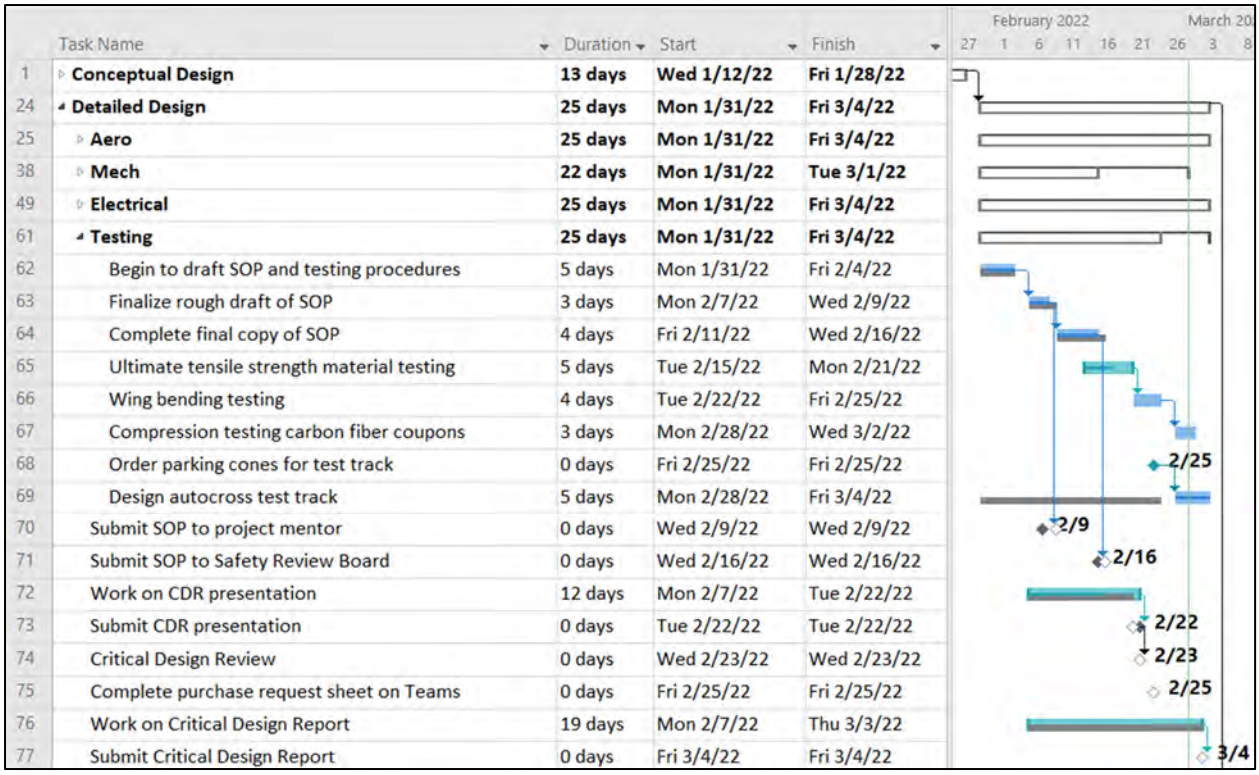

	Task Name	Duration	Start	Finish
1	**Conceptual Design**	**13 days**	**Wed 1/12/22**	**Fri 1/28/22**
24	**Detailed Design**	**25 days**	**Mon 1/31/22**	**Fri 3/4/22**
25	**Aero**	**25 days**	**Mon 1/31/22**	**Fri 3/4/22**
38	**Mech**	**22 days**	**Mon 1/31/22**	**Tue 3/1/22**
49	**Electrical**	**25 days**	**Mon 1/31/22**	**Fri 3/4/22**
61	**Testing**	**25 days**	**Mon 1/31/22**	**Fri 3/4/22**
62	Begin to draft SOP and testing procedures	5 days	Mon 1/31/22	Fri 2/4/22
63	Finalize rough draft of SOP	3 days	Mon 2/7/22	Wed 2/9/22
64	Complete final copy of SOP	4 days	Fri 2/11/22	Wed 2/16/22
65	Ultimate tensile strength material testing	5 days	Tue 2/15/22	Mon 2/21/22
66	Wing bending testing	4 days	Tue 2/22/22	Fri 2/25/22
67	Compression testing carbon fiber coupons	3 days	Mon 2/28/22	Wed 3/2/22
68	Order parking cones for test track	0 days	Fri 2/25/22	Fri 2/25/22
69	Design autocross test track	5 days	Mon 2/28/22	Fri 3/4/22
70	Submit SOP to project mentor	0 days	Wed 2/9/22	Wed 2/9/22
71	Submit SOP to Safety Review Board	0 days	Wed 2/16/22	Wed 2/16/22
72	Work on CDR presentation	12 days	Mon 2/7/22	Tue 2/22/22
73	Submit CDR presentation	0 days	Tue 2/22/22	Tue 2/22/22
74	Critical Design Review	0 days	Wed 2/23/22	Wed 2/23/22
75	Complete purchase request sheet on Teams	0 days	Fri 2/25/22	Fri 2/25/22
76	Work on Critical Design Report	19 days	Mon 2/7/22	Thu 3/3/22
77	Submit Critical Design Report	0 days	Fri 3/4/22	Fri 3/4/22

Figure 4.3.4 – Testing Detailed Design Review

Moving into a review of the fabrication phase, tasks in the project plan took longer than expected, were completed at later dates than planned, and more tasks had to be added for each sub team. This is due to the all-encompassing Murphy's Law, but the team was still able to complete the project on time. At this stage in the project, the aero and mechanical teams were all hands-on deck manufacturing the wing elements, ribs, and endplates. As outlined in Sections 2.1.4 and 2.1.5, the manufacturing process for the carbon fiber is time-consuming and labor intensive, so both teams worked together to fabricate all parts on time. The goal was to finish manufacturing and assembly a week before safety inspection for the team to have adequate time to troubleshoot any issues that arose, but this ended up happening only a day before safety inspection. For the aero team, the top of the main wing mold had to be resurfaced due to improper mixing of the tooling coat in the layup which multiplied the time required for sanding. For the mech team, the carbon fiber rods connecting the servo arms to the minor wing element arms had to be cut multiple times because the initial lengths were incorrect. Aero and mech team's fabrication phase project plan is shown below.

Task Name	Duration	Start	Finish
Fabrication	**15 days**	**Mon 3/14/22**	**Fri 4/1/22**
Aero	**14 days**	**Mon 3/14/22**	**Thu 3/31/22**
Spring break	**5 days**	**Mon 3/14/22**	**Fri 3/18/22**
Layup minor wing elements	5 days	Mon 3/14/22	Fri 3/18/22
Sand main wing mold	3 days	Mon 3/21/22	Wed 3/23/22
Prepare minor wing pieces for glueing together	3 days	Mon 3/21/22	Wed 3/23/22
Glue pieces together for minor wing with ribs	5 days	Mon 3/21/22	Fri 3/25/22
Layup main wing carbon fiber	1 day	Thu 3/24/22	Thu 3/24/22
Prepare main wing pieces for glueing together	3 days	Fri 3/25/22	Tue 3/29/22
Glue pieces together for main wing with ribs	1 day	Wed 3/30/22	Wed 3/30/22
Assemble wing kit	1 day	Thu 3/31/22	Thu 3/31/22
Mech	**14 days**	**Mon 3/14/22**	**Thu 3/31/22**
Spring Break	5 days	Mon 3/14/22	Fri 3/18/22
Weld tabs onto car for PCB mount	1 day	Tue 3/22/22	Tue 3/22/22
Cut rib and servo holes into top of main wing element	2 days	Tue 3/29/22	Wed 3/30/22
Cut carbon fiber rods to length	3 days	Mon 3/21/22	Wed 3/23/22
3D print carbon fiber rod ends	1 day	Wed 3/23/22	Wed 3/23/22
Assemble linkages	4 days	Thu 3/24/22	Tue 3/29/22
Weld tabs onto car for wing mount	1 day	Wed 3/30/22	Wed 3/30/22
Assemble and mount wing kit	1 day	Thu 3/31/22	Thu 3/31/22

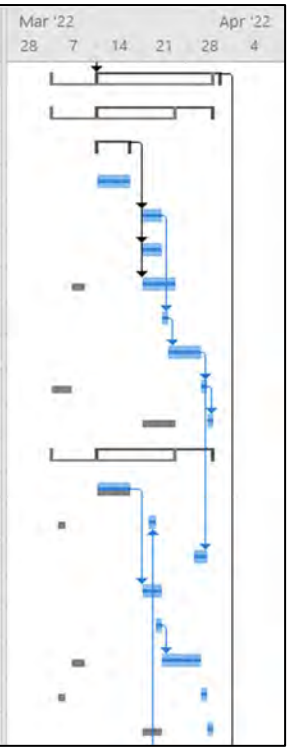

Figure 4.3.5 – Aero and Mech Fabrication Review

During the fabrication phase, the electrical team focused on wiring the wing kit, tuning the servo angles, and finishing the microcontroller code along with integrating the PCB into the car and wing kit. The testing team focused on designing test tracks and assisting with manufacturing wherever needed. Electrical and Testing teams' fabrication project plan is shown below.

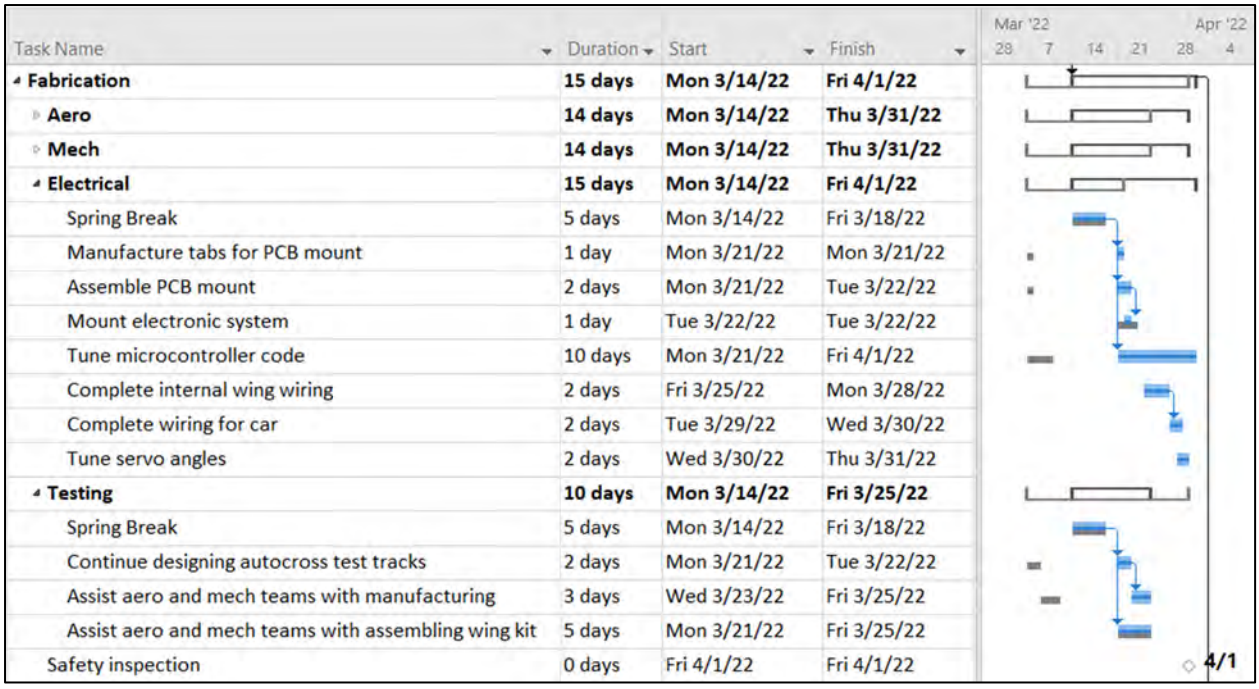

Task Name	Duration	Start	Finish
Fabrication	**15 days**	**Mon 3/14/22**	**Fri 4/1/22**
Aero	**14 days**	**Mon 3/14/22**	**Thu 3/31/22**
Mech	**14 days**	**Mon 3/14/22**	**Thu 3/31/22**
Electrical	**15 days**	**Mon 3/14/22**	**Fri 4/1/22**
Spring Break	5 days	Mon 3/14/22	Fri 3/18/22
Manufacture tabs for PCB mount	1 day	Mon 3/21/22	Mon 3/21/22
Assemble PCB mount	2 days	Mon 3/21/22	Tue 3/22/22
Mount electronic system	1 day	Tue 3/22/22	Tue 3/22/22
Tune microcontroller code	10 days	Mon 3/21/22	Fri 4/1/22
Complete internal wing wiring	2 days	Fri 3/25/22	Mon 3/28/22
Complete wiring for car	2 days	Tue 3/29/22	Wed 3/30/22
Tune servo angles	2 days	Wed 3/30/22	Thu 3/31/22
Testing	**10 days**	**Mon 3/14/22**	**Fri 3/25/22**
Spring Break	5 days	Mon 3/14/22	Fri 3/18/22
Continue designing autocross test tracks	2 days	Mon 3/21/22	Tue 3/22/22
Assist aero and mech teams with manufacturing	3 days	Wed 3/23/22	Fri 3/25/22
Assist aero and mech teams with assembling wing kit	5 days	Mon 3/21/22	Fri 3/25/22
Safety inspection	0 days	Fri 4/1/22	Fri 4/1/22

Figure 4.3.6 - Electrical and Testing Fabrication Review

After the fabrication phase was completed with the safety inspection on April 1st, the testing and validation phase began with the team fixing minor issues on the wing kit to prepare it for testing. The minor wing elements were resized to ensure proper tolerances between the endplates, and the electrical team had to install a new voltage regulator on the car because the built-in voltage regulators on the PCB failed. After the first day of autocross testing on April 10th, the endplates were resized to ensure proper ground clearance, and thread locker had to be placed on the bolts used for the wing elements to prevent them from falling out. In addition, one of the nuts in the 3D-printed carbon rod end came out and had to be reglued. Along with these minor wing failures, issues with the 20.5 Bullet Racing car slowed down the testing phase. The car leaked oil, the brake overtravel switch malfunctioned and caused the fuel pump to turn off, and the chain broke. Despite all these setbacks, we were able to complete four testing days, two for autocross and two for skid-pad, and collect a good amount of data. As the testing phase came to a close, we made an awesome marketing video and final presentation and finished the semester on a high note by winning first place at the Expo! Overall, the project was executed on time with a high degree of excellence. The testing and validation phase is shown below.

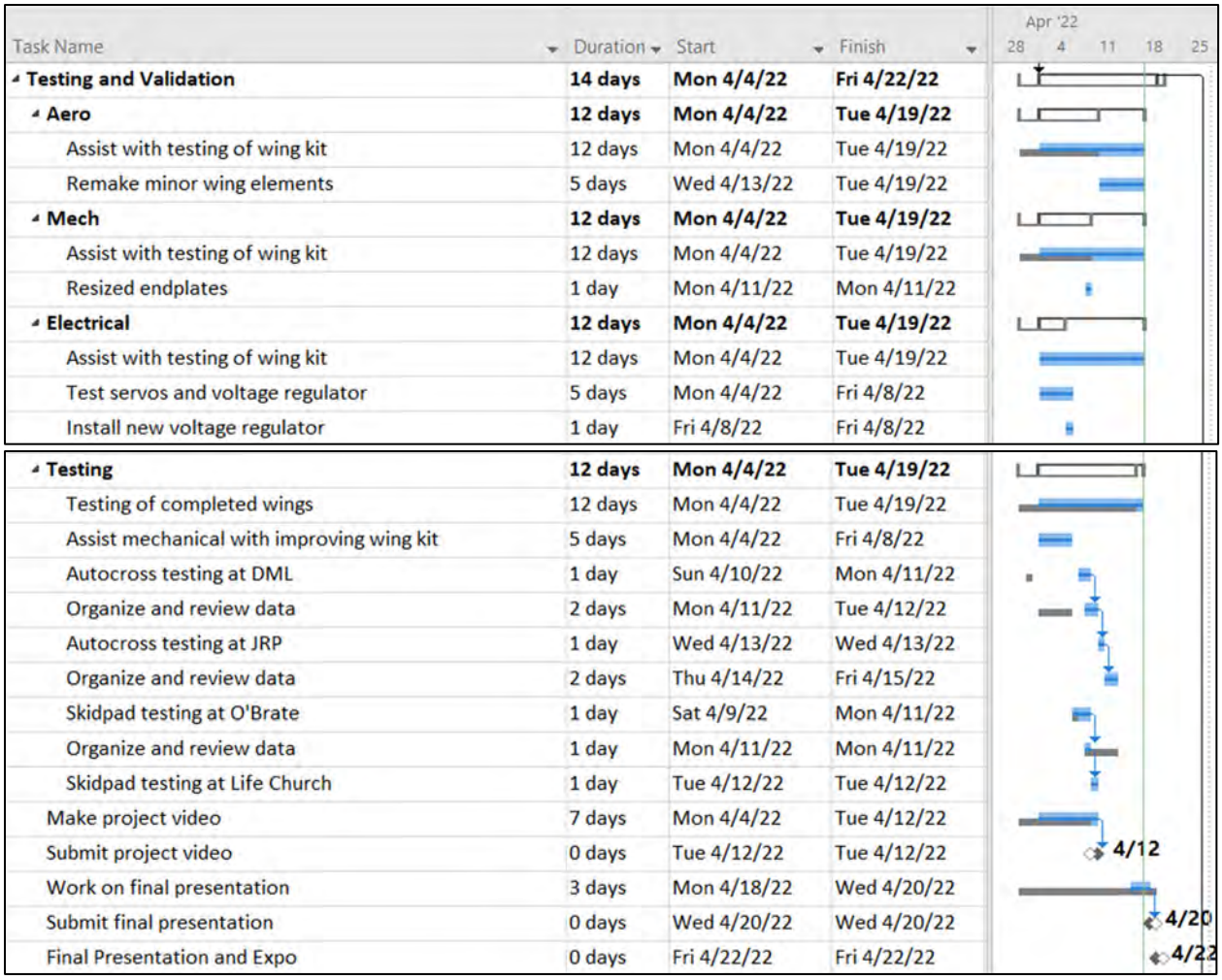

Task Name	Duration	Start	Finish
Testing and Validation	**14 days**	**Mon 4/4/22**	**Fri 4/22/22**
Aero	**12 days**	**Mon 4/4/22**	**Tue 4/19/22**
Assist with testing of wing kit	12 days	Mon 4/4/22	Tue 4/19/22
Remake minor wing elements	5 days	Wed 4/13/22	Tue 4/19/22
Mech	**12 days**	**Mon 4/4/22**	**Tue 4/19/22**
Assist with testing of wing kit	12 days	Mon 4/4/22	Tue 4/19/22
Resized endplates	1 day	Mon 4/11/22	Mon 4/11/22
Electrical	**12 days**	**Mon 4/4/22**	**Tue 4/19/22**
Assist with testing of wing kit	12 days	Mon 4/4/22	Tue 4/19/22
Test servos and voltage regulator	5 days	Mon 4/4/22	Fri 4/8/22
Install new voltage regulator	1 day	Fri 4/8/22	Fri 4/8/22
Testing	**12 days**	**Mon 4/4/22**	**Tue 4/19/22**
Testing of completed wings	12 days	Mon 4/4/22	Tue 4/19/22
Assist mechanical with improving wing kit	5 days	Mon 4/4/22	Fri 4/8/22
Autocross testing at DML	1 day	Sun 4/10/22	Mon 4/11/22
Organize and review data	2 days	Mon 4/11/22	Tue 4/12/22
Autocross testing at JRP	1 day	Wed 4/13/22	Wed 4/13/22
Organize and review data	2 days	Thu 4/14/22	Fri 4/15/22
Skidpad testing at O'Brate	1 day	Sat 4/9/22	Mon 4/11/22
Organize and review data	1 day	Mon 4/11/22	Mon 4/11/22
Skidpad testing at Life Church	1 day	Tue 4/12/22	Tue 4/12/22
Make project video	7 days	Mon 4/4/22	Tue 4/12/22
Submit project video	0 days	Tue 4/12/22	Tue 4/12/22
Work on final presentation	3 days	Mon 4/18/22	Wed 4/20/22
Submit final presentation	0 days	Wed 4/20/22	Wed 4/20/22
Final Presentation and Expo	0 days	Fri 4/22/22	Fri 4/22/22

Figure 4.3.7 – Testing and Validation Review

Works Cited

lady ada. (2018, May 27). *Introducing ItsyBitsy M0 Express - Pinouts*. Retrieved from Adafruit Learning System: https://learn.adafruit.com/introducing-itsy-bitsy-m0/pinouts

Steinberg, D. S. (2000). Designing Electronics for High Vibration and Shock. *Steinberg and Associates*.

Appendices

Appendix A: Summary of Contributions

Team Member	Contributions
Ian Babb	Linkage Design, System Drawings
Anthony Corpuz	Final Active Front Wing Configuration, Computational Fluid Dynamics Analysis, Manufacturing Plug and Wing Element Molds, Proof-reading and editing,
Carson Elmore	EHS, Control Logic, Electronic Components
Weston Gorham	Material Testing, Performance Testing, Risk Management, Bolt Pattern Conversion Plate, Manufacturing plug, overall formatting and editing
Brian Guthery	Bolt Pattern Conversion Plates, Material Testing, Driver Qualitative analysis, Manufacturing of all machined components
Gwangmin Kim	Manufacturing Plug and Wing Element Molds
Hunter Lovell	Cost Plan
Kyler Martinez	Risk Management
Erin Mathews	Linkage Design
Cameron Mendoza	Wing Material Selection
Levi Penwell	Final Active Front Wing Element Configuration
Tanner Price	Background, Problem Description
Jacob Robbins	Wiring Diagram and Harness

Team Member	Contributions
Michael Schlotthauer	Control Logic, Discrete Mode, PCB Enclosure, Project Plan, Overall Formatting and Editing
Luke Smith	2.2.3 Rib Design
Austin Wilkins	Composites Layup Knowledge Acquisition, Computational Fluid Dynamics Analysis

Appendix B: Videos

Project Marketing Video – Submitted for Grading

https://youtu.be/qDq571zTk1E

Expo Marketing Video – Displayed at Expo

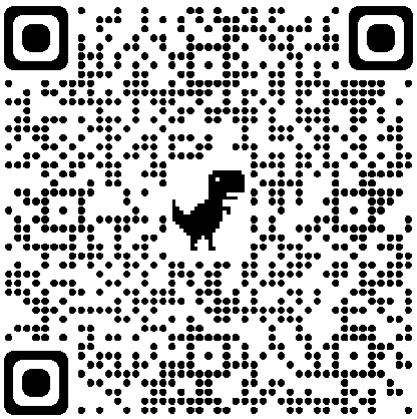

https://youtu.be/2CnIXy0sQ20

Appendix C: System Drawings

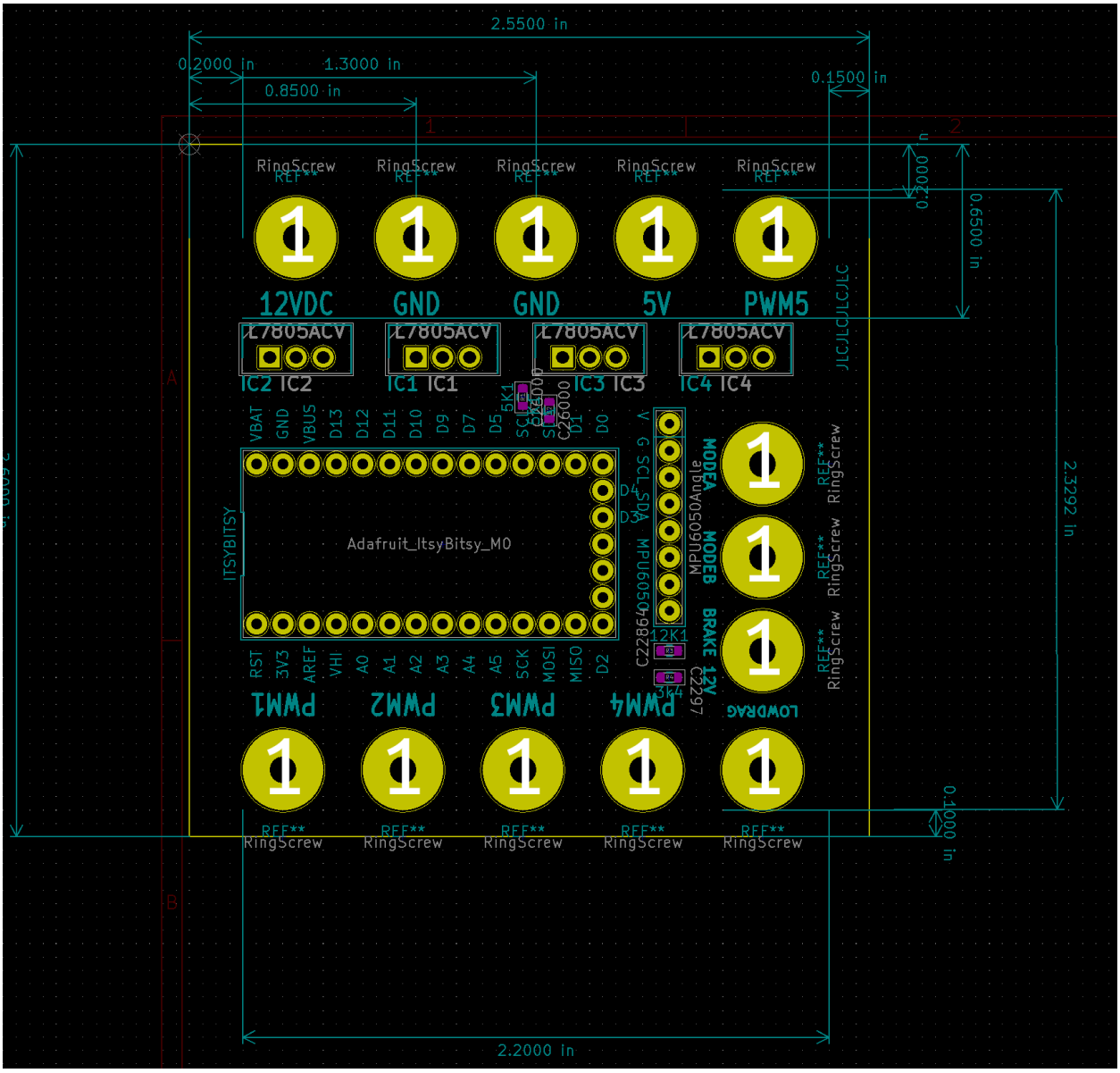

Figure 0.1 PCB physical dimensions

Appendix D: Wiring Diagram

Wing Wiring

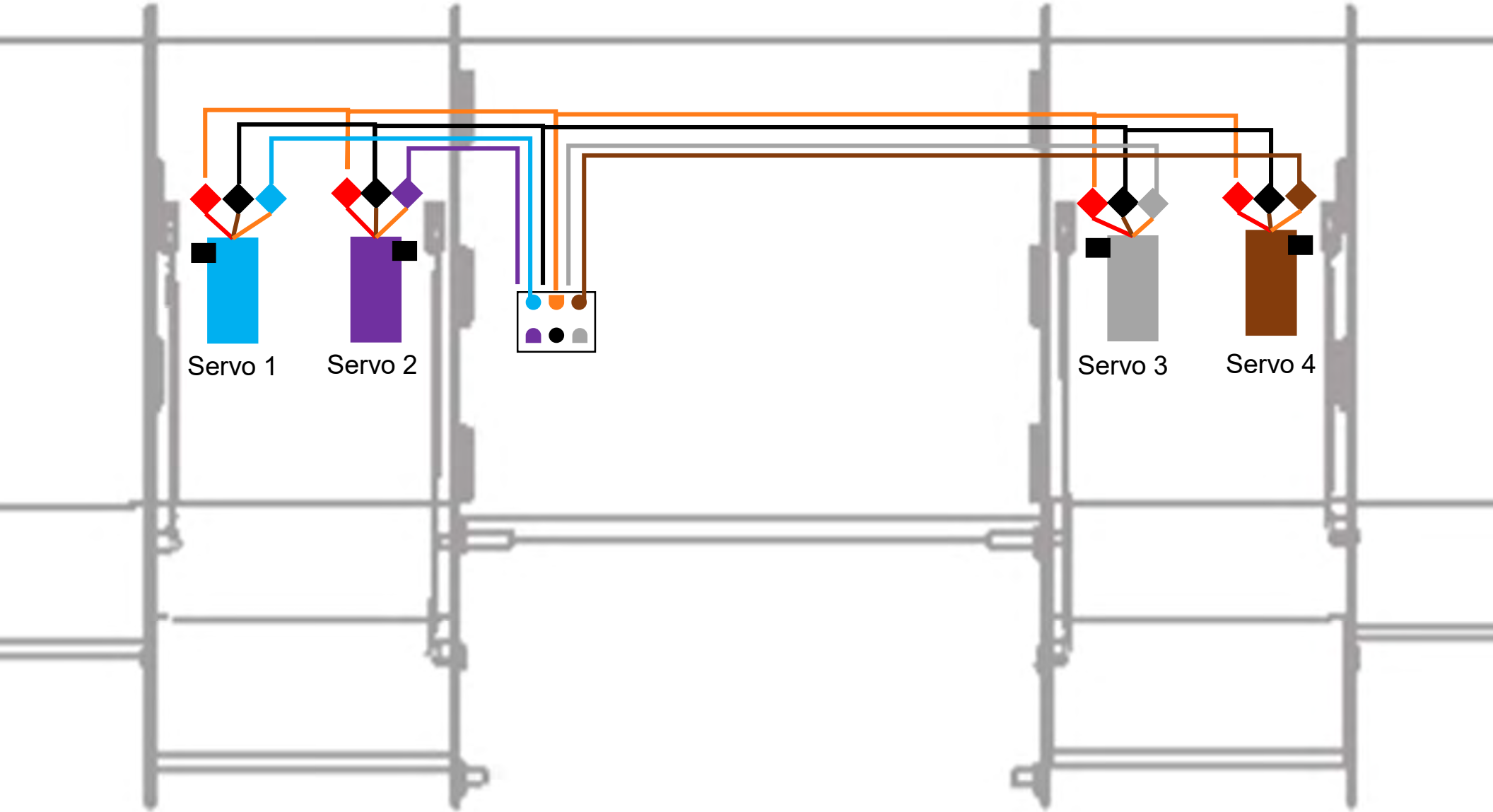

Front of car

KEY

◇ Automotive quick disconnect

Wing to PCB Wiring

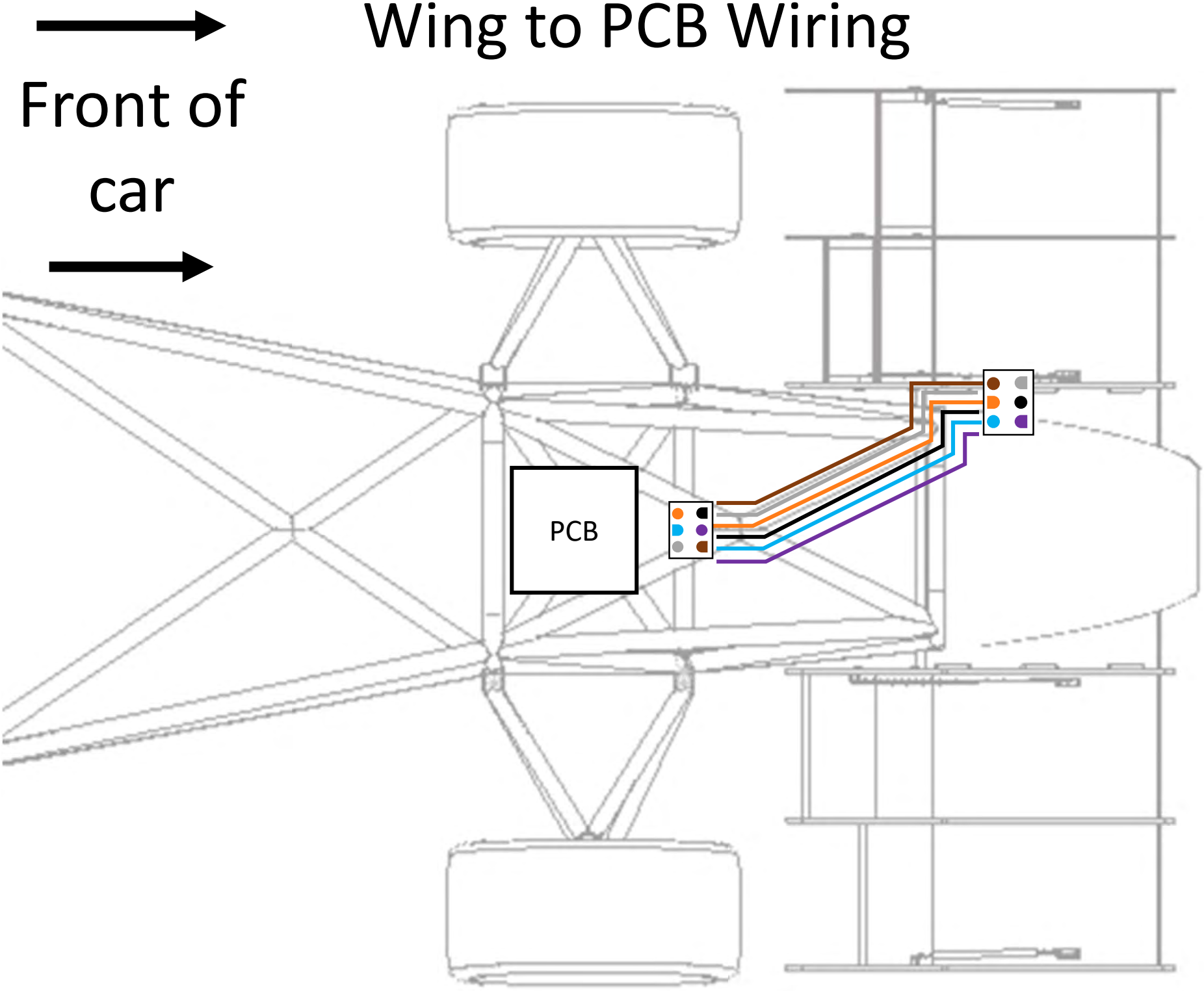

PCB Wiring

Front of car

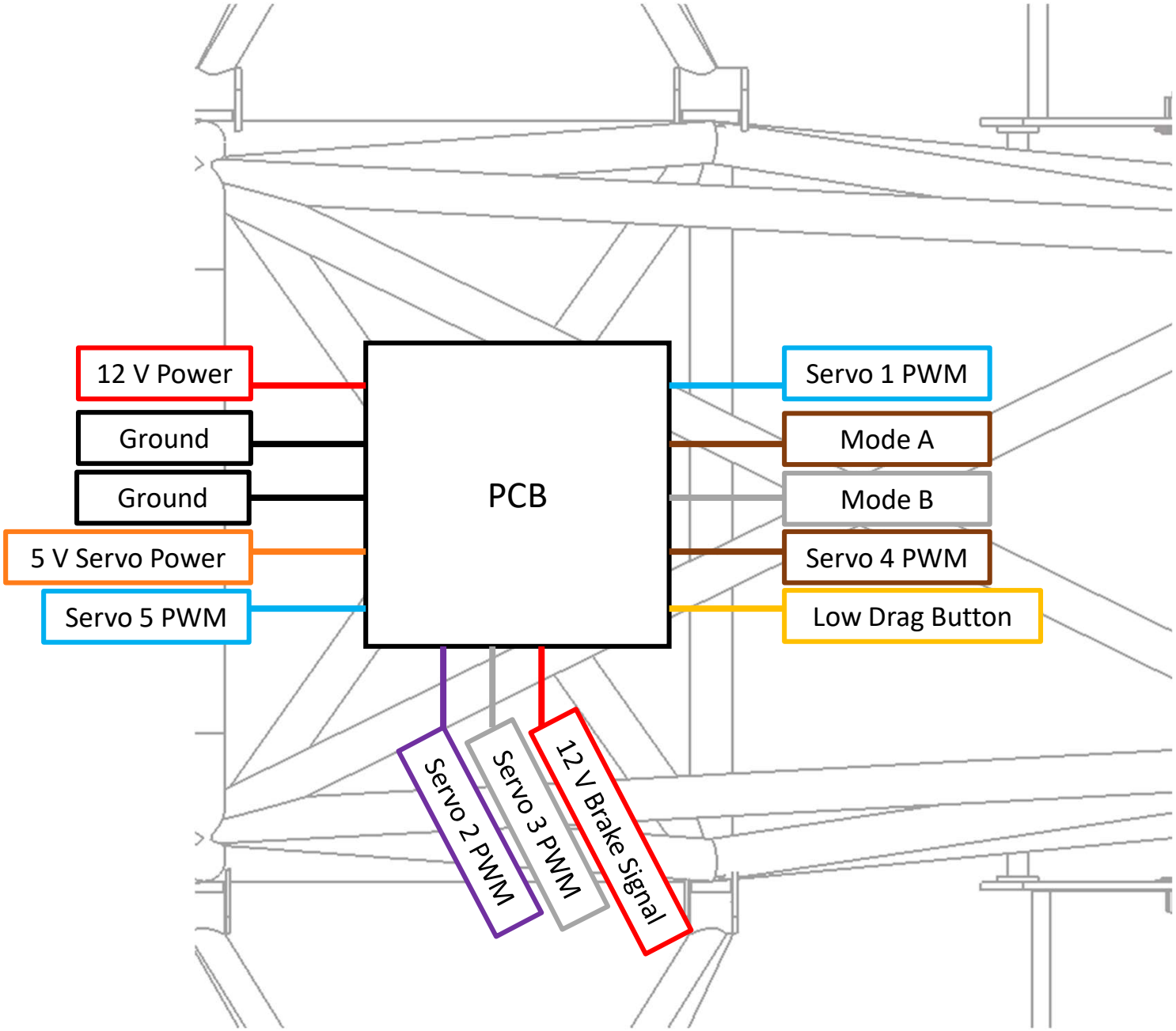

PCB Wiring

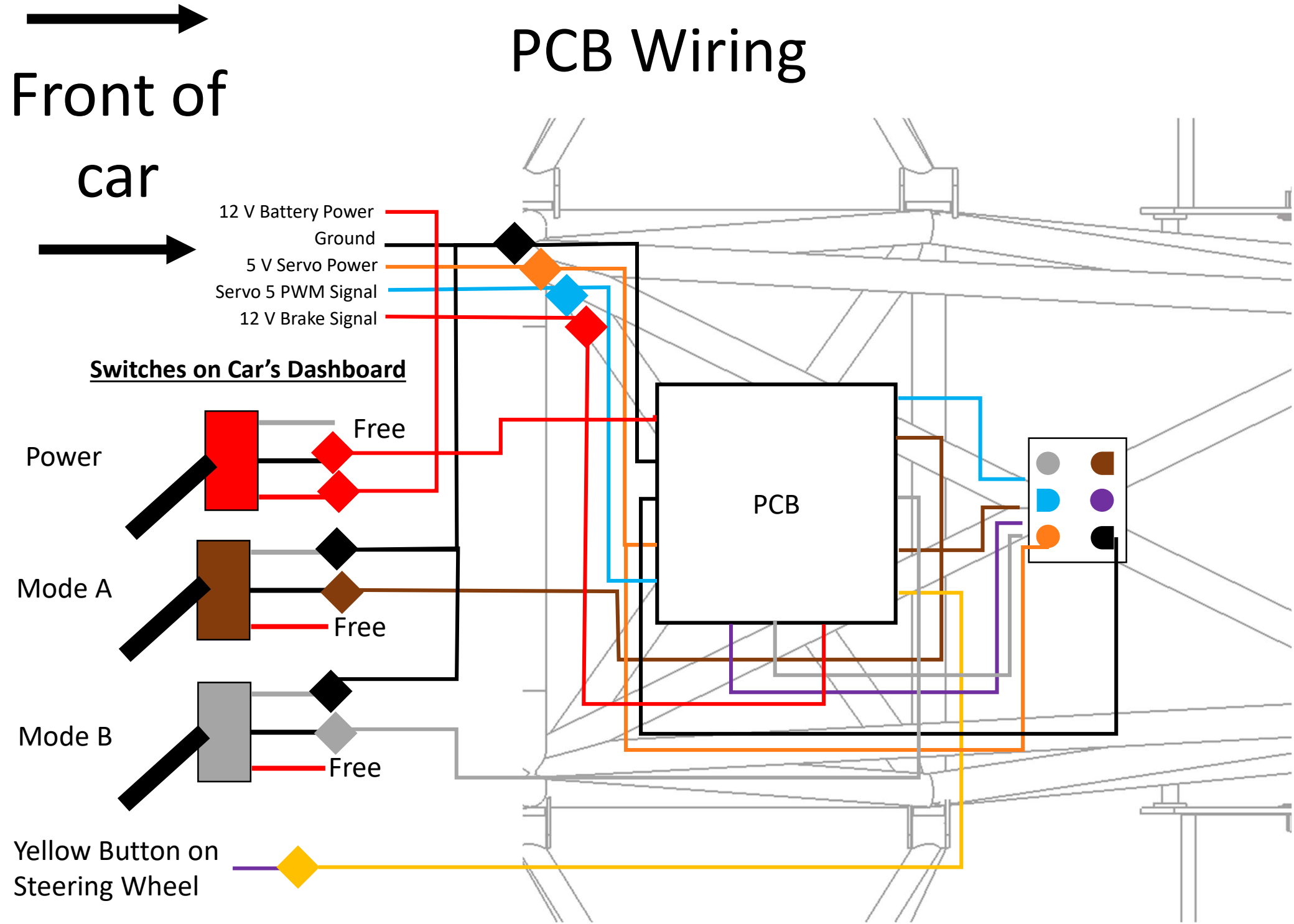
Front of car
12 V Battery Power
Ground
5 V Servo Power
Servo 5 PWM Signal
12 V Brake Signal
Switches on Car's Dashboard
Power
Free
Mode A
Free
Mode B
Free
Yellow Button on Steering Wheel
PCB

PCB to Rear of Car Wiring

Front of car

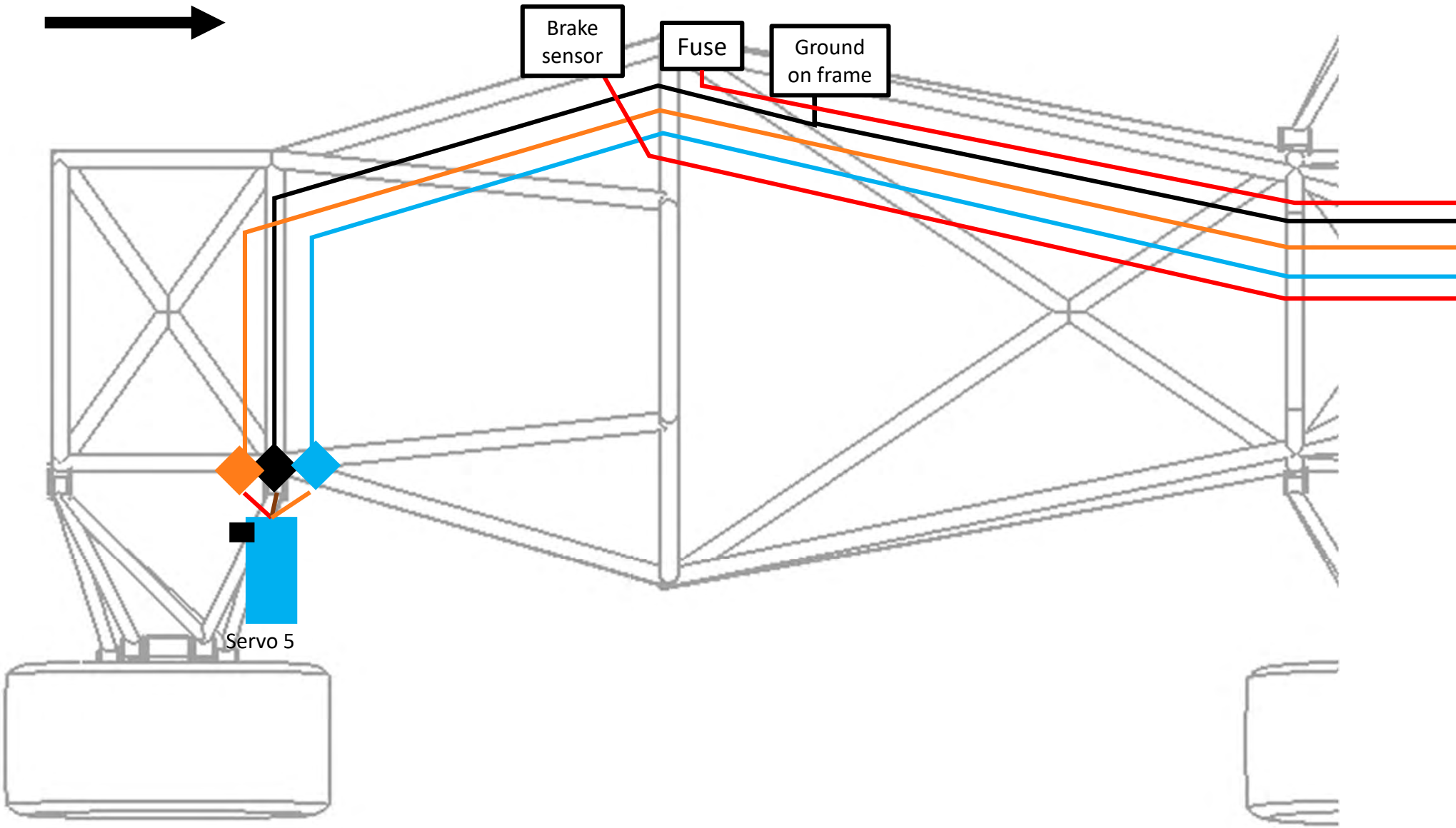

Switch Wiring

Dashboard from
driver's point of view

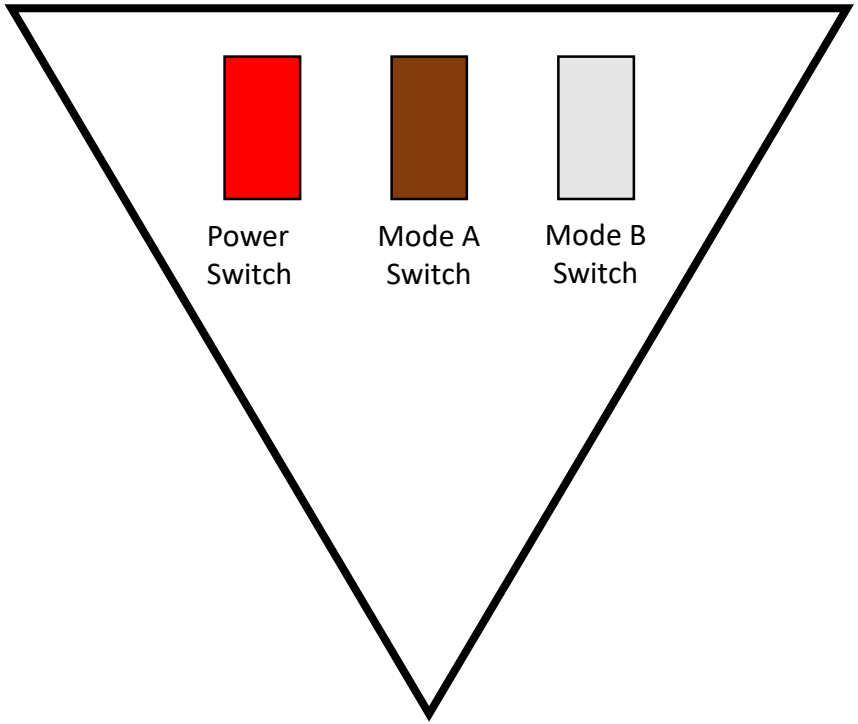

Wires from switch

Wires to PCB & from car

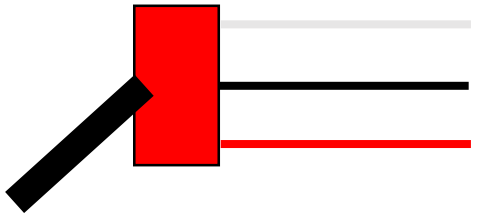

Free

5 V from voltage converter

5 V into PCB

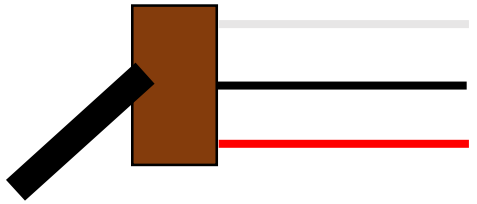

Ground

Mode A Pin

Free

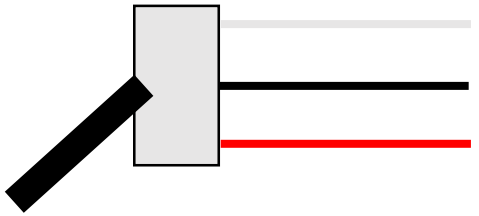

Ground

Mode B Pin

Free

Molex Connectors

Wing to Nose

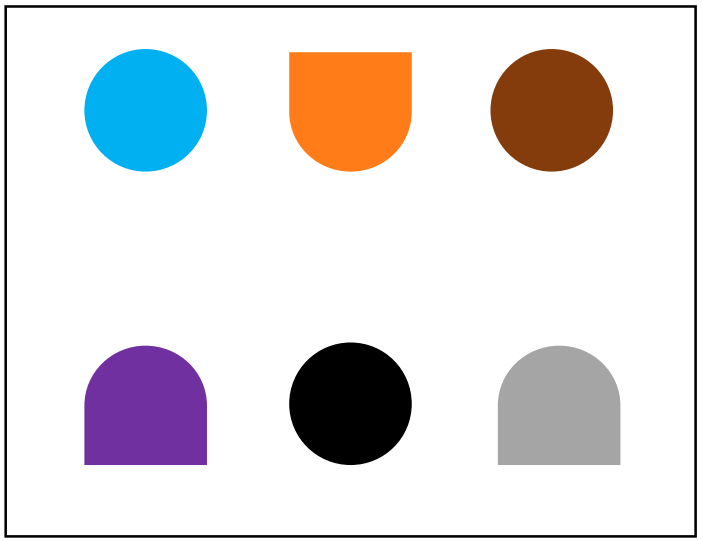

Nose to PCB

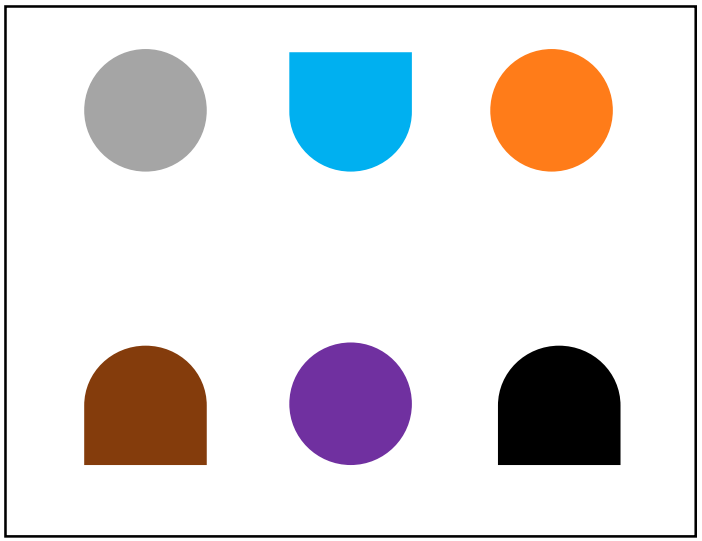

Servo 1 & 3 Orientation

Front of car →

0 degrees 90 degrees 180 degrees

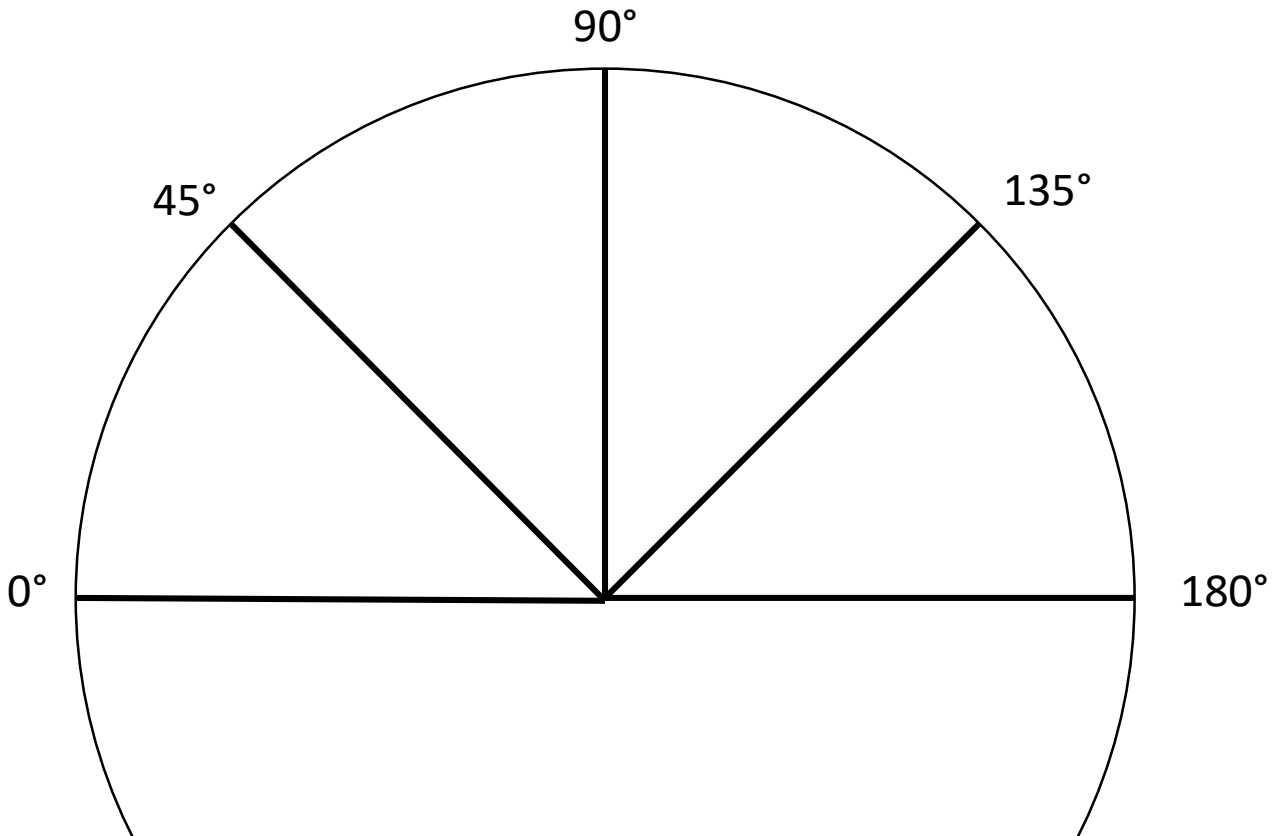

Servo 2 & 4 Orientation

Front of car →

180 degrees 90 degrees 0 degrees

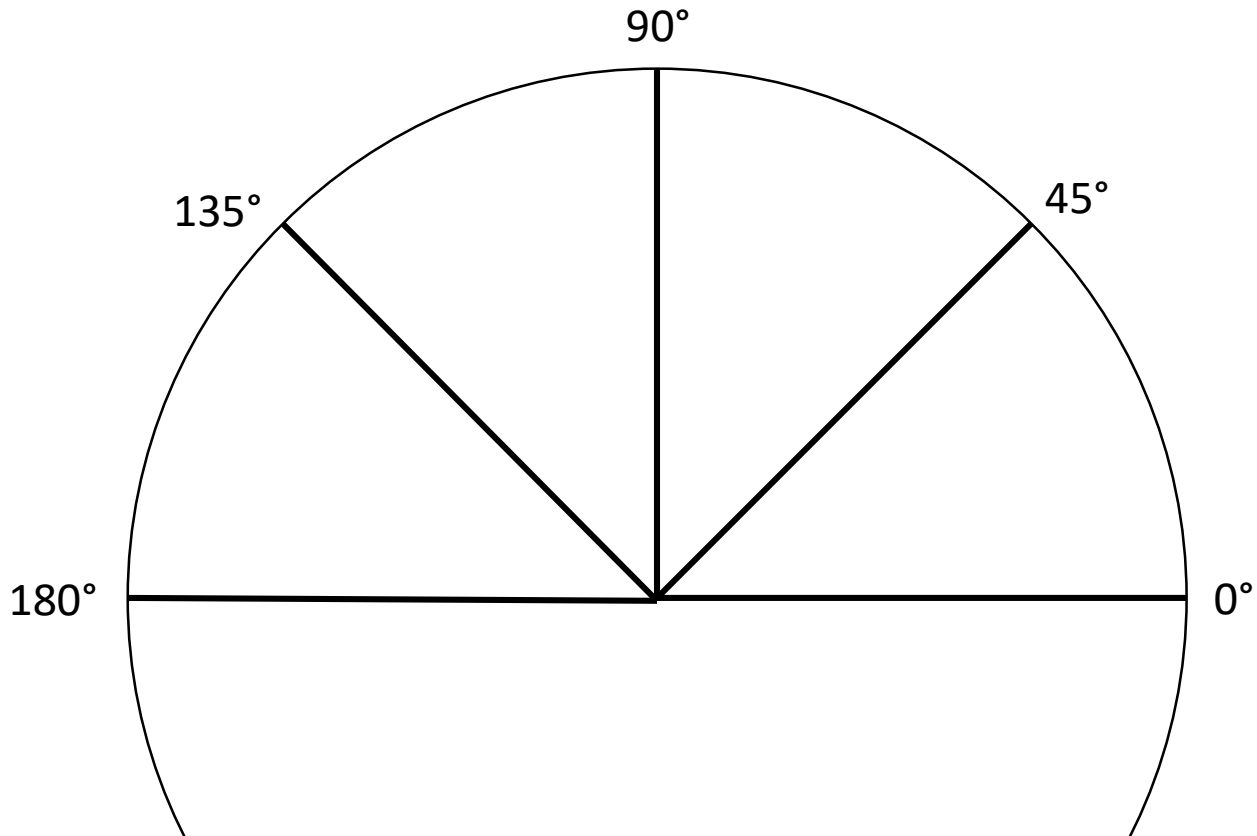

Appendix E: 3D CAD Drawings

D:\

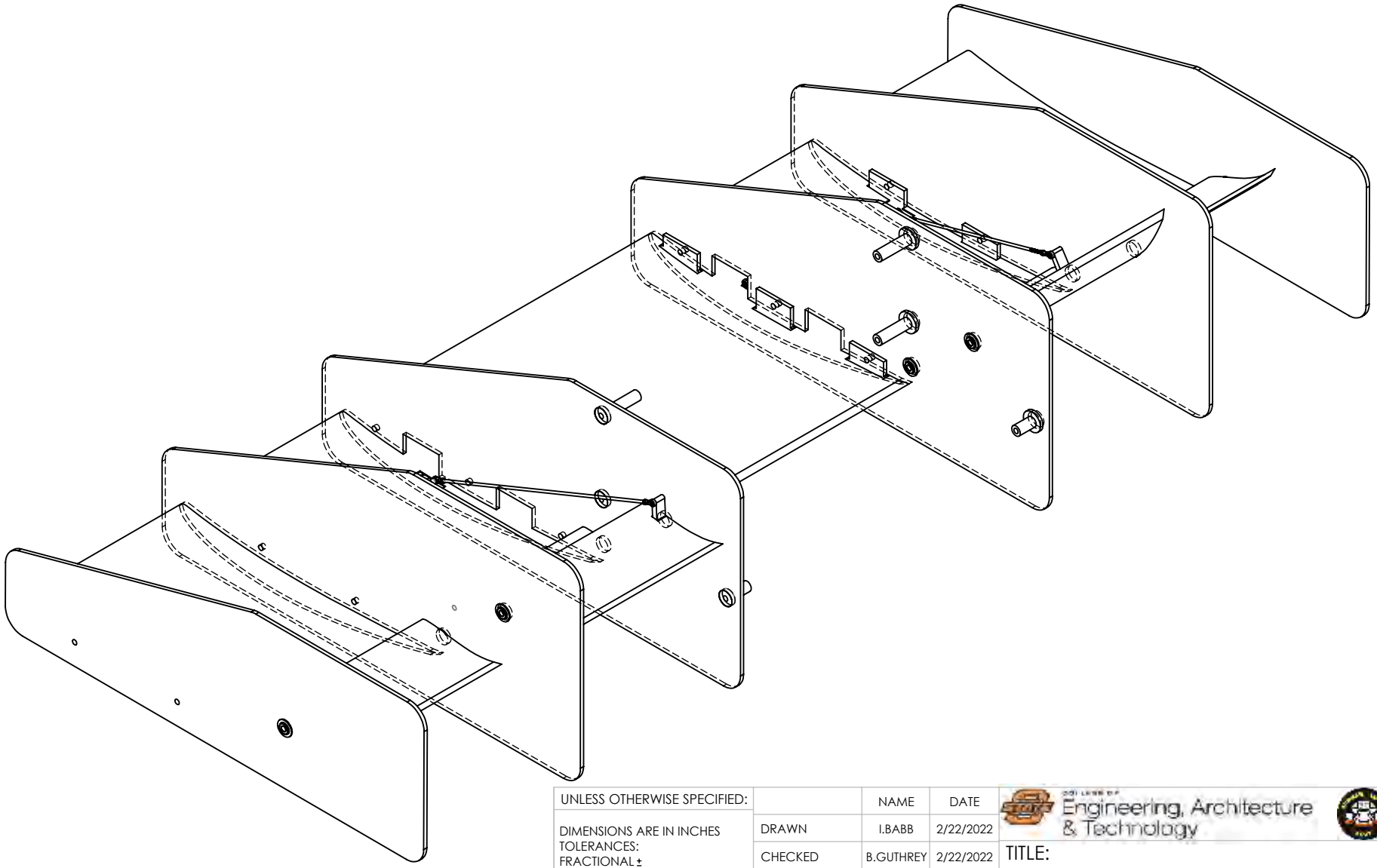

UNLESS OTHERWISE SPECIFIED:		NAME	DATE
DIMENSIONS ARE IN INCHES TOLERANCES: FRACTIONAL ± ANGULAR: MACH ± BEND ± TWO PLACE DECIMAL ± THREE PLACE DECIMAL ±	DRAWN	I.BABB	2/22/2022
	CHECKED	B.GUTHREY	2/22/2022
	ENG APPR.	DR.PAUL	1/20/2022
	MFG APPR.	-	-
INTERPRET GEOMETRIC TOLERANCING PER:	Q.A.	I.BABB	2/22/2022
MATERIAL EPOXY CARBON FIBER	COMMENTS: PARTS EDITED BY L.SMITH AND B.GUTHREY		
FINISH GLOSS			
DO NOT SCALE DRAWING			

Engineering, Architecture & Technology

TITLE:

Full Wing Assembly

SIZE	DWG.	REV
A	FULL ASSEMBLY DIMETRIC	3
	FILE NAME Spoiler alert CDR	

SCALE: 1:16 | WEIGHT: 10.33 | SHEET 1 OF 8

D:\

Ribs:

Scale 1:4

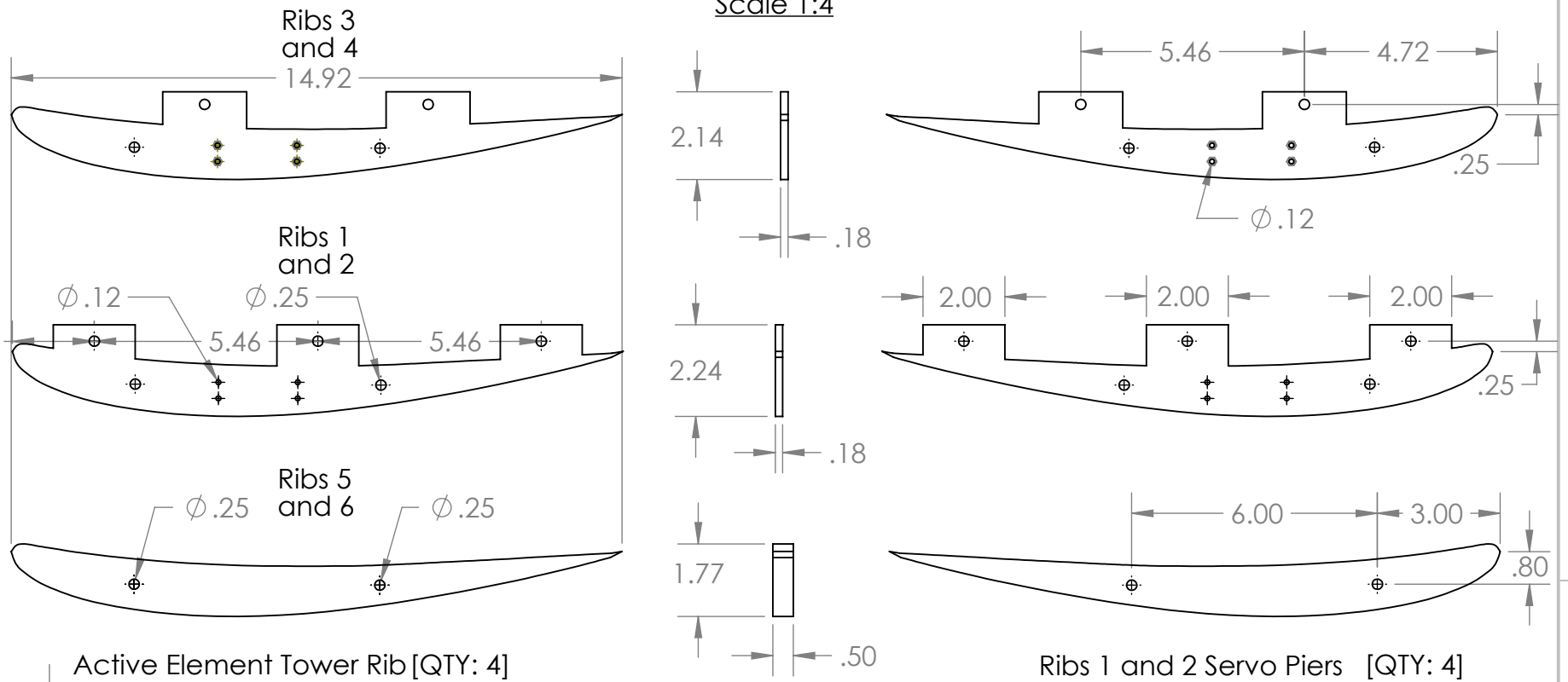

Active Element Tower Rib [QTY: 4]

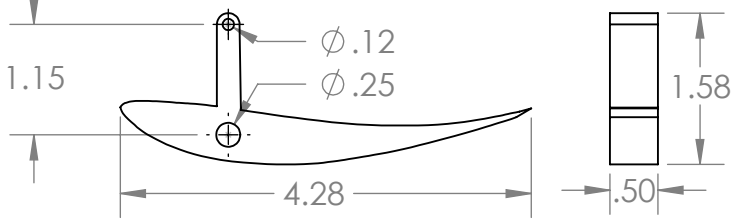

Scale 1:2

Ribs 1 and 2 Servo Piers [QTY: 4]

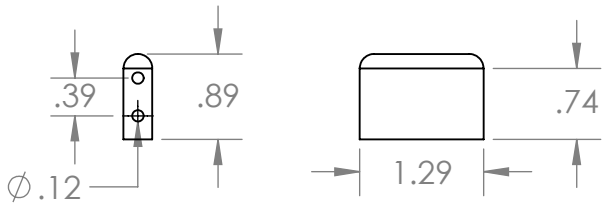

Active Element Pin Rib [QTY: 2]

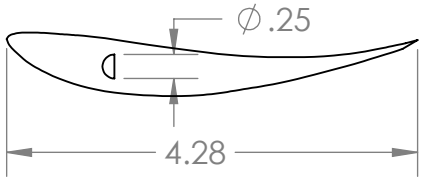

Active Element Rib [QTY: 6]

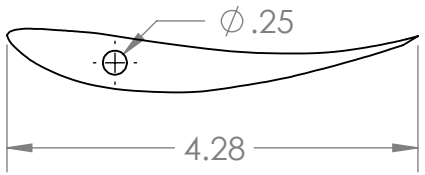

Engineering, Architecture & Technology

TITLE:

Full Wing Assembly

SIZE	DWG.	REV
A	RIB DESIGN	3
SCALE: 1:4		SHEET 2 OF 8

D:\

Wing Elements:

Main Element
[QTY: 1]

Scale 1:8

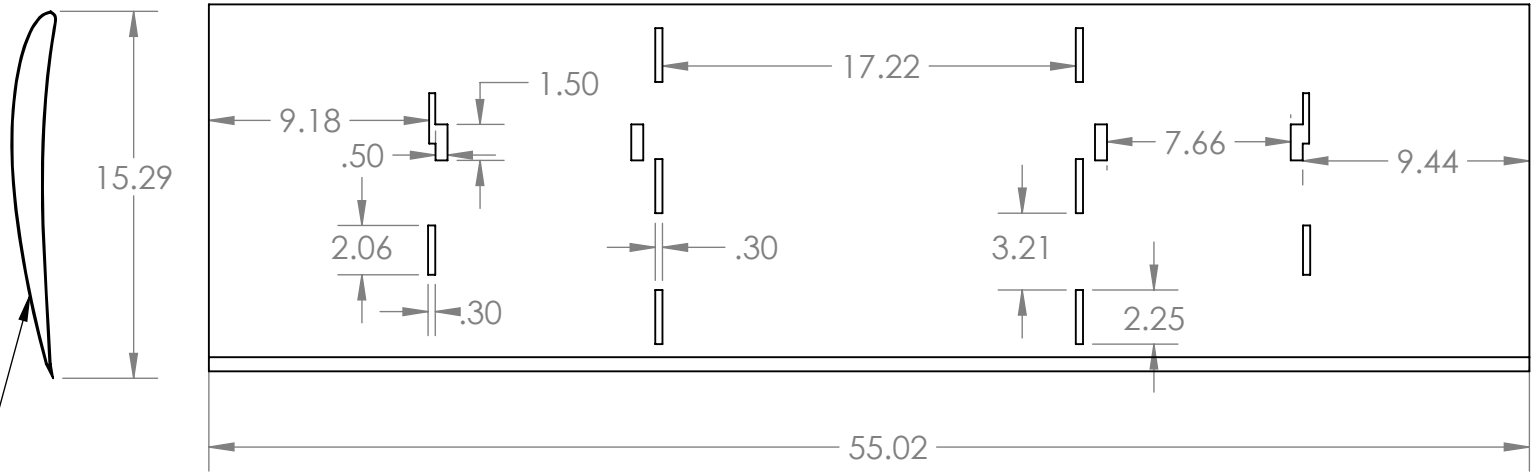

THICKNESS OF 0.05"

Active Element
[QTY: 6]

Scale 1:4

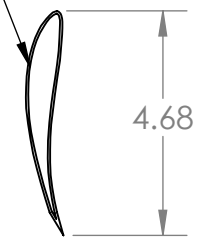

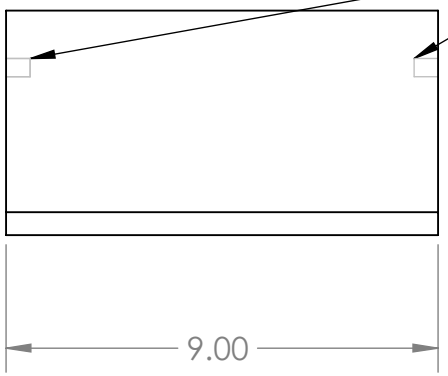

CUTOUT LOCATIONS FOR THE [ACTIVE ELEMENT TOWER RIB] TOWER TO PROTRUDE FROM THE ELEMENT

Engineering, Architecture & Technology

TITLE:

Full Wing Assembly

SIZE	DWG. NO.	REV
A	WING ELEMENT DESIGN	3
SCALE: 1:16		SHEET 3 OF 8

D:\

Endplates:

Scale 1:8

Endplates 1 and 2

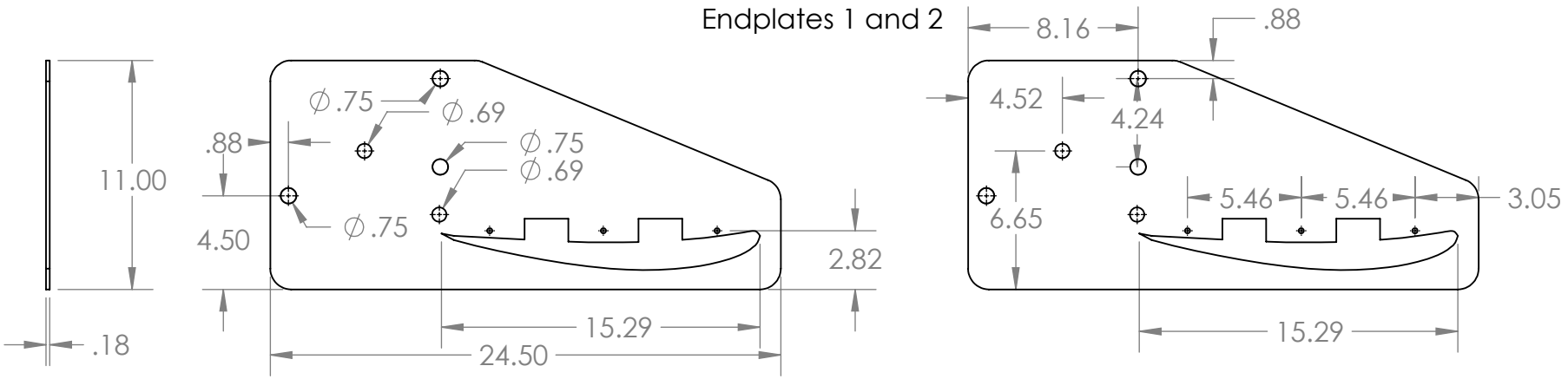

Endplates 3 and 4

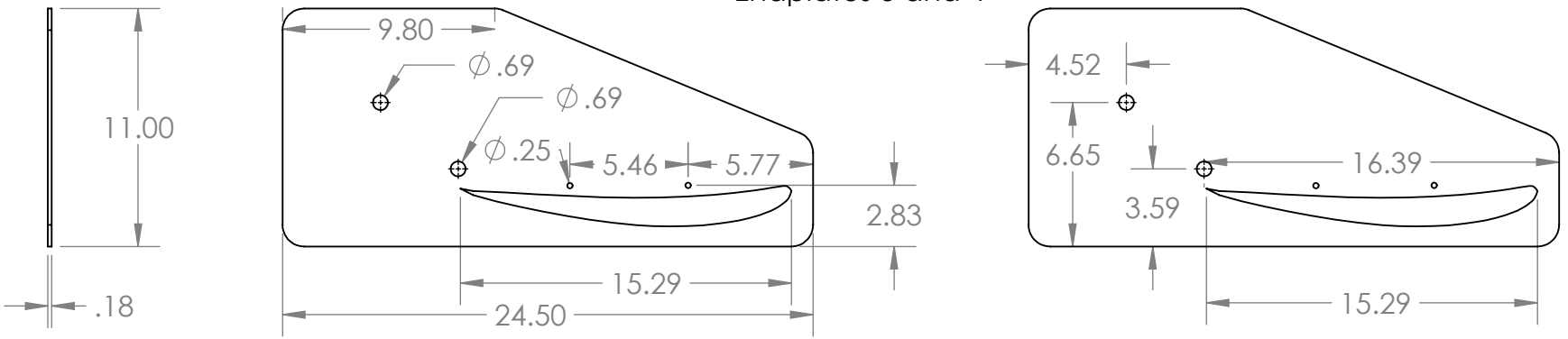

Endplates 5 and 6

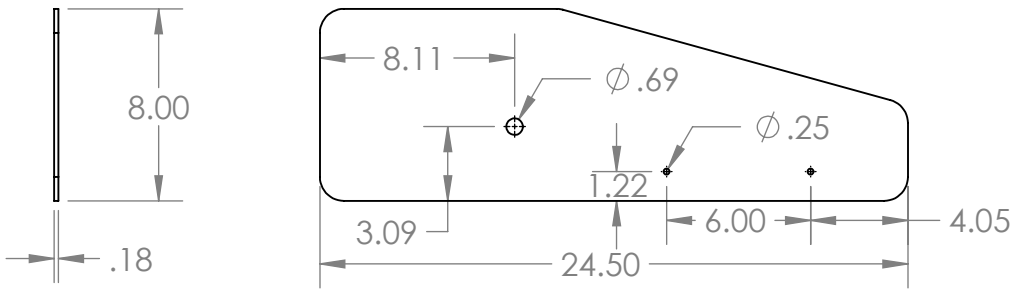

Engineering, Architecture & Technology

TITLE:

Full Wing Assembly

SIZE	DWG.	REV
A	ENDPLATE DESIGN	3

SCALE: 1:8 | SHEET 4 OF 8

D:\

Misc Parts:

Scale 1:1

Servo Motor [QTY: 4]

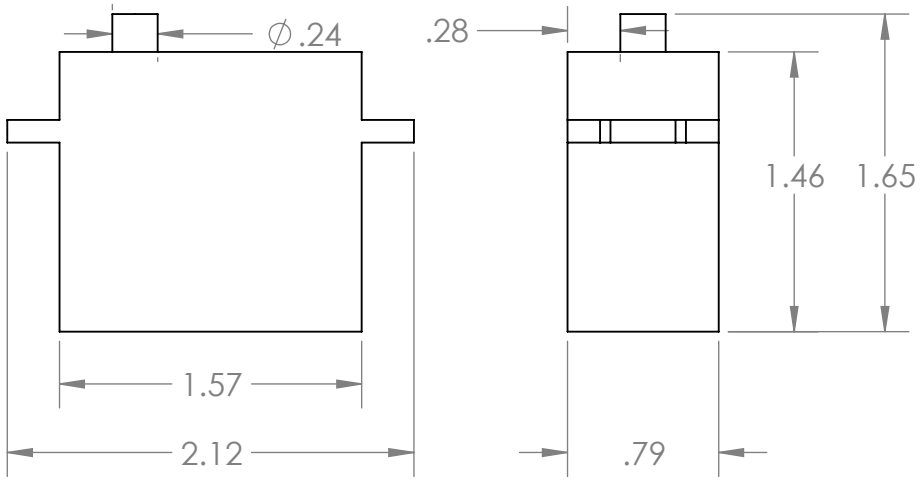

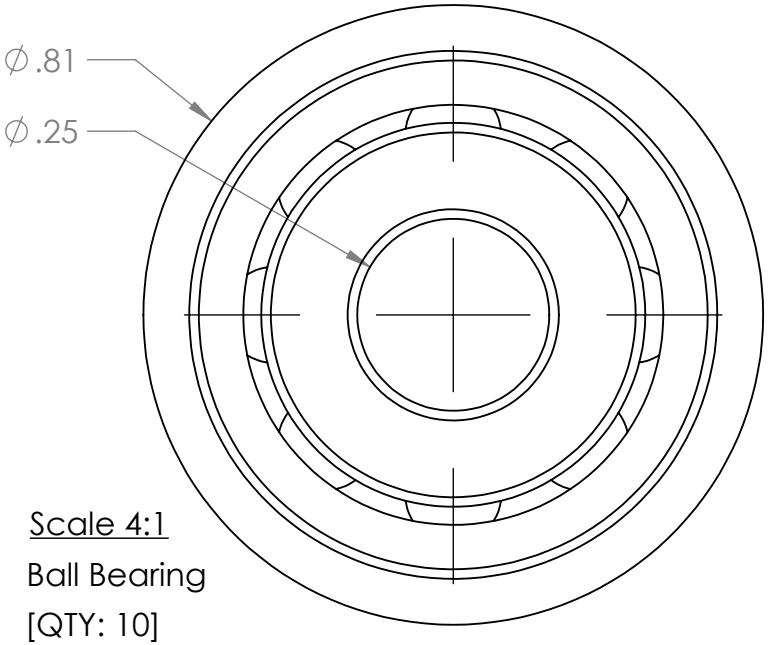

Scale 4:1

Ball Bearing

[QTY: 10]

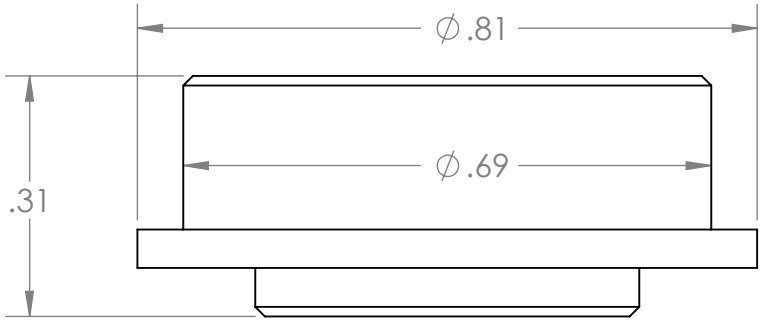

Scale 2:1

Servo Motor Arm [QTY: 4]

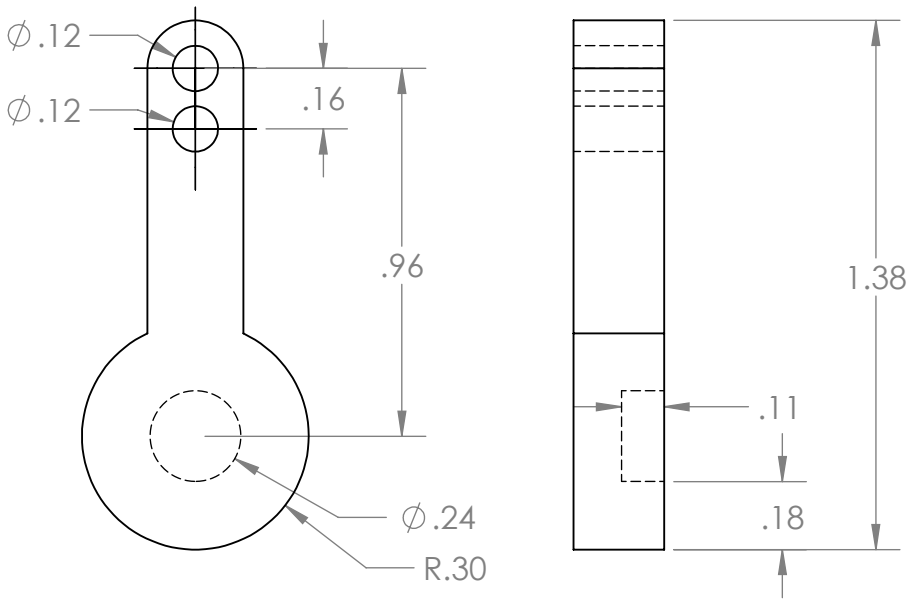

Engineering, Architecture & Technology

TITLE:

Full Wing Assembly

SIZE	DWG.	REV
A	MISC. PARTS	3
SCALE: 1:1		SHEET 5 OF 8

D:\

Misc Parts:

Tie Rod Linkages
[QTY: 2 EACH]

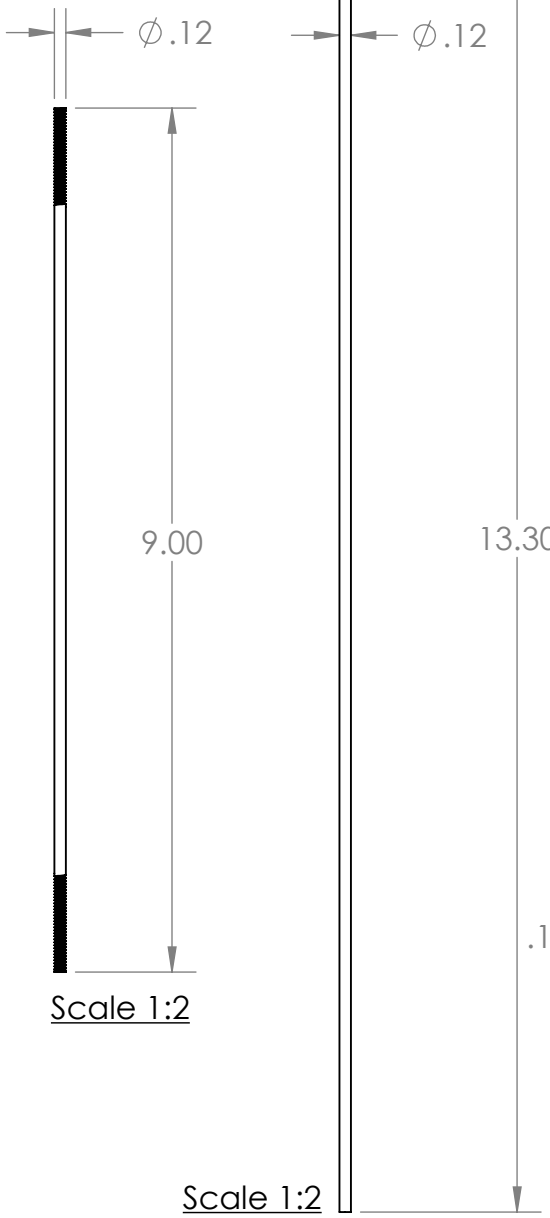

Scale 1:2

Scale 1:2

Wing Element Pin [QTY: 2]

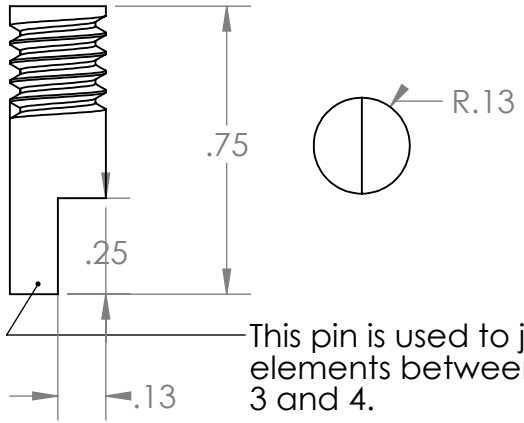

This pin is used to join the wing elements between the endplate 3 and 4.

Scale 4:1

Ball Joint Assembly [QTY: 8]

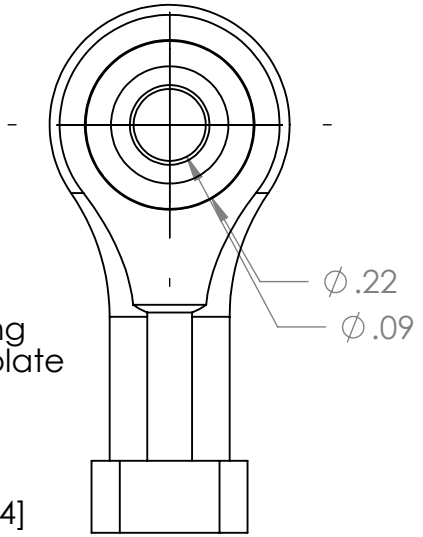

Scale 1:2

Rear Delrin [QTY: 2]

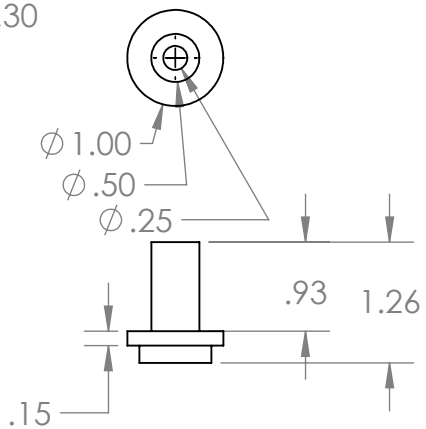

Front Delrin [QTY: 4]

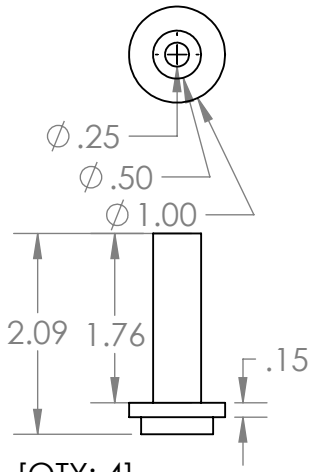

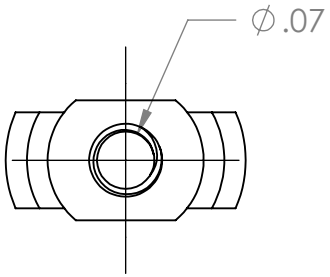

Scale 1:1

Ribs 1 and 2 Servo Piers [QTY: 4]

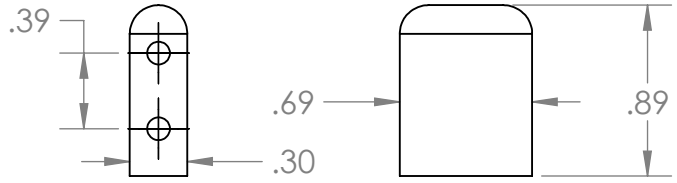

Engineering, Architecture & Technology

TITLE:

Full Wing Assembly

SIZE	DWG.	REV
A	MISC. PARTS	3
SCALE: 1:2		SHEET 6 OF 8

D:\

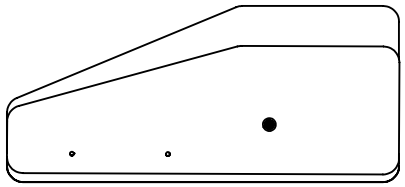

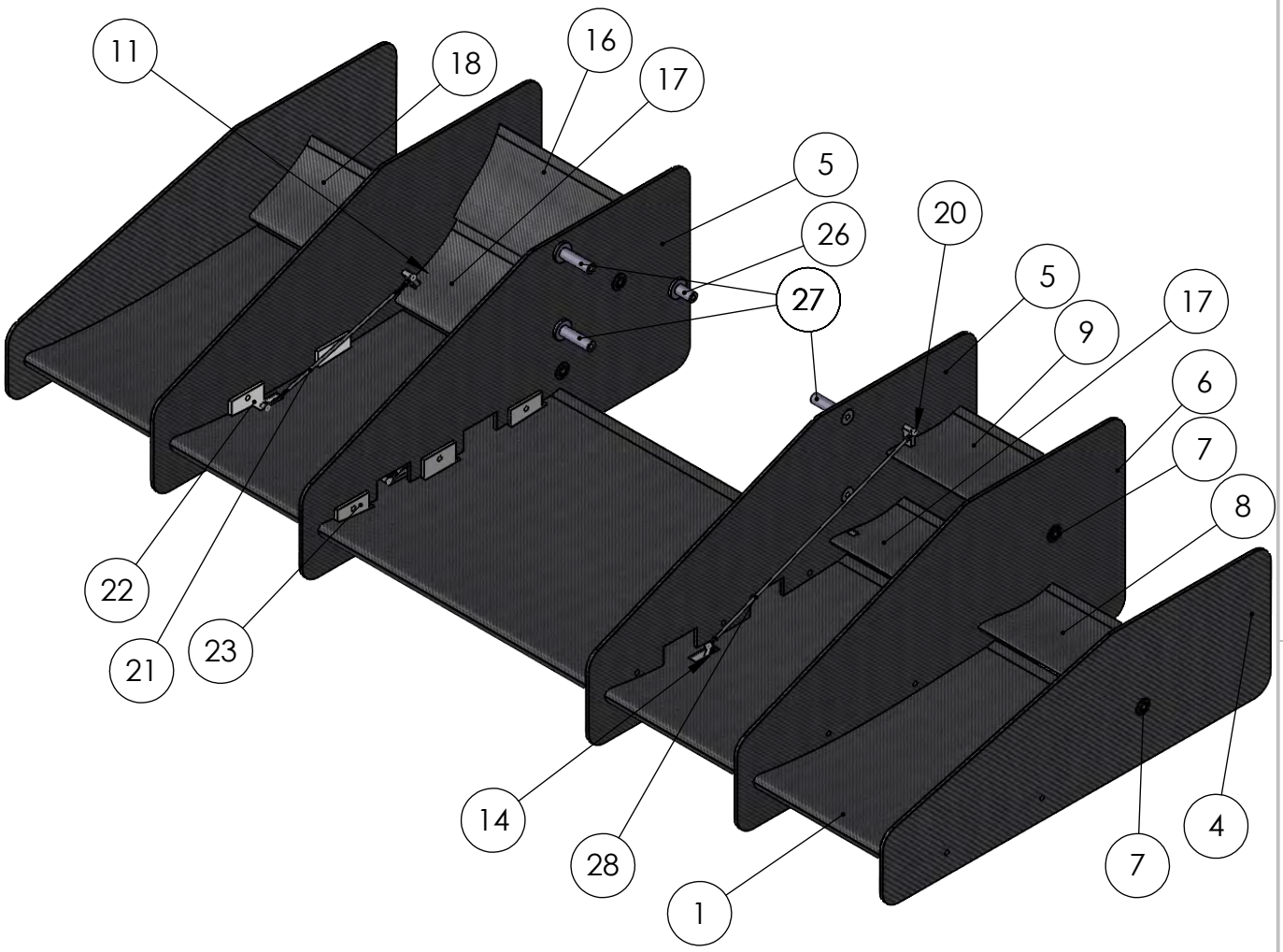

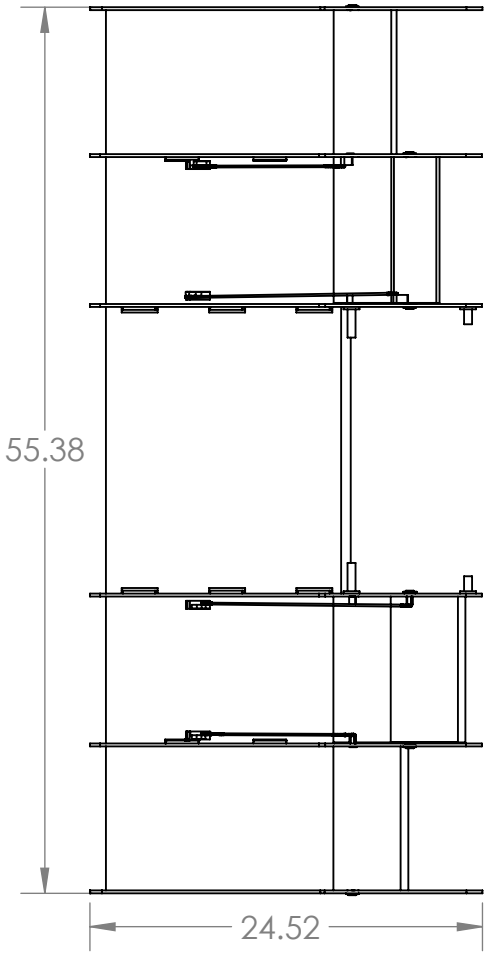

Engineering, Architecture & Technology

TITLE:

Full Wing Assembly

SIZE	DWG. NO.	REV
A	FULL ASSEMBLY	3

SCALE: 1:16 SHEET 7 OF 8

D:\

ITEM NO.	PART NUMBER	DESCRIPTION	QTY.
1	Main Element NACA 2412		1
2	NACA 2412 Rib Endplate With Servo Mount (Right)		1
3	NACA 2412 Rib Endplate With Servo Mount (Left)		1
4	Endplate_5,6		2
5	Endplate_1,2		2
6	Endplate_3,4-v3		2
7	6383K213	Ball Bearing	10
8	Active element outer Left-v2		1
9	Active element inner Left-v2		1
10	Active element rib_v3		6
11	Active element rib_v4		4
12	Mesh-Active element rib_v1		2
13	3,4 Active pin_v1		2
14	Motor Arm		4
15	Servo Motor		4
16	Active element inner Right-v2		1
17	Active element inner-v2		2
18	Active element outer Right-v2		1
19	6130K32	Ultra-Precision Ball Joint Rod End	8
20	ball		8
21	threaded rod		2
22	rib 3		2
23	Ribs 1,2		2
24	pier ribs 1,2		4
25	pier ribs 3,4		4
26	Bushingback_V1		2
27	BushingFront_V1		4
28	13.3 rod		2

TOTAL WEIGHT: 10.33 POUNDS

Engineering, Architecture & Technology

TITLE:

Full Wing Assembly

SIZE	DWG. NO.	REV
A	BILL OF MATERIALS	3
SCALE: 1:16		SHEET 8 OF 8